Respiratory Organ Motion in Interventional MRI: Tracking, Guiding and Modeling

Inauguraldissertation

zur Erlangung der Würde eines Doktors der Philosophie
vorgelegt der
Philosophisch-Naturwissenschaftlichen Fakultät
der Universität Basel

von
Žarko Ćeličanin
aus Trstenik, Serbien

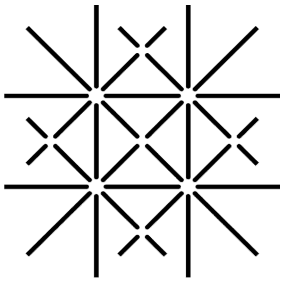

UNI
BASEL

Basel, 2016

Genehmigt von der Philosophisch-Naturwissenschaftlichen Fakultät

auf Antrag von:

Prof. Dr. Klaus Scheffler
Dissertationsleiter

Prof. Dr. Michael Bock
Korreferent

Basel, den 25. März 2014

Prof. Dr. Jörg Schibler
Dekan

Abstract

Respiratory organ motion is one of the major challenges in interventional MRI, particularly in interventions with therapeutic ultrasound in the abdominal region. High-intensity focused ultrasound found an application in interventional MRI for noninvasive treatments of different abnormalities. In order to guide surgical and treatment interventions, organ motion imaging and modeling is commonly required before a treatment start. Accurate tracking of organ motion during various interventional MRI procedures is prerequisite for a successful outcome and safe therapy.

In this thesis, an attempt has been made to develop approaches using focused ultrasound which could be used in future clinically for the treatment of abdominal organs, such as the liver and the kidney. Two distinct methods have been presented with its ex vivo and in vivo treatment results. In the first method, an MR-based pencil-beam navigator has been used to track organ motion and provide the motion information for acoustic focal point steering, while in the second approach a hybrid imaging using both ultrasound and magnetic resonance imaging was combined for advanced guiding capabilities.

Organ motion modeling and four-dimensional imaging of organ motion is increasingly required before the surgical interventions. However, due to the current safety limitations and hardware restrictions, the MR acquisition of a time-resolved sequence of volumetric images is not possible with high temporal and spatial resolution. A novel multislice acquisition scheme that is based on a two-dimensional navigator, instead of a commonly used pencil-beam navigator, was devised to acquire the data slices and the corresponding navigator simultaneously using a CAIPIRINHA parallel imaging method. The acquisition duration for four-dimensional dataset sampling is reduced compared to the existing approaches, while the image contrast and quality are improved as well.

Tracking respiratory organ motion is required in interventional procedures and during MR imaging of moving organs. An MR-based navigator is commonly used, however, it is usually associated with image artifacts, such as signal voids. Spectrally selective navigators can come in handy in cases where the imaging organ is surrounding with an adipose tissue, because it can provide an indirect measure of organ motion. A novel spectrally selective navigator based on a crossed-pair navigator has been developed. Experiments show the advantages of the application of this novel navigator for the volumetric imaging of the liver in vivo, where this navigator was used to gate the gradient-recalled echo sequence.

Publications Arising from this Thesis

Journal Papers

- **Z. Celicanin**, V. Auboiroux, O. Bieri, L. Petrusca, F. Santini, M. Viallon, K. Scheffler, R. Salomir. Real-time method for motion-compensated MR thermometry and MRgHIFU treatment in abdominal organs. Magn Reson Med 2013 doi: 10.1002/mrm25017.

- **Z. Celicanin**, O. Bieri, F. Preiswerk, P. Cattin, K. Scheffler, F. Santini. Simultaneous acquisition of image and navigator slices using CAIPIRINHA for 4D-MR imaging. Magn Reson Med 2013, doi: 10.1002/mrm.25134.

- **Z. Celicanin**, L. Petrusca, K. Scheffler, V. Auboiroux, Y. Natsuaki, F. Santini, O. Bieri, R, Salomir, "Hybrid US-MR guided treatment method with 3D motion compensation," submitted to *BioMed Research Journal*, 2014.

- L. Petrusca, P. Cattin, V. De Luca, F. Preiswerk, **Z. Celicanin**, V. Auboiroux, M. Viallon, P. Arnold, F. Santini, S. Terraz, K. Scheffler, C. Becker, R. Salomir. Hybrid ultrasound/magnetic resonance simultaneous acquisition and image fusion for motion monitoring in the upper abdomen. Invest Radiol. 2013;48(5):333-40.

Conference Proceedings

- **Z. Celicanin**, V. Auboiroux, O. Bieri, L. Petrusca, Y. Natsuaki, F. Santini, M. Viallon, K. Scheffler, R. Salomir. Hybrid US-MR guided HIFU treatment method with 3D motion compensation. Proceedings of the ISMRM 21st Annual Meeting and Exhibition, April 2013, Salt Lake City, USA.

- **Z. Celicanin**, V. Auboiroux, O. Bieri, L. Petrusca, F. Santini, M. Viallon, K. Scheffler, R. Salomir. Real-time treatment method with improved MR thermometry of mobile organs by MRgHIFU. Nouvelles methodologies en imagerie du vivant, December 2012, Lyon, France.

- **Z. Celicanin**, V. Auboiroux, O. Bieri, F. Santini, M. Viallon, K. Scheffler, R. Salomir. Real-time method for treatment of mobile organs and MR thermometry by MRgHIFU. The 12th International Symposium on Therapeutic Ultrasound, June 2012, Heidelberg, Germany.

- **Z. Celicanin**, O. Bieri, K. Scheffler, F. Santini. Spectrally selective crossed-pair navigator. Proceedings of the ISMRM 20th Annual Meeting and Exhibition, May 2012, Melbourne, Australia.

- **Z. Celicanin**, V. Auboiroux, O. Bieri, F. Santini, M. Viallon, K. Scheffler, R. Salomir. Real-time method for MR thermometry and treatment of mobile organs by MRgHIFU. Proceedings of the ISMRM 20th Annual Meeting and Exhibition, May 2012, Melbourne, Australia.

- **Z. Celicanin**, F. Preiswerk, P. Arnold, P, Cattin, K. Scheffler, F. Santini. Simultaneous acquisition of image and navigator slices using CAIPIRINHA. Proceedings of the ISMRM 19th Annual Meeting and Exhibition, May 2011, Montreal, Canada.

- L. Petrusca, V. De Luca, P. Arnold, **Z. Celicanin**, T. Goget, V. Auboiroux, M. Viallon, F. Santini, S. Terraz, K. Scheffler, C. Tanner, P. Cattin, R. Salomir. Ultrasound/MR hybrid imaging: truly simultaneous motion monitoring in the abdomen and image co-registration. Proceedings of the ISMRM 19th Annual Meeting and Exhibition, May 2011, Montreal, Canada.

- L. Petrusca, P. Arnold, Th. Goget, **Z. Celicanin**, V. Auboiroux, M. Viallon, F. Santini, V. De Luca, S. Terraz, C. Tanner, K. Scheffler, C. D. Becker, P. Cattin, R. Salomir. Simultaneous ultrasound/MRI montion monitoring in the abdomen. 8th Interventional MRI Symposium, September, 2010, Leipzig, Germany.

- **Z. Celicanin**, K. Scheffler, F. Santini. Fast interleaved sequence for 4D-MRI of organ motion. European IDEA Users Meeting, June 2010, Jülich, Germany.

Contents

Chapter 1

Introduction

Respiratory organ motion is a major issue in interventional magnetic resonance imaging (MRI) and in imaging with MRI in the abdominal and thoracic region. In this introductory chapter, the fundamental details of respiratory organ motion are provided with the focus on the current issues occurring in interventional MRI. The fundamental details of a relatively novel noninvasive treatment method, based on high-intensity focused ultrasound, are also provided. Fundamental principles of MR thermometry and the challenges with regard to respiratory organ motion are discussed. At the end, the aim and outline of the thesis are provided.

1.1 Introduction to Respiration

Respiration is the process of transporting the oxygen from the atmosphere into the bloodstream and releasing the carbon dioxide from the bloodstream to the atmosphere. These processes are enabled by a specific organ called the lung. The lung expends and contracts periodically by the diaphragm and inter-costal muscles which in fact enables breathing. The diaphragm causes changes of the vertical dimension of the lung, while the inter-costal muscles change the diameter of the chest cavity. A schematic plot of a respiratory waveform is shown on Fig. 1.1.

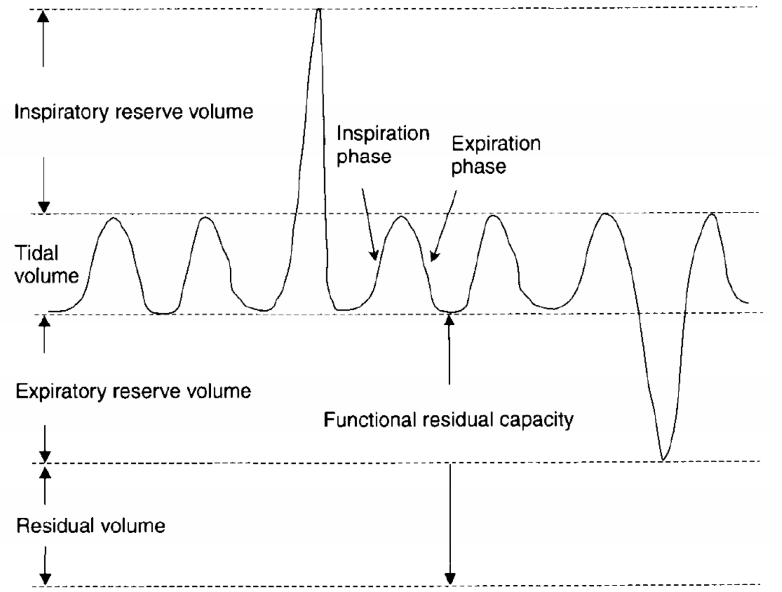

Figure 1.1 A schematic waveform of a respiratory signal. Respiratory phases, various lung volumes and functional residual capacity are marked. (Source [1])

During the inspiration phase, the alveolar pressure is negative (~ 2 mmHg) which causes the flow of the air inside the lung. It lasts approximately around 2 seconds in a health human subject. The expiration phase on the other hand is characterized by a positive alveolar pressure. This phase follows immediately

after the inspiration phase. There is a brief pause of around 1 second after the expiration phase is over before the next breathing cycle.

During the process of respiration, the air volume inside the lung is changing. The tidal volume (~ 0.5 L) is the volume of air that is normally exchanged during the breathing cycle. The maximum volume of air that can be inhaled beyond the tidal volume is called inspiratory reserve volume (~ 3.1 L), while the maximum volume of air that can be exhaled beyond the tidal volume is called expiratory reserve volume. The volume of air that remains inside the lung when the maximum exhalation is attained is called residual volume (~ 1.2 L). Functional residual capacity (~ 2.4 L) refers to the volume of air inside the lung after the ending of the expiration phase, i.e. it contains the residual and expiratory reserve volume.

1.2 Challenges Related to Organ Motion

Respiratory organ motion is a complicating factor in many treatment options of interventional MRI. The sites in the upper abdomen are influenced by the diaphragm and changes of the organ position occur during the respiratory cycle. The delivery of radiation therapy or acoustic energy at the desired spot requires tracking of organ motion. The goal of every therapy is to deliver the lethal dose of the therapy beam as much possible at the targeted region, while sparing the surrounding healthy tissue. Therefore, the accurate target localization is essential for interventional MRI. Organ motion tracking is an important part of the treatment procedure.

Patient positioning and interventional MRI treatment planning require the accurate images of the treated organs. If the organs are influenced by respiration, they are changing theirs position in time, which causes motion artifacts to appear in the images. These artifacts are ghosting and blurring. The standard Cartesian k-space trajectories are prone to ghosting in the phase-encoding direction if the imaging object is moving periodically (or nearly periodically) during the acquisition. This is due to the properties of k-space and MR signal acquisition. Therefore, it is essential that in MR imaging for treatment planning, motion compensation techniques are applied in order to eliminate the motion artifacts.

1.3 Tracking Respiratory Organ Motion

Many respiratory-motion compensation techniques, such as gating, triggering and view reordering, require the respiratory signal to be obtained during the MR imaging. During interventional MRI treatments, respiration causes abdominal organs to move, which requires some feedback control of the therapy. In order to have a visual feedback of the breath-holding, sometimes the acquisition of the respiratory waveform, interleaved with a desired pulse sequence, is performed. Different methods are used to obtain the signal correlated to respiration. Breathing

belts, navigators (or navigator echoes), and video cameras are the most commonly used.

1.3.1 Breathing Belts

A breathing belt is positioned around the chest or the abdomen of a human subject. It consists of a fabric belt, that goes around the subject's body while in front a pressure transducer is attached. The transducer converts the mechanical energy originating from lung volume changes into an analog voltage. After processing this analog signal, it is sent to the MRI unit. The optical transmission is normally used for the signal transmission from the belt to the MRI unit in order to minimize electromagnetic interference of the magnetic field gradients.

Figure 1.2 MR-compatible respiratory belt. (Source [2])

Although respiratory belts are often used to gate the MR signal acquisition, it is time consuming to place a breathing belt on a patient. Also, a signal obtained by respiratory belts is not reliable, since a delay between a change of the diameter of the chest cavity and motion of the diaphragm might produce motion artifacts in the abdominal MRI imaging. In clinical practice, respiratory belts are mainly replaced by MR-based navigators.

1.3.2 Optical Tracking

Organ motion tracking using an external tracking device such as an optical camera has been increasingly used for prospective motion correction in order to prevent motion artifacts from appearing. It was primarily used to track motion of a human head or brain [3, 4]. Recently, an optical tracking system was applied to interventional MRI for respiratory gating of MRgHIFU therapy using an in-bore digital camera [5].

The information about the movement of abdominal organs can be obtained using an optical camera. The idea is to place a marker on the skin of a human subject (e.g. a checker-board marker) and continually record the movement of the marker with an MR-compatible camera. Special digital image processing

algorithms can be subsequently used to extract organ motion information from the video sequence, which in fact provides an indirect respiratory signal.

1.3.3 MR-based Navigators

MR-based navigators (or navigator echoes) are used to acquire the signal from the parts of a human body that are moving due to respiration, such as the diaphragm. The acquired signal is then processed to reconstruct the spatial profile of the monitored region, which usually contains some transition area between different tissue types or a tissue-air interface. Temporal resolution of the navigators is usually much less compared to the one provided by respiratory belts. The MR-based navigators, used to correct motion artifacts, were first described by Ehman and Felmlee [6].

In general the navigators acquire a partial set of k-space data to track the effects of patient motion. The acquisition of the navigators precedes the acquisition of the imaging sequence and the two acquisitions are interleaved. The assumption of negligible organ motion during the period between the acquisitions of the navigator and the imaging sequence is required.

The most commonly used linear navigators are cross-paired and pencil-beam navigator. The information provided by the navigator can be used in two different manners: for prospective or retrospective motion correction. Prospective correction refers to an approach in which the navigator data is used to modify the subsequent imaging acquisition in order to prevent motion artifacts. On the other hand, in retrospective correction the navigator data is used only after the full acquisition of k-space is completed and the correction is applied to the raw data (before Fourier transform) or already reconstructed images. By looking into the nature of prospective correction, it can be concluded that it requires sufficiently fast real-time processing capabilities, if the modifications of the subsequent imaging sequence are to be performed on time. Slice following (or slice tracking) can be used on either periodic or aperiodic motion, and the concept is to move the scan volume in such a way as to be positioned always at the same location with respect to the imaging object [7]. Although the name implies that it can be used only for slice or two-dimensional acquisition, the volume or three-dimensional acquisition is also possible.

There are several methods to process the navigator data of which two methods are commonly used: the correlation method and least-squares method.

The navigators can be acquired in several ways. They can use 1D, 2D or 3D k-space trajectories. However, the 1D or linear navigators are used most commonly, and they are discussed in the section 1.2.2.1 cross-paired and 1.2.2.2 pencil-beam navigator. In the simplest form, one line passing through the origin of k-space is acquired and processed. This could be achieved with either a spin-echo or a gradient-echo pulse sequence. However, in many cases the navigator could be acquired without a separate RF excitation pulse by using the transverse magnetization already excited by the imaging RF pulse.

1.3.3.1 Cross-Paired Navigator

One method to excite a column of magnetization and so acquire a linear navigator is to use a spin echo sequence with two RF pulses, one excitation pulse and the other refocusing pulse with two slice selection gradients that are chosen in such a way that the corresponding slices intersect. To obtain a signal from a strip of magnetization, first the π/2 excitation RF pulse is used to select a plane, and then a plane which crosses the previous plane is excited with the π refocusing RF pulse. The desired planes are selected with the slice-selection gradients. The pulse sequence and the diagram showing a strip at the intersection of the two planes are shown on Fig. 1.3. Further details of this method of 2D excitation can be found in [8].

1.3.3.2 Pencil-Beam Navigator

Pencil-beam navigator can be acquired using a 2D RF pulse that sweeps k-space in a spiral or EPI-like trajectory, which excites a circular or strip column of spins. The pulse sequence of the pencil-beam navigator implemented with a spiral k-space trajectory is shown on Fig. 1.4.

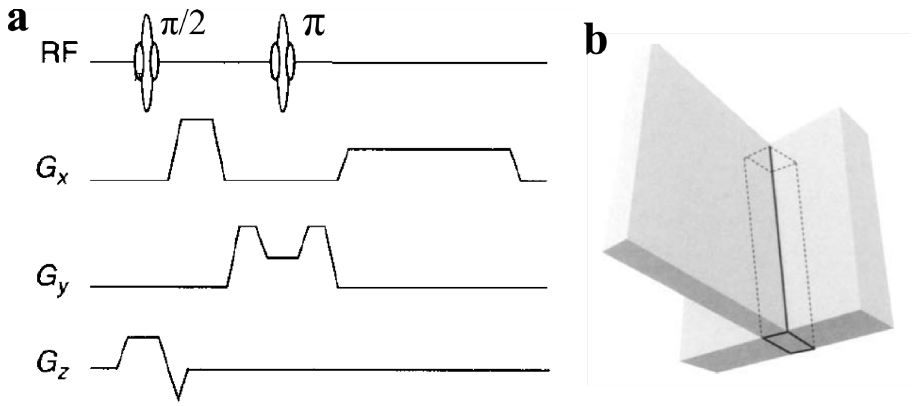

Figure 1.3 Pulse sequence of the cross-paired navigator **(a)**; a strip of magnetization excited in the intersection of the two planes **(b)**. (Adapted from [1])

1.3.3.3 Spectrally Selective Navigators

In order to provide fast and direct measurement of the bulk motion of the heart and the liver different spectrally selective navigators were proposed.

The cardiac fat navigator consisting of spatial-saturation pulses, spectral excitation and sampling the signal with multiple k-space trajectories were used to track the motion of the epicardial fat to image 3D magnetic resonance angiography of coronary arteries [9].

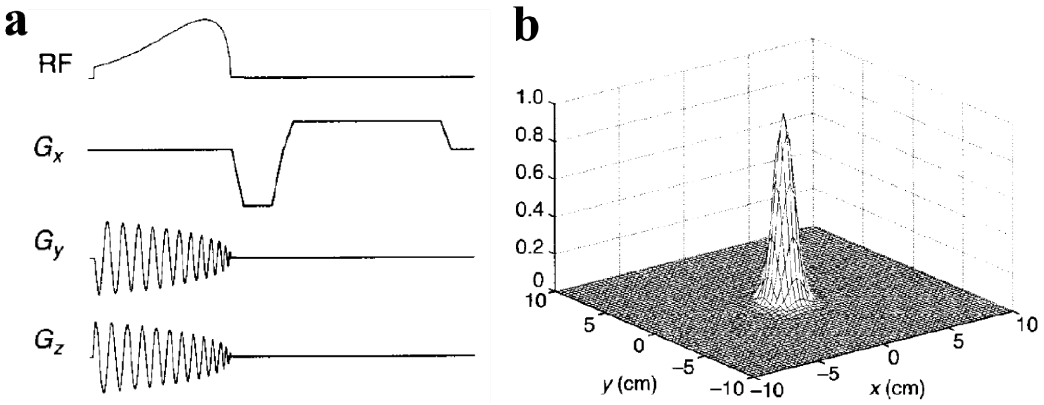

Figure 1.4 Pencil-beam navigator with spiral k-space trajectory **(a)**; calculated spatial profile **(b)**. (Source [1])

Spectrally selective pencil-beam navigator was used to track the motion of the adipose tissue around the liver and the kidney in order to guide the ablation with magnetic resonance guided high-intensity focused ultrasound [10]. The spectral selectivity of the navigator was achieved by converting the excitation to a 1-2-1 binomial pulse [11].

1.4 Imaging Respiratory Organ Motion

Different approaches were taken in the past to try to capture the whole motion of abdominal organs with the imaging modality such as MRI. Imaging with other modalities such as ultrasound and computed tomography (CT) will not be discussed here.

Dynamic imaging of organ motion offers many advantages over only static images, as it provides information about the organ deformation driven by respiration. Time-resolved imaging is used in interventional MRI for treatment planning, patient positioning, and control of the delivered treatment energy.

An ideal imaging of abdominal organ motion would provide an artifact-free imaging with high signal-to-noise ratio (SNR), high soft tissue contrast, high spatial and temporal resolution. However, due to the technical limitations of MRI this is currently not possible and different measures have to be taken in order to obtain satisfactory imaging.

Acquisition of full four-dimensional (4D) datasets (three-dimensional + time) of organs in the abdominal region during free-breathing is still a challenging problem. The current safety limitations and technical capabilities of the machines do not allow the acquisition of 4D MRI with the satisfactory image spatial and temporal resolution, and with high signal-to-noise ratio. To address this issue, different techniques are applied to deal with the organ motion.

Respiratory motion artifacts can be reduced by using ultrafast imaging, imaging during breath-hold (breath-holding), respiratory gating or respiratory phase encode reordering.

1.4.1 Breath-holding

A simple approach to suppress the motion of abdominal organs is to perform the breath-hold, either voluntarily or forcedly. In general, a healthy human subject can hold his or her breath for about 20 – 30 s. Although the breath-holding can be performed at any point in the respiratory waveform, it is usually done in the inspiratory reserve volume, since most of the subjects can perform breath-holding the longest at this stage of the respiration. Prior the breath-holding the operators usually instruct the patient to do hyperventilation, as this increases the time they can hold without breathing.

As only 20 – 30 sec. are available to acquire the images of the anatomy, fast imaging sequences, like gradient-recalled echo are used. Multiple breath-holding can be used in order to increase the number of slices or image resolution. Parallel imaging is commonly used to increase the speed of the acquisition.

However, 3D acquisition or 2D with higher spatial resolution in the phase-encoding direction is still challenging. Uncooperative patients, like children and geriatric patients still pose problems with this approach.

However, the dynamic information of the imaging organ (i.e. deformation or hysteresis) is not preserved, which could be problematic in a subsequent treatment in interventional MRI in case the treatment is to be performed in free-breathing. Sometimes the images acquired with a breath-holding method are used for a treatment which is also performed in a breath-hold, but this approach increases significantly the duration of the therapy.

1.4.2 Respiratory Gating

Respiratory gating is an approach in which the acquisition of images is only performed when the respiratory signal is within the certain range, determined by the upper and lower gating thresholds [12]. The gating is in general performed after the expiratory phase, i.e. at the functional residual capacity, as this is the longest relatively stable segment of the respiratory cycle. Schematic drawing of the respiratory gating is shown on Fig. 1.5.

The most important consideration when using gating is the prolonged time of the acquisition. As the acquisition is only performed during the gating window, which represents approximately about a third of the time of the overall respiratory cycle, the scan takes approximately three times more time. It is primarily used with fast sequences such as gradient-recalled echo. The treatments performed with the gating approach in interventional MRI are also significantly prolonged. One approach to improve gating is to instruct the patient to keep his or her breathing position in the gating window as much as possible, which could be done by a visual or audio feedback, or a combination of both.

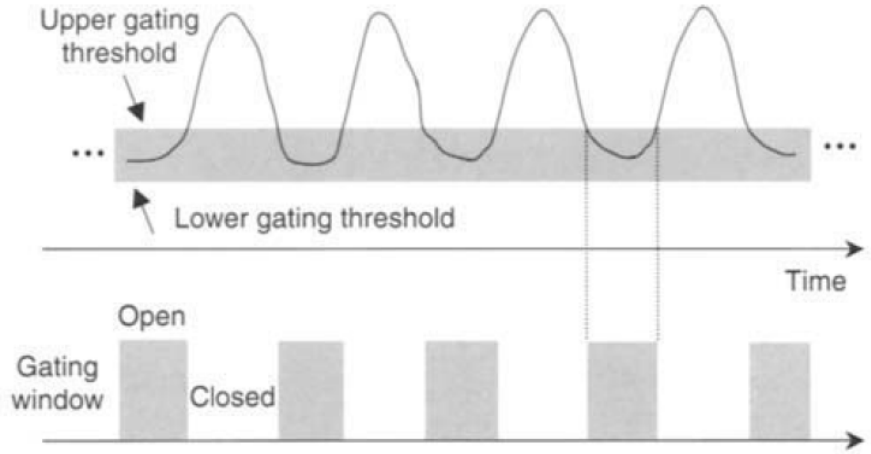

Figure 1.5 Schematic plot showing a respiratory breathing waveform with a gating window. Thresholds determine the size of the gating window. (Source [1])

1.5 Time-Resolved Volume Imaging of Organ Motion

If the precision and accuracy of interventional MRI treatments are to be improved, better control of abdominal organ motion must be achieved with tracking, organ motion modeling, and guidance of the treatments. To acquire images of organ motion during free-breathing and study various aspects of it, is a challenging problem. Due to the respiratory motion, an organ is always changing its position and so the compromise between spatial and temporal resolution and SNR have to be made during MR imaging.

One approach to get the 4D (3D + time) images of an organ, is to image only a part of the organ, for example a single slice. The respiratory phase is determined by the extra information acquired by a navigator, whose acquisition is interleaved with the acquisition of the desired imaging sequence. The navigator can be an external navigator, e.g. breathing belt or any kind of MR-based navigator. Retrospective sorting can be used after the acquisition to stack the images together [13].

Adaptive 4D MR imaging for real-time 3D visualization of respiratory organ motion for MRI-guided therapy based on the MR navigator echo and multiple gating windows was reported in [14]. It was designed to acquire a time series of volumetric 3D images of an organ to be used for a therapy guidance. A respiratory gating scheme was used in order to model nonrigid deformation of the liver from the acquired 3D undersampled high-resolution images combined with a fast and robust image registration [15].

One particularly interesting approach reported in [16], was based on a two-dimensional navigator, instead of a standard one-dimensional MR navigator in order to capture the different liver shapes during the respiration. The acquisition of the image and navigator slices was interleaved. The acquisition scheme is shown on Fig. 1.6.

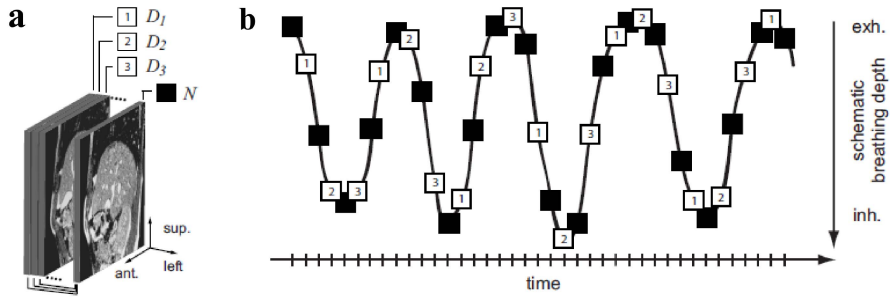

Figure 1.6 (a) Slices covering the organ of interest (D_1, D_2, D_3,…) and the navigator (N), **(b)** The interleaved acquisition scheme between the image slices and the navigator. (Source [17])

1.6 MR-guided high-intensity focused ultrasound

1.6.1 Introduction

The concept of using acoustic energy for noninvasive thermal ablation inside the human body was first suggested in 1940s for the ablation of central nervous system tissue [18]. However, due to the lack of an effective guiding modality for target visualization and exposure quantification, the high-intensity focused ultrasound (HIFU) had not become widely accepted till 1990s, when combining HIFU and MRI into MRgHIFU brought new applications: treatment of the eye [19], prostate [20, 21], bladder [22], kidney [22, 23], liver [22, 24, 25], breast [26], bone [27], and other cancers [28]. A good overview of the current treatment possibilities with MRgHIFU for different abnormalities is given in [29].

MRgHIFU utilizes the acoustic energy to induce thermal lesions inside the human body without any biological adverse effects. The concept of MRgHIFU is in a therapeutic sense superior to radiotherapy, commonly used in radiation oncology, by allowing smaller margins, being noninvasive and allowing therapy repetition multiple times.

MRI provides excellent soft tissue contrast, which is important for target definition and the detection of critical structures, such as bones, nerves, and gases. The only clinically proven method for noninvasive measurement of temperature inside the human body is enabled by MRI. MR thermometry based on proton resonance frequency (PRF) shift gave significant advantages to MRI as a guiding system [30]. Tissue independence, linearity and high signal-to-noise ratio (SNR) of PRF-based MR thermometry represent the major advantages compared to ultrasound (US) and computed tomography (CT). Excellent soft tissue contrast provided by MRI allows exceptional control of targeting, and setting accurate therapy margins.

The commercialization of the academic developments led to establishing several companies, of which one company got the approval by the Food and Drug Administration (FDA) for the treatment of uterine fibroids. Several clinical trials

are currently under way for the treatment of multiple organs and at different anatomic sites. To name some, palliative pain treatment of metastatic bone tumors [31], targeted drug delivery [32], focal blood-brain barrier disruption [33], and gene therapy [34, 35] are some of the currently recognized potential applications.

1.6.2 Principles

The principle of high-intensity focused ultrasound is based on acoustic power of ultrasound waves, which propagate though the body to reach a part of the body where treatment is sought. At the focal spot, the ultrasound waves interference constructively, which causes certain mechanical or thermal effects on a biological tissue. The main effect imposed on the living tissue is thermal, temperature elevation is caused by ultrasound pressure waves, while the propagation of mechanical energy is widely believed to be harmless below the cavitation threshold.

The increase of temperature is dependent on the duration of exposure and the intensity (power) of the HIFU system. For the short duration, the main effect causing the thermal cooling is thermal conduction, while for the longer duration the blood perfusion dominate the temperature distribution. In short ablations, the borders of thermal lesions are very sharp, in contrast to the ones when perfusion comes into play. In that case, tissue swelling and possible blood veins blockages could over- or under-estimation the ablated region.

The propagation of the acoustic pressure waves is shown on Fig. 1.7a, while the induced temperature elevation at the focal spot is shown on Fig. 1.7b.

The temperature elevation depends on the local absorption coefficient and on the attenuation in the overlying tissues, which causes a variability of temperature across the treated organ, and thus the need for thermal distribution assessment by MRI.

The bioeffects of the thermal energy affecting biological tissue was studied and reported in [37]. The biological effects of the different temperatures and time exposures have been quantified by an equivalent thermal damage at 43 ºC [38]. Although there is a variation across different tissue types, irreversible tissue damage is normally induced when a thermal dose at 43 ºC for 240 minutes is applied. Reversible tissue effects can also be caused by ultrasound energy, such as vasodilatation, vessel constriction, and permeability changes. These are transient changes after which the tissue comes back to normal after the ablation. However, proper measures should be taken during the treatment, as the ablation zone can be over- or under-estimated.

Other interesting bioeffects caused by ultrasound is the one mediated by micro-sized gas bubbles [39, 40]. There are two ways in which the effect, called cavitation, can present itself: a first, in which the bubbles contract and expand with the pressure waves and a second in which the bubbles burst violently. The latter case can cause a serious tissue damage and should be prevented, while on the other hand, the first one is used to transiently disrupt blood-brain barrier in the head, for local drug delivery, and also has some other potential applications.

The principle of MRgHIFU in the liver is schematically shown on Fig. 1.8. The induced elevated temperature inside the liver is shown in red. The lesion caused by the thermal energy is also shown after the necrotic tissue, which is white surrounding by red liver tissue. The ultrasound waves are produced by a HIFU transducer. In order to shape the beam, the transducer can have a lens, or can be made as a shaped crystal, a phased-array, or a combination of the previous. The extracorporeal spherical bowl transducer is shown on Fig. 1.8. As previously described, the HIFU transducer only ablates the tissue in the focal spot, while it leaves undamaged the surrounding tissue and the tissue though which the ultrasound waves are propagating.

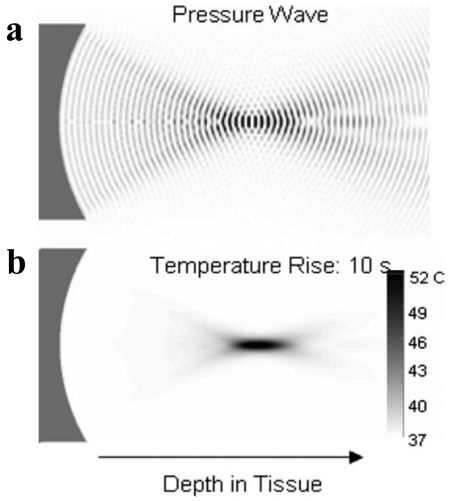

Figure 1.7 (a) Propagation of pressure waves though a tissue. Computer simulation with the frequency of the waves = 1 MHz, **(b)** The induced temperature elevation in the tissue, caused by the constructive interference of the pressure waves. (Source [36])

Fig. 1.8 Schematic representation of the ablation in the liver with the HIFU system. Standard shape of the focal point is presented, with the corresponding post-treatment necrotic tissue (white tissue around the red liver tissue).

1.6.3 MR Thermometry

Different intrinsic MR parameters are used to measure temperature: the T_1 and T_2 relaxation times, the diffusion coefficient, magnetization transfer and the proton resonance frequency [30]. Besides these parameter-based temperature methods, temperature-dependent contrast agents have been developed [30]. A relative change in temperature with respect to a baseline is commonly measured, although there exists an absolute temperature measurement by temperature-dependent contrast agents. The most commonly used method for temperature mapping in interventional MRI, especially in thermal treatment methods like high-intensity focused ultrasound, is based on the proton resonance frequency shift. A brief summary of this method is given in the following section.

The resonance frequency of a nucleus in a molecule can be written as:

$$\omega = \gamma B_{loc} = \gamma B_0 (1 - s), \tag{1.1}$$

where s is a shielding or screening coefficient, B_{loc} is the local magnetic field. It is linearly dependent with temperature in the temperature range, usually found in thermal ablations, and it can be written as:

$$s(T) = s_0 + s_T(T) = s_0 + \alpha T. \tag{1.2}$$

The shielding coefficient varies linearly for pure water molecules (H_2O) within the range of temperatures, which are of interest for interventional MRI procedures (-15 ºC to 100 ºC). The values are about -1.03 ± 0.02 * 10^{-8} /ºC. However, the lipid resonance frequency is almost temperature-independent, and completely determined by susceptibility effects.

Gradient-recalled echo pulse sequence [41] can be used to acquire temperature maps by encoding the temperature-dependent change in the phase change. An image is acquired before the temperature elevation in order to have a baseline and to eliminate the contributions from temperature-independent sources. The phase difference provides the relative change in temperature and can be written as:

$$\Delta T = \frac{\phi(T) - \phi(T_0)}{\gamma \alpha B_0 TE}, \tag{1.3}$$

where $\phi(T)$ is the phase of the acquired image (during heating), $\phi(T_0)$ is the baseline phase (acquired before heating), γ is the gyromagnetic ratio, α is the PRF shift coefficient, B_0 is the main magnetic field strength, and TE is the echo time.

Signal-to-noise ratio (SNR) of the temperature-dependent phase difference of a GRE pulse sequence can be estimated to be:

$$SNR_{\Delta\phi} \propto TE e^{-\frac{TE}{T_2^*}}. \tag{1.4}$$

By finding the maximum of $SNR_{\Delta\phi}$, the optimal echo time of $TE = T_2^*$ can be estimated [42].

Temperature sensitivity is tissue-independent, except for adipose tissue, and the PRF coefficient was measured to be around -0.009 and -0.01 ppm/°C [43]. The temperature dependence in adipose tissues is completely determined by susceptibility effects, since the temperature sensitivity is some orders of magnitude smaller than in aqueous tissues [44]. To overcome this issue of non-temperature dependency of PRF in adipose tissue, lipid suppression [45] or water-selective excitation is used. A hybrid (PRF)/T_1 approach was developed to accurately monitor temperature both in aqueous and adipose tissues based on PRF shift and T_1 change, respectively [46].

Proving precise temperature maps with high temporal and spatial resolution is the ideal goal of MR thermometry in guidance of thermal therapies. Depending on whether hyperthermia or thermal ablation regime is used, different temporal resolution is required. Fast temperature mapping can be achieved with gradient-recalled echo (GRE) echo-planar imaging (EPI) or segmented EPI acquisitions [47, 48]. Parallel imaging can be used in order to increase temporal resolution to reduce the artifacts caused by organ displacement [49].

Motion represents the major challenge in temperature mapping using proton resonance frequency. The artifacts produced by motion can be classified into two categories with respect to relation between the relative organ displacement frequency and the duration to acquire an MR image. Intrascan motion refers to motion that occurs during the acquisition an MR image, and it affects the image quality with typical blurring and ghosting artifacts. The usual solution to avoid this artifacts is to speed up the acquisition and consider the trade-offs between SNR (temperature uncertainty) and acquisition time. Interscan motion occurs between the two consecutive acquisitions and its effect on the images is the misregistration of them. To calculate temperature, baselines which are acquired before heating, are subtracted from the acquired images. This would be problematic in case interscan motion occurs, unless the acquired images are registered prior subtraction.

Different strategies were used to overcome the negative effects of motion on MR thermometry. Some of them are specifically designed for periodic motion, while the others are more general. As for the case of cardiac imaging, gating approach can be also applied to MR thermometry in the abdominal region. The gating was successfully applied in general anesthesia, in which case a periodic breathing pattern is established by mechanical respiration [50, 51]. In the case of free-breathing, the gating approach can fail due to the drifting organ motion during the procedure [52], or the irregularities in breathing make it hard to determine the gating window [53]. Navigator echoes were used for motion tracking and movement registration in ex vivo study [54]. A more advanced method that used triggering, navigator echoes for diaphragm tracking and acquisition of multiple baselines before temperature elevation was described in [55]. Matching baseline images according to non-similarity coefficients [56] or inter-correlation coefficients [57] has also been developed.

Reference-less or self-referenced temperature mapping is a method for which baselines acquired before heating are not needed. The background phase inside

the region of elevated temperature can be estimated based on the phase of the surround area by fitting a polynomial function to the unwrapped background phase [58] or a complex valued polynomial [59]. A reference-less method based on the theoretical framework of harmonic functions was suggested in [60], which enabled higher temporal resolution, eliminated the need for respiratory triggers, and was insensitive to jerky tissue motion.

1.6.4 HIFU Treatment of Abdominal Organs

The ultrasound-based therapy is already clinically applied for the treatment of uterine fibroids in the USA and for the treatment of prostate cancer in the European Union [29]. There are significant amount of studies currently under way for the treatment of different types of cancer. However, the application of the HIFU for the treatment of the liver and the kidney is still relatively underdeveloped.

Liver metastases and increases in hepatocellular carcinomas, which are related to a higher number of hepatitis c infections, pose a significant problem as the current treatments of the liver are associated with high levels of toxicity due to chemotherapy. A noninvasive approach is highly desirable. Thermal ablations in the liver have been tested and proofed to be effective [61-63], however, radiofrequency, microwave, laser ablation and cryotherapy have been utilized. Investigations to use HIFU to noninvasively target liver abnormalities was performed in China and UK with some promising results [64-65].

The major obstacles in the clinical implementation of HIFU-based liver treatments is respiratory organ motion and the ribs cage reducing the acoustic window. The previous attempts were focused on treating the lower liver lesions that peak out from below the ribs. The phase subtraction MR thermometry required the motionless organ, which was only possible to achieve with general anesthesia and without respiratory motion during sonication.

Renal carcinomas are slowly growing and relatively asymptomatic. Many patients seek minimally invasive options with thermal therapies, rather than aggressive surgical procedures. US-guided HIFU of the kidney was tried in the past [23]. The same problems are encountered in the HIFU treatments of the kidney which are come across in the liver therapeutic ultrasound ablations. However, the perfusion in the kidney makes it even more challenging to have the focal spot right on the targeted area in order to reach the high enough temperatures despite the additional cooling.

1.7 Aim of the Thesis

Interventional MRI is the field of applied radiology in which complicated interventional procedures and surgeries are performed under the guidance of MRI. HIFU is a relatively novel noninvasive treatment approach that is currently gaining significant interest of the medical community.

Respiratory organ motion is a complicating factor in various interventional MRI procedures and surgeries, and thus needs to be address in order to have better precision and more favorable outcomes of treatments. Performing HIFU ablation in free-breathing not only saves time and workflow, but is also necessary in certain regions with high perfusion or due to patient noncooperation.

Effort has been made to try to deal with respiratory organ motion in a most noninvasive manner, i.e. without employing any of the standard approaches like gating and trigging that are well-known in cardiac imaging. Two real-time methods have been outlined: in a first only MR-based motion tracking has been used implemented with a standard pencil-beam navigator, and a second hybrid US-MR guided HIFU in which an attempt was made to get the advantages of both imaging modalities with respect to their guiding capabilities.

Four-dimensional imaging for the purpose of organ motion modeling and prediction of its motion is an import part of interventional MRI when guiding surgical devices in the abdominal region during free-breathing. The previously suggested acquisition scheme of an interleaved image and navigator acquisition was modified to eliminate the delay between the two acquisitions, which reduces the required duration to acquire the dataset, before the interventional MRI procedure and improves the precision in the images as well.

Respiratory organ motion tracking is required for certain interventions, such as free-breathing HIFU ablation of the liver, or RF ablation of the cardiac muscle. By tracking the surrounding fatty tissue, an indirect measure of the organ motion can be obtained which in turn does save the regular imaging of saturation artifacts. A novel navigator approach was developed which is spectrally selective, meaning only excites fatty tissue, while sparing the imaging pulse sequence of signal voids.

All the presented material in this thesis is related to interventional MRI, more specifically to the application of HIFU to the abdominal region, and is readily applicable in the clinical practice.

1.8 Outline of the Thesis

In order to present the material as clearly as possible, the thesis is divided into six chapters, each presenting distinct material. Chapters two to five present different approaches taken in interventional MRI to combat the respiratory organ motion. The final chapter number six provides the summary and the speculation about the future prospects of the application of the acoustic-based treatments in the field of medicine and possible future techniques to deal with respiratory organ motion in interventional MR imaging.

Chapter two presents the treatment method in free-breathing with high-intensity focused ultrasound for therapy of the liver and the kidney, i.e. the organs in the abdominal region. Prospective motion compensation of the MR thermometry, acquired with gradient-recalled echo echo-planar imaging pulse sequence, was used to improve the accuracy of thermal doses. Ex vivo and in vivo experiments were performed, for which sheep and porcine livers were used. In order to protect the ribs against the collateral ablations, a special protection strips were placed in the acoustic propagation lines in front of the ribs. The pretreatment organ motion

modeling and MR thermometry baseline acquisitions were not compulsory before the treatment could start.

In chapter three, a novel acquisition method for four-dimensional (three dimensional + time) organ motion imaging is elaborated. Respiratory organ modeling is an important part of interventional MRI, and thus novel imaging approaches are needed to deal with respiratory organ motion, as the acquisition of time-resolved volumetric images with high spatial and temporal resolution is not possible with the current technology. The volumes are retrospectively stacked based on a method in which interleaved acquisition of image and navigator slices is used to infer a respiratory phase. The acquisition of the image and navigator slices was made simultaneous by the application of a CAIPIRINHA method. As the delay between the acquisition of slices is removed, this results in a more accurate organ motion models, while the signal-to-noise ratio is increased.

A spectrally selective navigator based on a cross-paired navigator is discussed in chapter four. Organ motion tracking is often needed in interventional MRI during surgeries and other medical interventions for which the information about the current position of the organ is crucial for the outcome. MR-based navigators are normally used for this application, however, they produce saturation artifacts, which could be resolved by tracking the surrounding adipose tissue instead, which resonant frequency is shifted. A cross-paired navigator was made spectrally selective. The results of tracking the respiratory organ motion of the liver and using this signal for gating gradient-recalled echo pulse sequence to acquire volumetric images of the liver are presented in this chapter. It is shown that the tracking signal is stable and accurate, without saturation artifacts.

In chapter five, a novel hybrid US-MR guided HIFU treatment is described with a complete three-dimensional organ motion compensation of the focal point steering and MR thermometry. US-based organ motion tracking was used in order to compensate for in-plane organ motion, while the MR-based pencil-beam navigator is used to track the out-of-plane motion, and thus full three-dimensional information about the target motion is attained. This chapter describes the ex vivo feasibility study, which demonstrates the improvements over the standard approach by having higher signal-to-noise ratio, less geometric distortion, and lock-on target motion of the focal spot in all three-dimensions.

Finally in chapter six, a brief summary of the thesis is added. Future applications of the HIFU are envisioned, as well possible novel four-dimensional acquisition strategies, as well spectral organ motion tracking. These were presented in the future outlook.

References

[1] M. A. Bernstein, K. F. King, and X. J. Zhou, "Handbook of MRI pulse sequences," *Academic Press*, 2004.

[2] http://www.biopac.com/Respiration-Transducer-MRI.

[3] M. Aksoy, C. Forman, M. Straka, S. Skare, S. Holdsworth, J. Hornegger, and R. Bammer, "Real-time optical motion correction for diffusion tensor imaging," *Magn Reson Med*, vol. 66, pp. 366-378, 2011.

[4] M. Zaitsev, C. Dold, G. Sakas, J. Hennig, O. Speck, "Magnetic resonance imaging of freely moving objects: prospective real-time motion correction using an external optical motion tracking system," *Neuroimaging*, vol. 31, pp. 1038-1050, 2006.

[5] V. Auboiroux, L. Petrusca, M. Viallon, A. Muller, S. Terraz, R. Breguet, X. Montet, C. D. Becker, and R. Salomir, "Respiratory-gated MRgHIFU in upper abdomen using an MR-compatible in-bore digital camera," *BioMed Research International*, vol. 2014, doi:10.1155/2014/421726.

[6] R. L. Ehman, and J. P. Felmlee, "Adaptive technique for high-definition MR imaging of moving structures," *Radiology*, vol. 173, pp. 255-263, 1989.

[7] P. G. Danias, M. V. McConnell, V. C. Khasgiwala, M. L. Chuang, R. R. Edelman, and W. J. Manning, "Prospective navigator correction of image position for coronary MR angiography," *Radiology*, vol. 203, pp. 733-736, 1997.

[8] D. A. Feinberg, J. C. Hoenninger, L. E. Crooks, L. Kaufman, J. C. Watts, and M. Arakawa, "Inner volume MR imaging: technical concepts and their application," *Radiology*, vol. 156, pp. 743-747, 1985.

[9] T. D. Nguyen, A. Nuval, S. Mulukutla, and Y. Wang, "Direct monitoring of coronary artery motion with cardiac fat navigator echoes," *Magn Reson Med*, vol. 50, pp. 235-241, 2003.

[10] M. O. Köhler MO, D. B. de Senneville, B. Quesson, C. T. Moonen, and M. Ries, "Spectrally selective pencil-beam navigator for motion compensation of MR-guided high-intensity focused ultrasound therapy of abdominal organs," *Magn Reson Med*, vol. 66, pp. 102-111, 2011.

[11] P. J. Hore, "A new method for water suppression in the proton NMR spectra of aqueous solutions," *J Magn Reson*, vol. 54, pp. 539-542, 1983.

[12] R. L. Ehman, M. T. McNamara, M. Pallack, H. Hricak, and C. B. Higgins, "Magnetic resonance imaging with respiratory gating: techniques and advantages," *AJR Am J Roentgenol*, vol. 143, pp. 1175-1182, 1984.

[13] G. Remmert, J. Biederer, F. Lohberger, M. Fabel, and G. H. Hartmann, "Four-dimensional magnetic resonance imaging for the determination of

tumour movement and its evaluation using a dynamic porcine lung phantom," *Phys Med Biol*, vol. 52, pp. N401-N415, 2007.

[14] J. Tokuda, S. Morikawa, H. A. Haque, T. Tsukamoto, K. Matsumiya, H. Liao, K. Masamune, and T. Dohi, "Adaptive 4D MR imaging using navigator-based respiratory signal for MRI-guided therapy," *Magn Reson Med*, vol. 59, pp. 1051-1061, 2008.

[15] C. Buerger, R. E. Clough, A. P. King, T. Schaeffter, and C. Prieto, "Nonrigid motion modeling of the liver from 3-D undersampled self-gated golden-radial phase encoded MRI," *IEEE Trans Med Imaging*, vol. 31, pp. 805-815, 2012.

[16] M. von Siebenthal, G. Szekely, U. Gamper, P. Boesiger, A. Lomax, and P. Cattin, "4D MR imaging of respiratory organ motion and its variability," Phys Med Biol, vol. 52, pp. 1547-1564, 2007.

[17] M. von Siebenthal, "Analysis and modeling of respiratory liver motion using 4DMRI," *PhD Thesis, ETH Zürich*, No. 17613.

[18] J. G. Lynn, R. L. Zwemer, A. J. Chick, and A. E. Miller, "A new for the generation and use of focused ultrasound in experimental biology," *J Gen Physiol*, vol. 26, pp. 179-193, 1942.

[19] D. J. Coleman, F. L. Lizzi, J. Driller, A. L. Rosado, S. E. Burgess, J. H. Torpey, M. E. Smith, R. H. Silverman, M. E. Yablonski, S. Chang, "Therapeutic ultrasound in the treatment of glaucoma. II. Clinical applications," *Ophthalmology*, vol. 92, pp. 347-353, 1985.

[20] R. Bihrle, R. S. Foster, N. T. Sanghvi, F. J. Fry, and J. P. Donohue, "High-intensity focused ultrasound in the treatment of prostatic tissue," *Urology*, vol. 43, pp. 21-26, 1994.

[21] J. Y. Chapelon, M. Ribault, F. Vernier, R. Souchon, and A. Gelet, "Treatment of localised prostate cancer with transrectal high intensity focused ultrasound," *Eur J Ultrasound*, vol. 9, pp. 31-38, 1999.

[22] G. Vallancien, M. Harouni, and B. Veillon, "Focused extracorporeal pyrotherapy: feasibility study in man," *J Endourol*, vol. 6, pp. 173-180, 1992.

[23] K. U. Köhrmann, M. S. Michel, J. Gaa, E. Marlinghaus, and P. Alken, "High intensity focused ultrasound as noninvasive therapy for multilocal renal cell carcinoma: case study and review of the literature," *J Urol*, vol. 167, pp. 2397-2403, 2002.

[24] F. Wu, Z. B. Wang, W. Z. Chen, H. Zhu, J. Bai, J. Z. Zou, K. Q. Li, C. B. Jin, F. L. Xie, and H. B. Su, "Extracorporeal high intensity focused ultrasound ablation in the treatment of patients with large hepatocellular carcinoma," *Ann Surg Oncol*, vol. 11, pp. 1061-1069, 2004.

[25] J. E. Kennedy, F. Wu, G. R. ter Haar, F. V. Gleeson, R. R. Phillips, M. R. Middleton, and D. Cranston, "High-intensity focused ultrasound for the treatment of liver tumours," *Ultrasonics*, vol. 42, pp. 931-935, 2004.

[26] F. Wu, Z. B. Wang, H. Zhu, W. Z. Chen, et al., "Extracorporeal high intensity focused ultrasound treatment for patients with breast cancer" *Breast Cancer Res Treat*, vol. 92, pp. 51-60, 2005.

[27] F. Wu, W. Z. Chen, J. Bai, J. Z. Zou JZ, et al., "Pathological changes in human malignant carcinoma treated with high-intensity focused ultrasound," Ultrasound Med Biol, vol. 27, pp. 1099-1106, 2001.

[28] F. Wu, "Extracorporeal high intensity focused ultrasound in the treatment of patients with solid malignancy" *Minim Invasive Ther Allied Technol*, vol. 15, pp. 26-35, 2006.

[29] F. A. Jolesz, and K. H. Hynynen, "MRI-guided focused ultrasound surgery" *Informa Healthcare*; 2008.

[30] V. Rieke, K. B. Pauly, "MR thermometry," *J Magn Reson Imaging*, vol. 27, pp. 376-390, 2008.

[31] A. Konski, "High-intensity focused ultrasound in the treatment of bone tumors: another treatment option for palliation and primary treatment?," *Cancer*, vol. 116, pp. 3754-3755, 2010.

[32] M. D. Bednarski, J. W. Lee, M. R. Callstrom, and K. C. Li, "In vivo target-specific delivery of macromolecular agents with MR-guided focused ultrasound," *Radiology*, vol. 204, pp. 263-268, 1997.

[33] K. Hynynen, N. McDannold, N. Vykhodtseva, and F. A. Jolesz, "Noninvasive MR imaging-guided focal opening of the blood-brain barrier in rabbits," *Radiology*, vol. 220, pp. 640-646, 2001.

[34] M. D. Bednarski, J. W. Lee, E. L. Yuh, and K. C. P. Li, "In vivo target-specific delivery of genetic materials with MR-guided focused ultrasound," *Ultrasonics*, vol. 30, pp. 325-330, 1998.

[35] C. E. Silcox, R. C. Smith, R. King, N. McDannold, P. Bromley, K. Walsh, and K. Hynynen, "MRI-guided ultrasonic heating allows spatial control of exogenous luciferase in canine prostate," *Ultrasound Med Biol*, vol. 31, pp. 965-970, 2005.

[36] K. Hynynen, "MRIgHIFU: a tool for image-guided therapeutics," *J Magn Reson Imaging*, vol. 34, pp. 482-493, 2011.

[37] M. W. Dewhirst, B. L. Viglianti, M. Lora-Michiels, M. Hanson, and P. J. Hoopes, "Basic principles of thermal dosimetry and thermal thresholds for tissue damage from hyperthermia," *Int J Hyperthermia*, vol. 19, pp. 267-294, 2003.

[38] S. A. Sapareto, and W. C. Dewey, "Thermal dose determination in cancer therapy," *Int J Radiat Oncol Biol Phys*, vol. 10, pp. 787-800, 1984.

[39] L. A. Crum, R. A. Roy, M. A. Dinno, et al., "Acoustic cavitation produced by microsecond pulses of ultrasound: a discussion of some selected results," *J Acoust Soc Am*, vol. 91, pp. 1113-1119, 1992.

[40] J. Wu, and W. L. Nyborg, "Ultrasound, cavitation bubbles and their interaction with cells," *Adv Drug Deliv Rev*, vol. 60, pp. 1103-1116, 2008.

[41] Y. Shihara, A. Calderon, H. Watanabe, K. Okamoto, Y. Suzuki, K. Kuroda, and Y. Suzuki, "A precise and fast temperature mapping using water proton chemical shift," *Magn Reson Med*, vol. 34, pp. 814-823, 1995.

[42] K. Kuroda, R. V. Mulkern, K. Oshio, L. P. Panych, T. Nakai, T. Moriya, S. Okuda, K. Hynynen, and F. A. Jolesz, "Temperature mapping using the water proton chemical shift: self-referenced method with echo-planar spectroscopic imaging," *Magn Reson Med*, vol. 43, pp. 220-225, 2000.

[43] N. McDannold, "Quantitative MRI-based temperature mapping based on the proton resonant frequency shift: a review of validation studies," *Int J Hyperthermia*, vol. 21, pp. 533-546, 2005.

[44] K. Kuroda, K. Oshio, R. V. Mulkern, and F. A. Jolesz, "Optimization of chemical shift selective suppression of fat," *Magn Reson Med*, vol. 40, pp. 505-510, 1998.

[45] J. A. de Zwart, F. C. Vimeux, C. Delalande, P. Canioni, and C. T. Moonen, "Fast lipid-suppressed MR temperature mapping with echo-shifted gradient-echo imaging and spectral-spatial excitation," *Magn Reson Med*, vol. 42, pp. 53-59, 1999.

[46] N. Todd, M. Diakite, A. Payne, and D. L. Parker, "Hybrid proton resonance frequency/T1 technique for simultaneous temperature monitoring in adipose and aqueous tissues," *Magn Reson Med*, vol. 69, pp. 62-70, 2013.

[47] C. Weidensteiner, B. Quesson, B. Caire-Gana, N. Kerioui, A. Ruillier, H. Trillaud, and C. T. Moonen, "Real-time MR temperature mapping of rabbit liver in vivo during thermal ablation," *Magn Reson Med*, vol. 50, pp. 322-330, 2003.

[48] R. J. Stafford, R. E. Price, C. J. Diederich, M. Kangasniemi, L. E. Olsson, and J. D. Hazle, "Interleaved echo-planar imaging for fast multiplanar magnetic resonance temperature imaging of ultrasound thermal ablation therapy," *J Magn Reson Imaging*, vol. 20, pp. 706-714, 2004.

[49] K. P. Pruessmann, M. Weiger, M. B. Schneidegger, and P. Boesiger, "SENSE: Sensitivity encoding for fast MRI," *Magn Reson Med*, vol. 42, pp. 952-962, 1999.

[50] S. Morikawa, T. Inubushi, Y. Kurumi, et al., "Feasibility of respiratory triggering for MR-guided microwave ablation of liver tumors under general anesthesia," *Cardiovasc Intervent Radiol*, vol. 27, pp. 370-373, 2004.

[51] M. Lepetit-Coiffe, B. Quesson, O. Seror, et al., "Real-time monitoring of radiofrequency ablation of rabbit liver by respiratory-gated quantitative temperature MRI," *J Magn Reson Imaging*, vol. 24, pp. 152-159, 2006.

[52] F. Preiswerk, P. Arnold, B. Fasel, P. C. Cattin, "Towards more precise, minimally-invasive tumour treatment under free breathing," *Conf Proc IEEE Eng Med Biol Soc*, vol. 2012, pp. 3748-3751, 2012.

[53] C. Weidensteiner, N. Kerioui, B. Quesson, B. D. de Senneville, H. Trillaud, and C. T. Moonen, "Stability of real-time MR temperature mapping in healthy and diseased human liver," *J Magn Reson Imaging*, vol. 19, pp. 438-446, 2004.

[54] J. A. de Zwart, F. C. Vimeux, J. Palussiere, et al., "On-line correction and visualization of motion during MRI-controlled hyperthermia," *Magn Reson Med*, vol. 45, pp. 128-137, 2001.

[55] K. K. Vigen, B. L. Daniel, J. M. Pauly, and K. Butts, "Triggered, navigated, multi-baseline method for proton resonance frequency temperature mapping with respiratory motion," *Magn Reson Med*, vol. 50, pp. 1003-1010, 2003.

[56] A. V. Shmatukha, P. R. Harvey, and C. J. Bakker, "Correction of proton resonance frequency shift temperature maps for magnetic field disturbances using fat signal," *J Magn Reson Imaging*, vol. 25, pp. 579-587, 2007.

[57] B. D. de Senneville, C. Mougenot, and C. T. Moonen, "Real-time adaptive methods for treatment of mobile organs by MRI-controlled high-intensity focused ultrasound," *Magn Reson Med*, vol. 57, pp. 319-330, 2007.

[58] V. Rieke, K. K. Vigen, G. Sommer, B. L. Daniel, J. M. Pauly, and K. Butts, "Referenceless PRF shift thermometry," *Magn Reson Med*, vol. 51, pp. 1223-1231, 2004.

[59] K. Kuroda, D. Kokuryo, E. Kumamoto, K. Suzuki, Y. Matsuoka, and B. Keserci, "Optimization of self-reference thermometry using complex field estimation," *Magn Reson Med*, vol. 56, pp. 835-843, 2006.

[60] R. Salomir, M. Viallon, A. Kickhefel, J. Roland, D. R. Morel, L. Petrusca, V. Auboiroux, T. Goget, S. Terraz, C. D. Becker, and P. Gross, "Reference-free PRFS MR-thermometry using near-harmonic 2-D reconstruction of the background phase," *IEEE Trans Med Imaging*, vol. 31, pp. 287-301, 2012.

[61] S. G. Silverman, K. Tuncali, P. R. Morrison, "MR Imaging-guided percutaneous tumor ablation," Acad Radiol, vol. 12, pp. 1100-1109, 2005.

[62] S. N. Goldberg, J. Bonn, G. Dodd, et al., "Society of Interventional Radiology Interventional Oncology Task Force: interventional oncology research vision statement and critical assessment of the state of research affairs," J Vasc Interv Radiol, vol. 16, pp. 1287-1294, 2005.

[63] S. N. Goldberg, "Science to practice: can we differentiate residual untreated tumor from tissue responses to heat following thermal tumor ablation?," Radiology, vol. 234, pp. 317-318, 2005.

[64] J. F. Aubry, K. B. Pauly, C. Moonen, et al., "The road to clinical use of high-intensity focused ultrasound for liver cancer: technical and clinical consensus," *J Therap Ultras* 2013, doi:10.1186/2050-5736-1-13.

[65] K. Fischer, W. Gedroyc, and F. A. Jolesz, "Focused ultrasound as a local therapy for liver cancer," *Cancer J*, vol. 16, pp. 118-124, 2010.

Chapter 2

Real-Time Method for Motion-Compensated MR Thermometry and MRgHIFU Treatment in Abdominal Organs

An adapted version of this chapter has been published as:
Z. Celicanin, V. Auboiroux, O. Bieri, L. Petrusca, F. Santini, M. Viallon, K. Scheffler, R. Salomir, "Real-Time Method for Motion-Compensated MR Thermometry and MRgHIFU Treatment in Abdominal Organs," *Magn Reson Med* 2013; doi 10.1002/mrm.25017.

2.1 Introduction

Magnetic resonance-guided high-intensity focused ultrasound (MRgHIFU) is considered a promising approach for non-invasive and spatio-temporal controlled tissue ablation [1, 2]. Its applicability to the clinical field has been demonstrated primarily in the treatment of uterine fibroids [3, 4], breast cancer [5] and prostate cancer [6], while ultrasound-triggered local drug delivery was under investigation in vivo [7]. Treatment of organs located in the upper abdomen could benefit from this technology, but significant improvement of the clinical treatment method is required. Respiratory and other physiological motion makes treatment difficult, since MR thermometry (MRT) is affected by organ motion, and it also requires continuous correction of the HIFU focal point position, while the rib cage reduces the available acoustic window hindering effectiveness of tissue ablation. Prevention of collateral heating and thermal coagulation of ribs and their surrounding tissue has to be considered in cases when upper abdominal organs are to be treated by HIFU. Rib sparing procedures have been reported in the past [8, 9], while in [10] a dedicated MR-guided positioning method of specific reflective strips for acoustic masking of the ribs has been suggested. Although respiratory gated treatment approaches have been reported [11, 12], sustained sonication is still preferred due to the high perfusion rates of organs such as liver and kidney, increased treatment duration for gated approach, and differing breath-hold positions of different gating windows.

The first report on irregular motion correction in MR-guided focused ultrasound thermotherapy [13] described the use of MR navigator echoes, in-plane registration of the images as post-processing, and redefinition of the reference phase map following the motion. The MRgHIFU treatment method, reported in [14], was based on fast MR thermometry and advanced image post-processing to extract organ motion displacement in real-time. Modeling of organ motion was performed during a so-called initial learning phase, while during the treatment, the motion field of the most similar image was used retrospectively to correct the focal point position. This method required the hypothesis of a periodical motion, since the focal point position was extrapolated for the next cycle. The delay of estimation was around 2 s, and thus not negligible, which imposed restriction of high periodicity of the motion pattern, and was incapable of handling non-rigid deformations caused by intestinal activity or muscle relaxation. In [15], the previous work was improved by reducing the delay with predictive filtering, while the out-of-plane motion was compensated by an one-dimensional (1D) pencil-beam navigator. In [16], an optimized principal component analysis (PCA)-based motion descriptor was used to characterize organ motion during treatment. During a so-called preparative learning step, the PCA was used to detect spatio-temporal coherences in the organ motion, which were later used during treatment for the adjustment of the beam position and the compensation of motion-related errors in thermal maps. In [17], a recent method was reported for focus steering dedicated to periodic motion, using a retrospective lookup table of images correlated to the breathing signal by assuming a regular pattern of respiratory motion. Although the previous work represents significant progress towards safe and successful MRgHIFU treatment of abdominal organs, there are still important issues to be

resolved. Neither of the previous solutions tried to use any prospective motion correction for improved MR thermometry accuracy, although it meant imaging with heavily T2* weighting and low signal-to-noise ratio (SNR). Methods for temperature mapping and/or motion compensation requiring acquisition of baselines during the preparative learning step are incapable of dealing with aperiodic motion and are prone to significant inaccuracy after short time (5-10 min) due to the drifting organ motion [18]. The necessity of periodically updating look up tables may yield workflow drawbacks.

Recently, hybrid ultrasound-MR guided HIFU sonication was reported in [19, 20], using an optical flow tracking in ultrasound images to obtain organ motion information. Although accurate performance of the method was demonstrated, additional instrumentation complicates the set-up.

Motion artifacts can be classified in two categories based on the time scale of motion with respect to the image acquisition time. Physical displacement of the spins of an imaging object during the MR image acquisition causes an intra-scan motion artifact, which manifests itself as blurring and ghosting, which can be surmounted by accelerating acquisition rate in a trade-off between acquisition time on one side, and SNR and temperature accuracy on the other. The inter-scan motion, the movement of organs during the period between the consecutive slice acquisition, does not affect image quality directly, but complicates the reconstruction of temperature map and thermal dose. Non-invasive temperature measurement based on temperature-sensitive MR proton resonance frequency (PRF) shift is currently the preferred method of choice due to its excellent linearity and near independence of tissue type [21].

Tissue motion is the most challenging problem of PRF shift-based MRT, and it hinders clinical applications of MRgHIFU that involve organ motion. A reference-less MRT method [22, 23] uses the phase information from outside the heated region to estimate the background phase inside the region of interest, unlike the standard baseline MRT method which is based on subtraction of temporal reference phase maps acquired before heating. The reference-less method is preferable in terms of robustness against tissue motion and magnetic perturbations, permitting also interactive repositioning of MR thermometry slices if required. The benefits of reference-less and multi-baseline temporal referenced methods can be obtained with a combined approach [24].

Respiratory induced patterns of organ motion in the abdomen were quantitatively and qualitatively examined by varies groups [25, 26]. Liver motion driven by the diaphragm is predominantly along the superior-inferior (S/I, equivalent cranial-caudal) direction and its largest extent appertains to regions below the diaphragm. An inter-subject modeling of liver deformation during quasi-periodic respiratory motion was reported in [26]. The principal component of liver motion is along SI direction, enabling a 1D navigator to track it.

Unlike the retrospective motion correction [27], the prospective motion correction [28] (PMC) is applied prior to the acquisition of a complete set of raw image data. The PMC can be implemented with MR navigator echoes [29] that are used for tracking organ motion during k-space acquisition, and based on this information subsequent correction of slice position and orientation in real-time is

applied by adjusting MR pulse sequence acquisition parameters, ensuring steady acquisition in the anatomy of interest.

Here, a novel MRgHIFU treatment method is presented, where tracking of the organ motion, carried out by MR navigator echo originally suggested in [29] and further refined in [30], provides real-time organ position information which is used for HIFU focal point position correction and PMC of MRT simultaneously. To the best of the authors' knowledge, this is the first attempt of using near real-time organ motion tracking for PMC of MR thermometry and simultaneous HIFU beam steering requiring neither preparative learning step nor any organ motion modeling, i.e. prediction of organ motion. The novel developments reported here, are parts of a long-term project, and the motion-compensation system was added on top of our previously described methodological functionalities.

2.2 Methods

2.2.1 MR Thermometry

All experiments were performed on a 3 T whole-body MRI clinical scanner (MAGNETOM Trio - A TIM System, Siemens Medical Solutions, Erlangen, Germany).

Real-time PRF shift-based MR thermometry based on RF-spoiled lipid-suppressed, using 1-2-1 binomial frequency-selective RF pulse, segmented gradient-recalled echo (GRE) echo-planar imaging (EPI), was modified to acquire a 1D MR navigator echo (pencil-beam navigator) before each segment of k-space (pulse sequence principle, navigator profiles and a navigator histogram are shown on Fig. 2.1). Flow compensation was available in the sequence (nulling the first moment of the gradient). MRT slice position was readjusted, facilitating motion correction on a segment-per-segment basis using the real-time feedback prospective motion correction (PACE) method, available on the clinical Siemens scanner, based on the tissue displacement information measured by the MR navigator echo. Note that the motion correction sampling time is equal to TR and thus much shorter than the temporal resolution of MR thermometry. This approach achieved the intra-scan motion correction. For future compatibility with more complex correction of the motion, the 1D navigator feedback data was converted into full 3D spatial coordinates of the scanner reference system, knowing the orientation vector of that user-defined navigator (e.g. parallel to the Oz-axis of the scanner). For the current implementation, the vector's coordinates perpendicular to the SI direction were zero-filled when sent to the HIFU beamformer. These spatial coordinates were fed in real-time to a HIFU system to adapt focal point position accordingly, as shown on Fig. 2.1a, which also provides detailed information on system architecture and latencies. The following acquisition parameters were used for MR thermometry: TE/TR = 8.69/80 ms, EPI factor = 9, slice thickness = 5 mm, in-plane resolution = 1.5 × 1.5 mm2 ex vivo and 1.88 x 1.88 mm2 in vivo, readout bandwidth 700 Hz/pixel, reconstructed image matrix = 128 × 128, acquisition time per slice = 1.04 s.

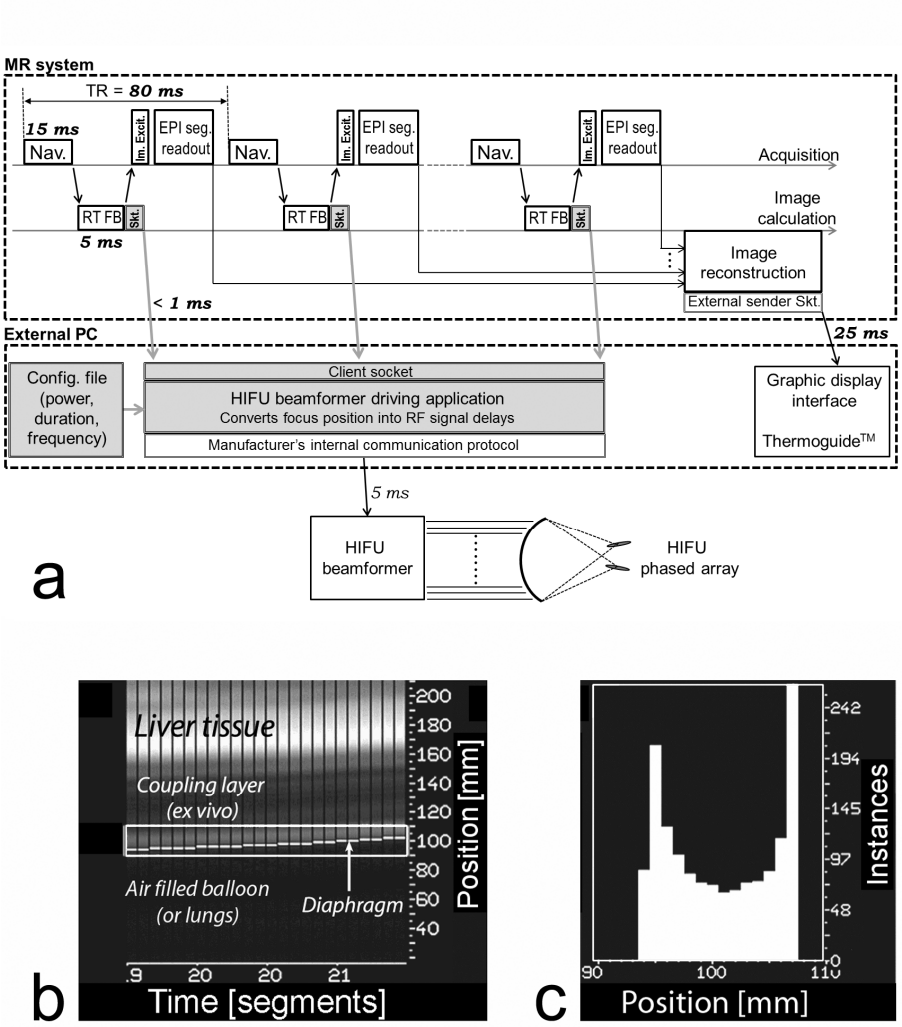

Figure 2.1 (a) Comprehensive system architecture diagram for the motion-compensated MRgHIFU treatment. Standard subsystems are shown as white background boxes, while custom built ones are represented with shaded background boxes. Time delays for data acquisition, calculation and transfer inside the system are indicated. Pulse sequence diagram of principle is shown inside the MR system providing details of real-time navigator feedback functionality, which communicates the tracking information for HIFU focal point position correction and PMC of MRT. (Abbreviations: RT FB – Real-time feedback; Skt. – Socket; Nav. – Navigator; Im. Excit. – Image Excitation). **(b)** Navigator profiles with real-time extraction of motion information. **(c)** Histogram of the tracked feature positions along the direction of the navigator.

The pencil-beam navigator was used for slice tracking of MR thermometry. It comprised of a 2D spatially-selective echo-planar RF pulse, used to excite a pencil-beam-shaped column, followed by a gradient echo. The acquisition duration of the pencil-beam navigator was approximately 20 ms, while the navigator volume was rectangular column with dimensions of (5 to 10) × (5 to

10) × 180 mm. Note that the TR parameter provided above, also includes the duration of the navigator. Exemplary navigator profiles and a histogram of motion tracking ex vivo are shown on Fig. 2.1b and 2.1c, respectively.

Magnitude and phase images were sent in real-time to an external computer and used for temperature visualization and control of the HIFU platform.

The temperature elevation profile was calculated on the external computer based on the reference-less method (for details, cf. Ref. [23]), which exploits mathematical properties of the magnetic field in a near-homogeneous medium and reconstructs the background phase inside the region of interest by solving a 2D Dirichlet problem based on iterative convolution. This calculation was performed with a typical ROI diameter of 20 to 25 pixels, requiring less than 50 ms of CPU time, making the temperature and thermal dose subsequently available in real-time. The calculation ROI was set larger in motion non-compensated sonications to encompass the elongated thermal build-up in the focal plane.

2.2.2 MR-guided HIFU Platform

The randomized 256-element phased-array transducer (Imasonic, Besançon, France) was used for the MRgHIFU experiment with the following characteristics: frequency range = 974 – 1049 kHz, natural focal length = 130 mm, aperture = 140 mm, diameter of each element = 6.6 mm. The HIFU transducer was driven by a 256-channel beam former (Image Guided Therapy, Pessac-Bordeaux, France). Electronic steering of the focal point was performed within -3 dB revolution ellipsoid of axes 30 mm (Ox), 30 mm (Oz), and 50 mm (Oy) around the natural focus. The maximum switching rate of the beam-former's RF signals to change the focal point position was 20 frames per second. Further details on this device can be found in [19].

In-house written software enabled treatment planning and on-line correction of the focal point position during the treatment in order to follow organ motion and avoid collateral damage of the surrounding healthy tissue, using a special TCP/IP socket which was independent of the socket dedicated to the transfer of reconstructed MR data to the external PC. The reconstructed magnitude and phase images were transferred by the standard Siemens mechanism, provided with its "Thermo" work-in-progress (WIP) package. A single Ethernet cable physically connected the local network of the MR system to the external PC (i.e. the two sockets used different ports). Original image calculation environment (ICE) program, used for the image reconstruction, was modified to facilitate the communication of MR navigator data between the MR system and a client application running on the external computer via the special TCP/IP socket. As soon the navigator data was available on the MR image calculation computer, the ICE program tried connecting to the external computer, and when that connection was established the navigator data was sent though. The navigator information was transferred to the external PC as absolute coordinates and the relative displacement was further calculated in the external PC application relative to the time point when the sonication started. The client application interpreted the

navigator information from the MR and updated on-the-fly the RF delays of the HIFU beam-former to change the focal point position accordingly.

2.2.3 Description of the Experiments

A dedicated experimental set-up was designed for ex vivo measurements (see Fig. 2.2). The equipment was placed on the MR bed with the main axis of simulated organ motion along the direction of the main magnetic field or along the z-axis. Ex vivo tissue was placed in water coupled bath, while the inflating balloon simulated a breathing-like motion pattern, mimicking diaphragm displacement. The balloon was filled and drained by a mechanical ventilator (Anesthesia Delivery Unit (ADU™) Plus Carestation® GE Healthcare, Madison, WI, USA). A sheep liver and a turkey pectoral muscle were alternately used in the experiments. Remote control of the organ motion amplitude and period was possible from the outside the scanner room. The typical period was set in the range of 6 to 10 s.

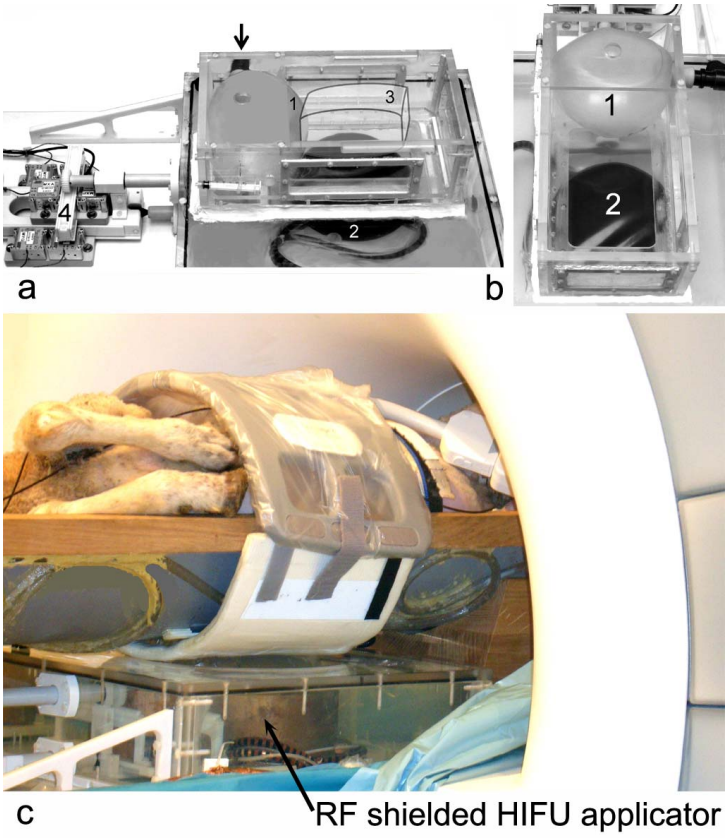

Figure 2.2 (a-b) Ex vivo experimental set-up: 1. Inflating balloon simulating breathing motion with diaphragm-like shape, 2. Water coupled bath, in which an ex vivo organ was placed, 3. Phantom, 4. Electrical motor used for positioning HIFU platform in two axis. **(c)** In vivo set-up. Note the HIFU applicator and the MR coil combination.

The simulated tissue motion pattern was non-rigid with compressional deformation similar to that found in natural breathing. The non-rigid spatio-temporal rearrangement of the susceptibility distribution during motion-caused magnetic field perturbation, requiring the reference-less PRF shift thermometry to filter out this effect.

The performance of the new motion tracking method was compared in this study with “ground truth” approach, namely, the well known respiratory gated sonication and MR thermometry. This comparison took advantage of the periodic motion patterns generated by the mechanical ventilator. A “start” trigger was sent to the MR system and to the HIFU beam former when the applied air over-pressure fell below 15% of the peak value, while a “stop” trigger was sent to the HIFU beam former when the over-pressure rose above 25% of the peak value.

A standard Siemens single loop receiver coil (11 cm diameter) was used for MR signal acquisition for ex vivo experiments, while for in vivo experiments, two phased-array coils wrapped around the animal were combined (see Fig. 2.2c). A standard 4-channel flex large coil (Siemens Medical Solutions, Erlangen, Germany) was placed on top of the abdomen, and a dedicated interventional 3-channel coil (Clinical MR Solutions, Brookfield, WI, USA) with 14 x 16 cm2 aperture, enabling HIFU beam propagation, was placed under the animal. The scanner built-in adaptive coil combine algorithm was used. The pencil-beam navigator tracked the diaphragm motion in the close proximity of the MRT slice.

Independent single-point sonications of the sheep liver in vivo were performed inter-costally in two animals (both female, mean weight= 25-35 kg). Ethical approval was granted by the Geneva University Institutional Animal Care and Use Committee and by the Cantonal Veterinary Authority of Geneva. The animals were intubated and mechanically ventilated. Anaesthesia was maintained by continuous inhalation of 2% isoflurane (Abbott AG, Baar, Switzerland). The breathing rate was approximately 7-10 breaths/min. The pencil beam navigator was placed parallel to the SI direction, crossing the right half of the diaphragm and avoiding the proximity of large blood vessels. A preliminary acquisition was performed to calibrate the tracking factor between the navigator measurements and the subsequent applied slice displacements. A tracking factor was considered appropriate if the anatomic structures around the planned position of the HIFU focus (mainly the blood vessels within the liver parenchyma) appeared as static in the motion-compensated GRE-EPI magnitude data. Typically, a range of tracking factors between 0.5 and 1 was tested with an incremental step of 0.05. Therefore, a maximum of 10 scout acquisitions were performed, requiring in total approximately 10 minutes. For the in vivo experiments, the navigator tracked organ motion over the right hemi-diaphragm, which caused that the targets more distal to that tracking position required varying correction factors. A rib protection method, described in [10], was used to protect against collateral thermal damage. The animals were awoken after the experiment and followed up for 7 days. Further details on the MRgHIFU protocol in the sheep liver in vivo can be found in [19].

2.3 Results

2.3.1 Ex vivo experiments

On Fig. 2.3, the need for a reference-less reconstruction method and the effectiveness of the HIFU focal point position correction for the ex vivo experiment is demonstrated. The amplitude of ex vivo muscle motion was 12 mm, while the period was 7.5 s. Every shown case on Fig. 2.3 was acquired with slice tracking of MR thermometry. The average SNR was approximately 35. The reference-less MR thermometry method delivered a baseline stability of 0.4 ±0.1 ºC.

Although the images were acquired with the motion-compensated segmented GRE-EPI sequence, inhomogeneous magnetic susceptibility field variations due to motion yielded large phase changes inside the breathing cycle (see Figs. 3a and 3b). This effect required the use of a motion-insensitive PRF shift thermometry method. The reference-less approach was chosen because of the advantageous workflow (no need to map the space of events before the treatment) and for future compatibility with free-breathing condition on patients. Repositioning of the Dirichlet's domain was not required with motion-compensated magnitude data as the tissue motion appeared motion-less.

Fig. 2.3c corresponds to continuous HIFU sonication with fixed focus position in a moving ex vivo turkey pectoral muscle (non motion-compensated sonication and motion-compensated MR thermometry acquisition), while for Fig. 2.3d the focal point position was steered in real time to lock on tissue motion. It can be observed from the figure that the in-plane thermal build-up in the left image is elongated, while the one on the right is sharply focused in one spot. The in-plane extension of the thermal build-up in the left image is around 12 mm, which corresponds well with the pre-set amplitude of motion. The maximum temperature achieved with the HIFU sonication (36 s, 108 ac W) was around 20ºC in the focal spot for the compensated approach, while only around 10ºC for the non-compensated. This corresponds to a ratio of 2 between the highest temperature elevations in tissue at equal HIFU energy for the compensated versus non compensated approach.

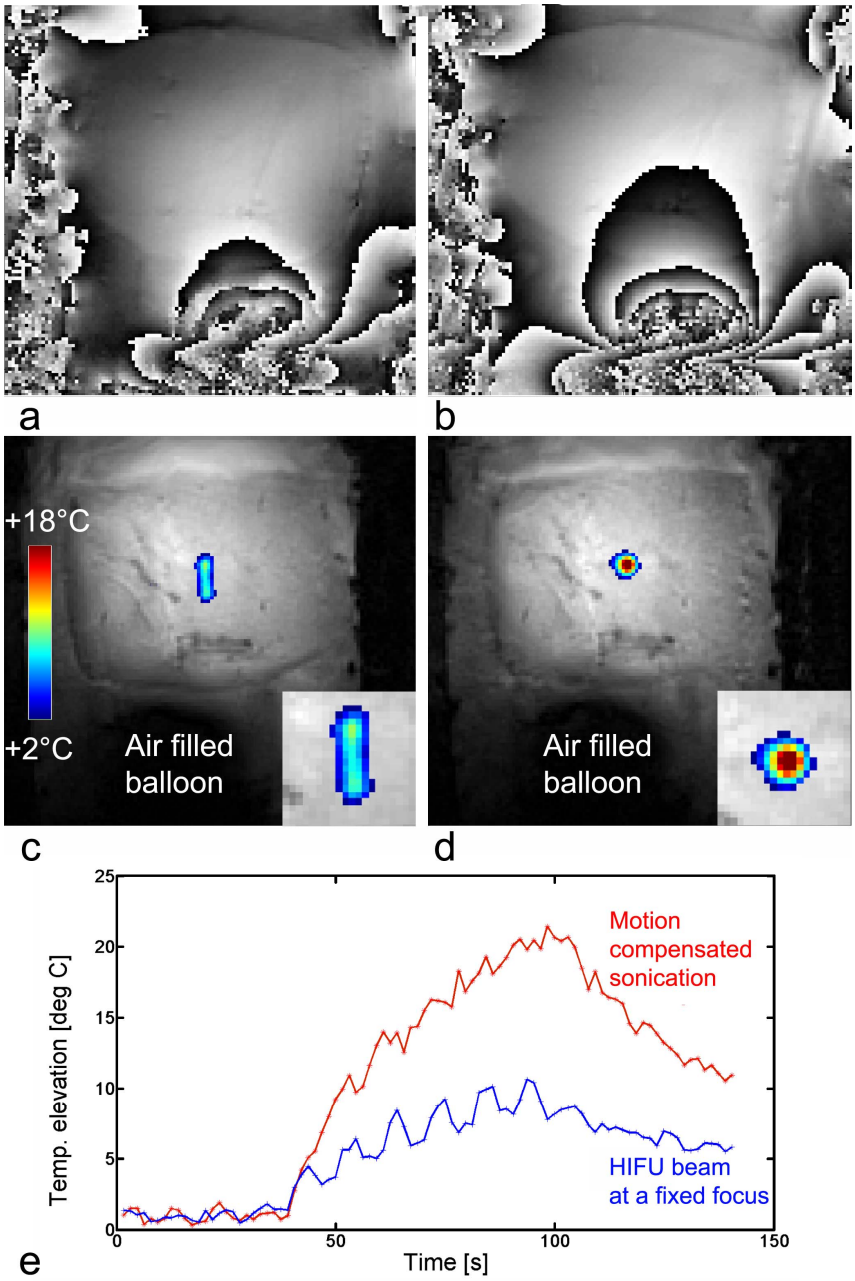

Figure 2.3 Baseline phase maps of motion-compensated MR thermometry, showing significant difference in the local magnetic field due to breathing motion. Phase maps are shown at the end of **(a)** inspiration **(b)** expiration. (c – d) Ex vivo exemplary slice tracking thermometry images showing significant difference in the thermal build-up when the HIFU focal point position was motion-compensated or not. Sonication end point thermal maps are shown: without focal point position correction **(c)** and with correction **(d)** (FOV = 192 mm). **(e)** Comparison of temporal curves of temperature elevation in the highest temperature voxel corresponding to the cases (c-d), respectively.

The comparative experiments conducted under various conditions: motion-compensated (new method) or non-compensated sonication in moving tissue (monitored with motion-compensated MR thermometry), respiratory gated sonication and MR thermometry (i.e. “ground truth” motion compensation) and, respectively, fixed focus sonication in static tissue (i.e. reference experiment) led to following observations based on 4 repeated experiments per method, see Fig. 2.4 for exemplary results on ex vivo liver: 1) fixed focus sonication in moving tissue yielded an elongated thermal build-up, approximating the histogram of mass-point positions during the motion cycle. Motion amplitude higher than 10 mm tended to split the lesion into two separate “satellites” corresponding to the inhalation and exhalation positions (see Fig. 2.4b); 2) the new method of motion tracking as well as the respiratory gating sonication yielded basically isotropic thermal build-up but the ablation efficiency was significantly higher for the active motion tracking, when the duty cycle was near 100%; 3) the reference sonication in static conditions confirmed the precise beam forming without inherent acoustic aberration. Note, a quantitative correlation ex vivo between cumulated thermal dose [31] (calculated here for a virtual baseline temperature of 37°C) and thermally decolored tissue is not meaningful as the two processes rely on different mechanisms. When considering the thermal patterns induced by the non-compensated sonication on Fig. 2.3b (turkey pectoral muscle) and Fig. 2.4b (sheep liver), differences could be observed, especially accentuated splitting hot spots in the second case, although the motion amplitude was comparable (12 mm and 14 mm, respectively). The different elasticity of various tissues probably yields slightly different patterns of motion during the breathing cycle, thus different histograms of mass-point position in the fixed focus reference frame and therefore different topology of the heating patterns.

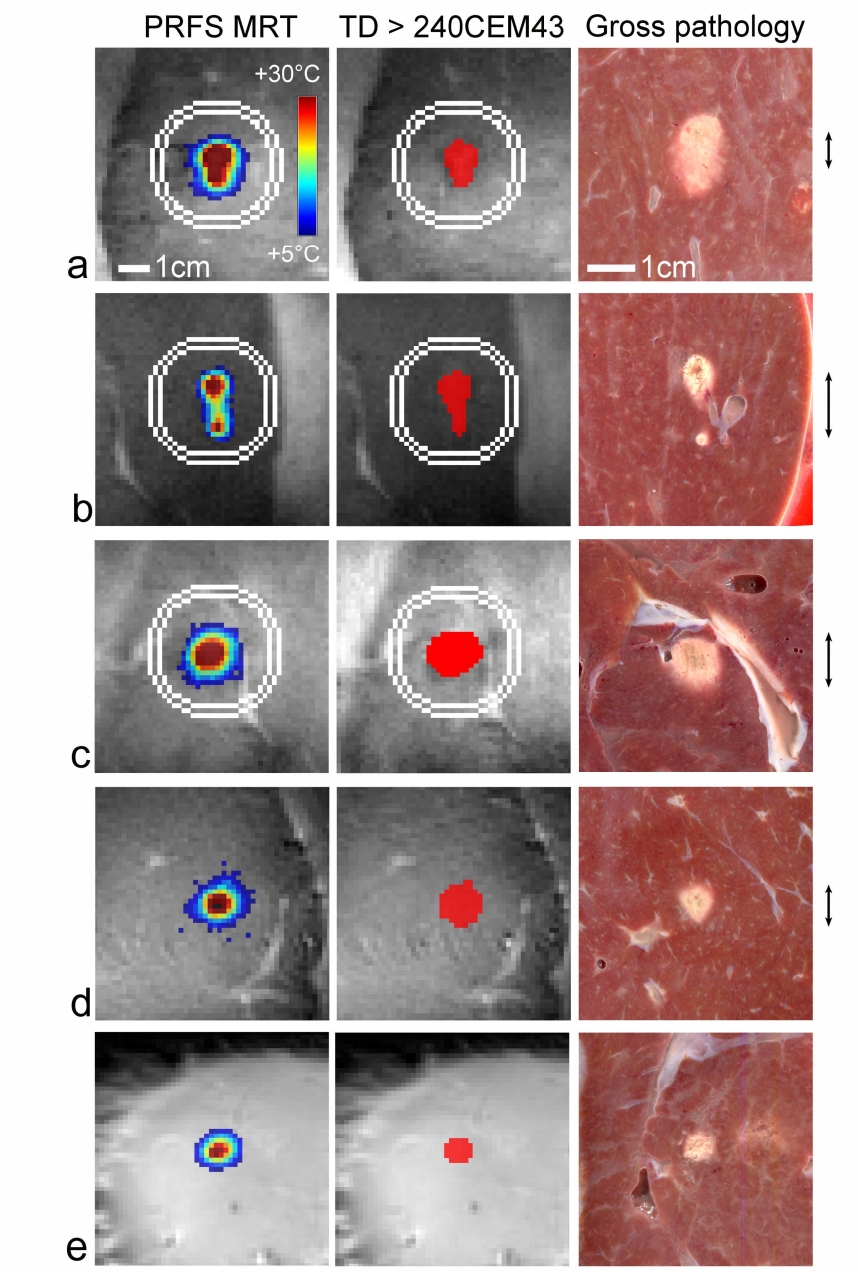

Figure 2.4 Pictorial comparison between ex vivo results of MRgHIFU sonication in moving tissue. The focal plane is shown each time. Left column: MR thermometry (relative values above the baseline, see color bar) at the end-point of sonication. Middle column: cumulated thermal dose exceeding the 240CEM43 threshold. Right column: gross pathology and the amplitude of motion (double head arrow). A distance scale is provided for each type of image. When the reference-less PRF shift calculation was used for MR thermometry, the double border of the Dirichlet's domain is indicated. The sonication parameters are provided in each case as (power [W], duration [s], duty cycle [%], motion amplitude [mm]). The following conditions apply: **(a)** Fixed focus sonication in moving tissue (192 W, 30 s, 100%, 8 mm). **(b)** Fixed focus sonication in moving tissue with larger displacement amplitude (192 W, 30 s, 100%, 14 mm). **(c)**

Motion-compensated sonication using the new method of tracking (192 W, 30 s, 100%, 14 mm). **(d)** Respiratory gated sonication synchronized to the quiet phase of exhalation (240 W, 60 s, 33%, 9 mm). **(e)** Static sample, fixed focus sonication, i.e. reference experiment (108 W, 40 s, 100%, 0 mm). In the last case, the applied energy was deliberately lower to avoid non-linear disruption (cavitation, boiling). Note the essentially isotropic spot of decoloration within the tissue for the three last rows.

The comparative experiments conducted under various conditions: motion-compensated (new method) or non-compensated sonication in moving tissue (monitored with motion-compensated MR thermometry), respiratory gated sonication and MR thermometry (i.e. “ground truth” motion compensation) and, respectively, fixed focus sonication in static tissue (i.e. reference experiment) led to following observations based on 4 repeated experiments per method, see Fig. 2.4 for exemplary results on ex vivo liver: 1) fixed focus sonication in moving tissue yielded an elongated thermal build-up, approximating the histogram of mass-point positions during the motion cycle. Motion amplitude higher than 10 mm tended to split the lesion into two separate “satellites” corresponding to the inhalation and exhalation positions (see Fig. 2.4b); 2) the new method of motion tracking as well as the respiratory gating sonication yielded basically isotropic thermal build-up but the ablation efficiency was significantly higher for the active motion tracking, when the duty cycle was near 100%; 3) the reference sonication in static conditions confirmed the precise beam forming without inherent acoustic aberration. Note, a quantitative correlation ex vivo between cumulated thermal dose [31] (calculated here for a virtual baseline temperature of 37°C) and thermally decolored tissue is not meaningful as the two processes rely on different mechanisms. When considering the thermal patterns induced by the non-compensated sonication on Fig. 2.3b (turkey pectoral muscle) and Fig. 2.4b (sheep liver), differences could be observed, especially accentuated splitting hot spots in the second case, although the motion amplitude was comparable (12 mm and 14 mm, respectively). The different elasticity of various tissues probably yields slightly different patterns of motion during the breathing cycle, thus different histograms of mass-point position in the fixed focus reference frame and therefore different topology of the heating patterns.

2.3.2 In vivo experiments

Both sheep studies yielded similar results. On Fig. 2.5, two images from one in vivo sheep liver sonication (40 s, 240 ac W) experiment are shown, acquired at the end of a) inspiration and b) expiration. The apparent motion of the ribs can be observed, although they were static, due to the use of PMC. The maximum temperature elevation was found to slightly exceed 10 ºC. It reached a steady state regime after approximately 30 s and longer treatment duration did not increase the temperature. The HIFU acoustic energy was delivered as a single spot. MRI follow up and animal necropsy indicated no burning of the tissue surrounding the

ribs or at other abdominal interfaces for the actual conditions of sonication (power, duration, F-number and dynamic steering range). SNR of the liver MR thermometry images ranged between 20 and 25. At the given TE and B0, this corresponds to approximately 0.5°C intrinsic standard deviation of MR thermometry [32]. This is considered sufficient to enable accurate monitoring of the HIFU sonication. The combination of a limited acoustic window of inter-costal sonication with conservative ribs' protection, liver perfusion and limited available acoustic power yielded insufficient temperature elevation to cause irreversible tissue damage.

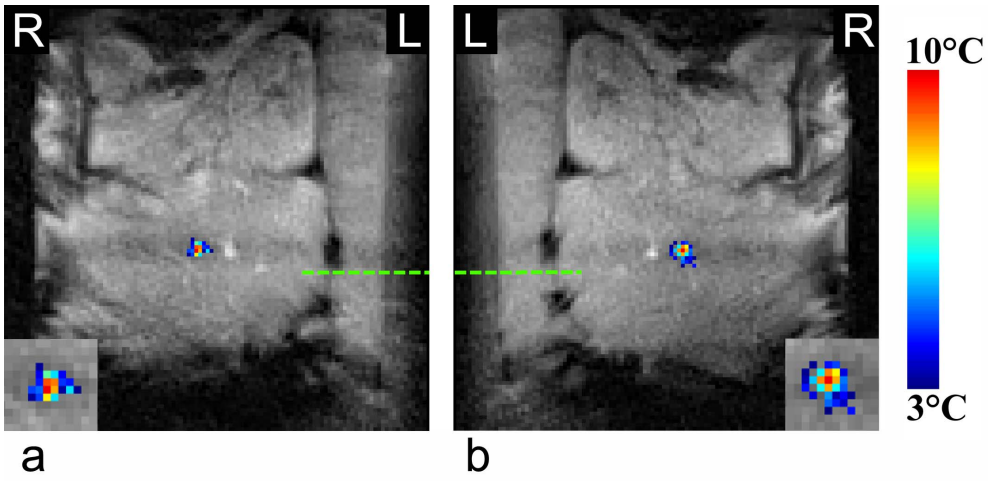

Figure 2.5 In vivo exemplary thermometry images of sheep liver during motion-compensated inter-costal HIFU ablation. Apparent motion of the ribs of approximately 6 mm amplitude can be observed due to the use of PMC, although the ribs were static in the laboratory frame. The thermometry images were acquired within the same breathing cycle at the end of **(a)** inspiration **(b)** expiration (FOV = 240 mm). Note frame (a) was deliberately flipped L/R to facilitate the visual comparison of apparent motion of static structures (e.g. ribs).

2.4 Discussion

Two fundamental issues of MRgHIFU treatment have been addressed in the presented work, namely the real-time control of acoustic energy targeting and motion correction of MR thermometry. The MR thermometry developments are not restricted to MRgHIFU, but are applicable to any other thermal therapy in abdomen (e.g. LITT or RFA).

Here, the monitoring of HIFU ablation was performed by PRF shift-based MR thermometry implemented by segmented GRE EPI pulse sequence. Segmented k-space acquisition was used in the phase-encode direction to minimize T2* apodization effects on the image. The position of the focal point as well as the position of imaging slice were updated according to the organ displacement measured by the segment-based MR navigator, and thus achieving intra- and

inter-scan MR motion compensation. The treatment method here described, does not rely on reconstructed magnitude nor phase MR images, and therefore potential latency from data reconstruction and export to the external computer is not involved in the feedback process. The temporal resolution of the motion correction was 80 ms, while the readout bandwidth per pixel was reduced by a factor larger than 2 as compared to the one suggested in [15]. Obtained SNR was larger than 20 in vivo for a voxel volume of 0.017 mL. Since the motion compensation was applied, the imaged object appeared motion-less in the image. This allowed easier implementation of reference-less thermometry, as it was not necessary to reposition the ROI due to motion.

As the pencil-beam navigator remains the most robust organ-motion tracking method currently available on clinical MR systems, it was used for slice tracking of MR thermometry to provide accurate compensation of tissue displacement along the SI direction (i.e. principal component of motion). The correction factor of motion between the tracked diaphragm position and the ROI for sonication in liver was manually adjusted on an individual basis, aiming to cancel the apparent motion in magnitude GRE-EPI data around the location of the HIFU focus. While this empirical methodology enabled the proof of concept in vivo, the adjustment of the correction factor may be done automatically, e.g. a closed loop algorithm iteratively changing the tracking factor until nulling the motion field vectors in the MR thermometry magnitude image.

By the means of the pencil-beam navigator, the focal point position could be updated at an effective frame rate of 1/TR, here 12.5 Hz. Steering the beam induced a decrease in focal point intensity, here -3dB at 15 mm lateral steering. This condition was due to the relatively narrow radiation diagram of each elementary source of the phased-array (circular piston with the ratio diameter/wavelength = 4.2). This effect lowered the effectively delivered average energy, especially for large motion amplitudes. Upon the hardware capability, the instantaneous power may be increased as a function of beam steering to compensate for the mentioned effect.

In vivo experiments have demonstrated the ability of MRgHIFU treatment of moving organs, with high spatial accuracy and a near 100% duty cycle. Neither predictive modeling of organ motion nor the requirement of mapping a motion atlas before the active phase of the treatment was required. The challenge of ablation through the rib cage was addressed by the use of protective reflective strips. The value of the correction factor was 0.7. Given the liver's anatomy of the treated animals, the focal point was positioned typically 2.5 to 3 cm behind the rib cage, yielding a significant angular masking effect of the acoustic window. By scaling the temperature elevation obtained in our experiments versus the applied power, we estimate at least twice higher acoustic output would have been necessary for effective tissue ablation in our study.

Previous studies on MRgHIFU treatment of abdominal organs [13-17] relied on heavily T2*-weighted MR images acquired with gradient-recalled echo (GRE) single-shot echo-planar imaging (ssEPI) sequence dedicated to MR thermometry, which is generally of low contrast and limited SNR, and thus sub-optimal for motion information extraction. Since MR thermometry data, besides aiming to provide temperature maps, were also used to track organ motion, the requirement

of high temporal resolution inflicted imaging with low SNR and high geometric distortion. The compulsory pretreatment data acquisition prior to thermal treatment renders the methods inapplicable to aperiodic free-breathing motion patterns with deep inspiration or expiration phases.

The ballistic accuracy of the MRgHIFU treatment performed in this work was not assessed. The anisotropy factor of the motion-compensated thermal build-up was found to be close to 1, and the shape of the decolorized coagulated tissue specimen in the post-operatory gross pathology ex vivo was found to be basically circular. However, positing of the focal point on a true target was not examined here. Moreover, the delivered energy was insufficient to induce in vivo thermal lesions in liver parenchyma. Although only 2 in vivo animal sonications were performed and evaluated here, our preliminary results show interesting potential of our robust treatment method, which could motivate further large scale studies to prepare clinical translation of the method.

The PRF shift reference-less approach is suitable in the presence of a large volume of unheated homogeneous tissue (e.g. liver), which provides spatial reference information. Its applicability may be challenging in a more complicated anatomic environment where susceptibility variation, adipose tissue or flow phenomena are present, e.g. prostate, breast, kidney. An extension to reference-less thermometry allowing background phase estimation in the presence of phase discontinuities between aqueous and fatty tissues was described in [24]. That method was based on a multi-echo sequence and binary water and fat maps generated using a Dixon reconstruction.

Another limitation of the implemented method was the lack of automatic feedback control of the temperature elevation, i.e. no objective function was defined for the time course of the focal point heating. The engineering architecture of our solution is readily compatible with integration of a spatial-temporal temperature controller that will be addressed in future studies.

Only the SI component of the motion was corrected for in this study. Although this is, in general, the main component of the abdominal motion, correcting for the complete 3D motion may be required in some specific situations where the spatial accuracy is critical.

2.5 Conclusion

This paper demonstrates motion compensation during MRgHIFU utilizing prospective motion corrected segmented EPI for thermal mapping and control of the HIFU focal spot. Accurate focal point lock-on target was achieved in ex vivo moving phantoms and sheep. The proposed MR thermometry motion compensation method produced accurate temperature maps with good SNR and low geometric distortion.

References

[1] H. E. Cline, J. F. Schenck, K. Hynynen, R. D. Watkins, S. P. Souza, and F. A. Jolesz, "MR-guided focused ultrasound surgery," *J Comput Assist Tomogr*, vol. 16, pp. 956-965, 1992.

[2] K. Hynynen, W. R. Freund, H. E. Cline, A. H. Chung, R. D. Watkins, J. P. Vetro, and F. A. Jolesz, "A clinical, noninvasive, MR imaging-monitored ultrasound surgery method," *Radiographics*, vol. 16, pp. 185-195, 1996.

[3] O. C. Smart, J. T. Hindley, L. Regan, and W. M. Gedroyc, "Magnetic resonance guided focused ultrasound surgery of uterine fibroids – the tissue effects of GnRH agonist pre-treatment," *Eur J Radiol*, vol. 59, pp. 163-167, 2006.

[4] C. M. Tempany, "From the RSNA refresher courses: Image-guided thermal therapy of uterine fibroids," *Radiographics*, vol. 27, pp. 1819-1826, 2007.

[5] A. C. Schmitz, M. A. van den Bosch, V. Rieke, F. M. Dirbas, K. Butts Pauly, W. P. Mali, and B. L. Daniel, "3.0-T MR-guided focused ultrasound for preoperative localization of nonpalpable breast lesions: an initial experimental ex vivo study," *J Magn Reson Imaging*, vol. 30, pp. 884-889, 2009.

[6] R. Chopra, A. Colquhoun, M. Burtnyk, W. A. N'djin, I. Kobelevskiy, A. Boyes, K. Siddiqui, H. Foster, L. Sugar, M. A. Haider, M. Bronskill, and L. Klotz, "MR imaging-controlled transurethral ultrasound therapy for conformal treatment of prostate tissue: initial feasibility in humans," *Radiology*, vol. 265, pp. 303-313, 2012.

[7] R. Staruch, R. Chopra, and K. Hynynen, "Localised drug release using MRI-controlled focused ultrasound hyperthermia," *Int J Hyperthermia*, vol. 27, pp. 156-171, 2011.

[8] J. Civale, R. Clarke, I. Rivens, and G. ter Haar, "The use of a segmented transducer for rib sparing in HIFU treatments," *Ultrasound Med Biol*, vol. 32, pp. 1753-1761, 2006.

[9] B. Quesson, M. Merle, M. O. Köhler, C. Mougenot, S. Roujol, B. D. de Senneville, and C. T. Moonen, "A method for MRI guidance of intercostal high intensity focused ultrasound ablation in the liver," *Med Phys*, vol. 37, pp. 2533-2540, 2010.

[10] R. Salomir, L. Petrusca, V. Auboiroux, A. Muller, M. I. Vargas, D. R. Morel, T. Goget, R. Breguet, S. Terraz, J. Hopple, X. Montet, C. D. Becker, and M. Viallon, "Magnetic resonance-guided shielding of prefocal acoustic obstacles in focused ultrasound therapy: application to intercostal ablation in liver," *Invest Radiol*, vol. 48, pp. 366-380, 2013.

[11] D. Kopelman, Y. Inbar, A. Hanannel, D. Freundlich, D. Castel, A. Perel, A. Greenfeld, T. Salamon, M. Sareli, A. Valeanu, and M. Papa, "Magnetic

resonance-guided focused ultrasound surgery (MRgFUS): ablation of liver tissue in a porcine model," *Eur J Radiol*, vol. 59, pp. 157-162, 2006.

[12] A. Okada, T. Murakami, K. Mikami, H. Onishi, N. Tanigawa, T. Marukawa, and H. Nakamura, "A case of hepatocellular carcinoma treated by MR-guided focused ultrasound ablation with respiratory gating," *Magn Reson Med Sci*, vol. 5, pp. 167-171, 2006.

[13] J. A. de Zwart, F. C. Vimeux, J. Palussière, R. Salomir, B. Quesson, C. Delalande, and C. T. Moonen, "On-line correction and visualization of motion during MRI-controlled hyperthermia," Magn Reson Med, vol. 45, pp. 128-137, 2001.

[14] B. D. de Senneville, C. Mougenot, and C. T. Moonen, "Real-time adaptive methods for treatment of mobile organs by MRI-controlled high-intensity focused ultrasound," *Magn Reson Med*, vol. 57, pp. 319-330, 2007.

[15] M. Ries, B. D. de Senneville, S. Roujol, Y. Berber, B. Quesson, and C. Moonen, "Real-time 3D target tracking in MRI guided focused ultrasound ablations in moving tissues," *Magn Reson Med*, vol. 64, pp. 1704-1712, 2010.

[16] B. D. de Senneville, M. Ries, G. Maclair, and C. Moonen, "MR-guided thermotherapy of abdominal organs using a robust PCA-based motion descriptor," *IEEE Trans Med Imaging*, vol. 30, pp. 1987-1995, 2011.

[17] A. B. Holbrook, P. Ghanouni, J. M. Santos, C. Dumoulin, Y. Medan, and K. B. Pauly, "Respiration based steering for high intensity focused ultrasound liver ablation," *Magn Reson Med*, doi: 10.1002/mrm.24695.

[18] M. von Siebenthal, G. Székely, U. Gamper, P. Boesiger, A. Lomax, and P. Cattin, "4D MR imaging of respiratory organ motion and its variability," *Phys Med Biol*, vol. 52, pp. 1547-1564, 2007.

[19] V. Auboiroux, L. Petrusca, M. Viallon, T. Goget, C. D. Becker, and R. Salomir, "Ultrasonography-based 2D motion-compensated HIFU sonication integrated with reference-free MR temperature monitoring: a feasibility study ex vivo," *Phys Med Biol*, vol. 57, pp. N159-N171, 2012.

[20] Z. Celicanin, V. Auboiroux, O. Bieri, L. Petrusca, Y. Natsuaki, F. Santini, M. Viallon, K. Scheffler, and R. Salomir, "Hybrid US-MR Guided HIFU Treatment Method with 3D Motion Compensation," In: Proceedings of the 21th Annual Meeting of ISMRM, Salt Lake City, USA, 2013. p. 233.

[21] V. Rieke, K. and Butts Pauly, "MR thermometry," *J Magn Reson Imaging*, vol. 27, pp. 376-390, 2008.

[22] V. Rieke, K. K. Vigen, G. Sommer, B. L. Daniel, J. M. Pauly, and K. Butts, "Referenceless PRF shift thermometry," *Magn Reson Med*, vol. 51, pp. 1223-1231, 2004.

[23] R. Salomir, M. Viallon, A. Kickhefel, J. Roland, D. R. Morel, L. Petrusca, V. Auboiroux, T. Goget, S. Terraz, C. D. Becker, and P. Gross, "Reference-

free PRFS MR-thermometry using near-harmonic 2-D reconstruction of the background phase," *IEEE Trans Med Imaging*, vol. 31, pp. 287-301, 2012.

[24] V. Rieke, A. M. Kinsey, A. B. Ross, W. H. Nau, C. J. Diederich, G. Sommer, and K. B. Pauly, "Referenceless MR thermometry for monitoring thermal ablation in the prostate," *IEEE Trans Med Imaging*, vol. 26, pp. 813-821, 2007.

[25] S. C. Davies, A. L. Hill, R. B. Holmes, M. Halliwell, and P. C. Jackson, "Ultrasound quantitation of respiratory organ motion in the upper abdomen," *Br J Radiol*, vol. 67, pp. 1096-1102, 1994.

[26] M. von Siebenthal, G. Székely, A. Lomax, and P. Cattin, "Inter-subject modeling of liver deformation during radiation therapy," *Med Image Comput Comput Assist Interv*, vol. 10, pp. 659-666, 2007.

[27] R. L. Ehman, and J. P. Felmlee, "Adaptive technique for high-definition MR imaging of moving structures," *Radiology*, vol. 173, pp. 255-263, 1989.

[28] M. V. McConnell, V. C. Khasgiwala, B. J. Savord, M. H. Chen, M. L. Chuang, R. R. Edelman, and W. J. Manning, "Prospective adaptive navigator correction for breath-hold MR coronary angiography," *Magn Reson Med*, vol. 37, pp. 148-152, 1997.

[29] C. J. Hardy, J. D. Pearlman, J. R. Moore, P. B. Roemer, and H. E. Cline, "Rapid NMR cardiography with a half-echo M-mode method," *J Comput Assist Tomogr*, vol. 15, pp. 868-874, 1991.

[30] K. Nehrke, P. Börnert, J. Groen, J. Smink, and J. C. Böck, "On the performance and accuracy of 2D navigator pulses," *Magn Reson Imaging*, vol. 17, pp. 1173-1181, 1999.

[31] S. A. Sapareto, and W. C. Dewey, "Thermal dose determination in cancer therapy," *Int J Radiat Oncol Biol Phys*, vol. 10, pp. 787-800, 1984.

[32] R. Salomir, J. Palussière, F. C. Vimeux, J. A. de Zwart, B. Quesson, M. Gauchet, P. Lelonq, J. Perqrale, N. Grenier, and C. T. Moonen, "Local hyperthermia with MR-guided focused ultrasound: spiral trajectory of the focal point optimized for temperature uniformity in the target region," *J Magn Reson Imaging*, vol. 12, pp. 571-582, 2000.

Chapter 3

Simultaneous Acquisition of Image and Navigator Slices using CAIPIRINHA for 4D-MR Imaging

---

An adapted version of this chapter has been published as:
Z. Celicanin, O. Bieri, F. Preiswerk, P. Cattin, K. Scheffler, F. Santini, "Simultaneous acquisition of image and navigator slices using CAIPIRINHA for 4D MRI," *Magn Reson Med* 2013; doi 10.1002/mrm.25134.

3.1 Introduction

Respiratory organ motion represents one of the key problems in various novel minimally invasive treatment methods, such as high-intensity focused ultrasound [1], radiotherapy [2] and proton therapy [3]. These treatment methods require not only high-quality static images of treated organs, but also models of respiratory organ motion. Magnetic resonance imaging (MRI) is commonly used as a guiding tool due to its excellent soft tissue contrast and high image quality. However, artifacts caused by respiratory motion are one of the major causes of image degradation, especially for three-dimensional (3D) MRI of moving organs, potentially obscuring important anatomic structures and lesions. Moreover, irregularities in organ motion during free breathing over an extended period of time are not addressed, since common imaging methods rely on simplified breathing patterns to acquire one generalized breathing cycle [4-6].

To overcome these limitations, a four-dimensional (4D) MRI was proposed [7]. This method neither assumes a constant breathing depth nor a strict breathing periodicity, and it is not dependant on any external breathing signal. Retrospective stacking is performed on dynamic 2D images using internal image-based sorting to produce a series of time-resolved 3D images. As a result, precise tracking of organ motion, including drifts and deformations, over the range of tens of minutes has been successfully demonstrated [7].

At present, 4D-MRI requires the interleaved acquisition of two-dimensional (2D) “image” and “navigator” slices. Image and navigator are originally acquired both in sagittal orientation, with the navigator slice locked to the same position for the whole acquisition, whereas the image position changes over time to cover the whole organ of interest. The navigator images provide information about the breathing state, and the image slice position is indirectly inferred by the position of the navigators immediately before and after [7, 8], resulting in a time difference between the image and the navigator slice. Generally, from the interleaved acquisition scheme, the construction of accurate 3D organ motion models from 4D-MRI data is currently limited by its temporal resolution, as well as sampling efficiency. Notably, image and navigator slices, however, are acquired in the same sagittal orientation, providing access to multislice acquisition techniques [9-11].

Controlled aliasing in parallel imaging results in higher acceleration (CAIPIRINHA) is a parallel multislice imaging technique that modifies the appearance of aliasing artifacts during the acquisition to improve the subsequent parallel image reconstruction procedure [11]. Multiple slices are simultaneously excited by multiband RF pulses, resulting in superimposed slices. By modulating the radiofrequency (RF) phase of the individual slices in the multiband excitation pulses, the two (or more) superimposed slices appear shifted with respect to each other. Commonly, for simultaneous excitation of two slices, a π phase cycle is applied to the RF pulses of one of the slices to induce a shift equal to half the field-of-view (FOV). Implementation of this concept to steady state free precession (SSFP), however, is not straightforward, since similar RF phase cycles are required to maintain the steady state. To this end, linear RF phase cycles were introduced to solve the issue of the required phase shift between slices and the maintenance of the steady state in each slice [12].

Commonly, simultaneous 2D multi-slice imaging is performed using multiband RF pulses, being the optimal choice for a fixed distance between the slices. With 4D-MRI, however, the distance between the navigator and the image slice is variable, making the multiband pulse approach less practical, due to the requirement of pulses with variable gaps and variable flip angles.

The use of CAIPIRINHA method for simultaneous acquisition of image and navigator slices for 4D-MRI was first presented in [13]. Subsequently, a similar approach was reported in [14]. Here, a new approach for simultaneous acquisition of image and navigator slices with 4D-MRI is introduced based on the one previously reported in [13]. The proposed method is based on the CAIPIRINHA technique and evaluated in phantoms and in vivo. Our results indicate that this method can achieve higher accuracy in the generation of motion models and improved signal-to-noise ratio (SNR) with respect to the original approach.

3.2 Methods

A standard balanced SSFP (bSSFP) sequence was modified to simultaneously excite two slices, namely an image and a navigator slice. An exemplary diagram of the modified bSSFP pulse sequence is shown on Fig. 3.1a. The image slice is excited by the first RF pulse, while the second RF pulse excites the navigator slice. The corresponding slice selection gradients have an opposite polarity to achieve nulling of the zeroth-order moment of the gradients at the echo (TE) and repetition (TR) time. This introduces a gap between the two pulses equal to twice the ramp time of the gradients (approximately 250 μs). Since both slices share the same frequency and phase encodings, they become superimposed on top of each other in the acquired image. Different phase cycling schemes are thus applied to the two RF pulses in order to both keep the bSSFP signal of the two slices in the passband regime and to distribute the acquired slices over the FOV. In order to achieve a shift of half the FOV, which maximizes the coil sensitivity variations and subsequently the reconstruction accuracy, the phase increment for the phase cycling of the image slices was manually selectable (to minimize banding artifacts, with a default of $+\pi/2$), while the phase cycling of the navigator slice was fixed to an offset of π with respect to the image excitation RF pulse.

With 4D-MRI, the navigator slice position is kept constant, but the image slice position is changing sequentially during the data acquisition [7]. To enhance transition into steady state, every time the slice position was changed, a series of 10 preparation pulses of increasing flip angles (Kaiser-Bessel preparation) was used to suppress transient signal oscillations [15]. For the navigator slice, the steady state was maintained by dummy RF pulses of a constant amplitude and the same phase cycling scheme as during imaging (see Fig. 3.1b). For a special case when the slice and navigator positions were identical, only one RF pulse was played, i.e. only the navigator slice was acquired.

The sequence was evaluated on a phantom and in vivo on a 1.5 T whole-body MRI clinical scanner (MAGNETOM Avanto – Siemens Medical Solutions, Erlangen, Germany). The modified 4D-MRI bSSFP sequence was used with the following parameters: TE = 1.84 ms, TR = 3.18 ms, FA = 50º, FOV = 22.5 × 24

cm2, matrix = 120 × 128, slice thickness = 6 mm, partial Fourier factor = 6/8, BW = 1184 Hz/pixel. The total acquisition time for a stack of 20 images and 20 navigators was approximately 6s. The phase cycling angle was manually optimized on a case-by-case basis by repeating the acquisition until an optimal image quality was obtained.

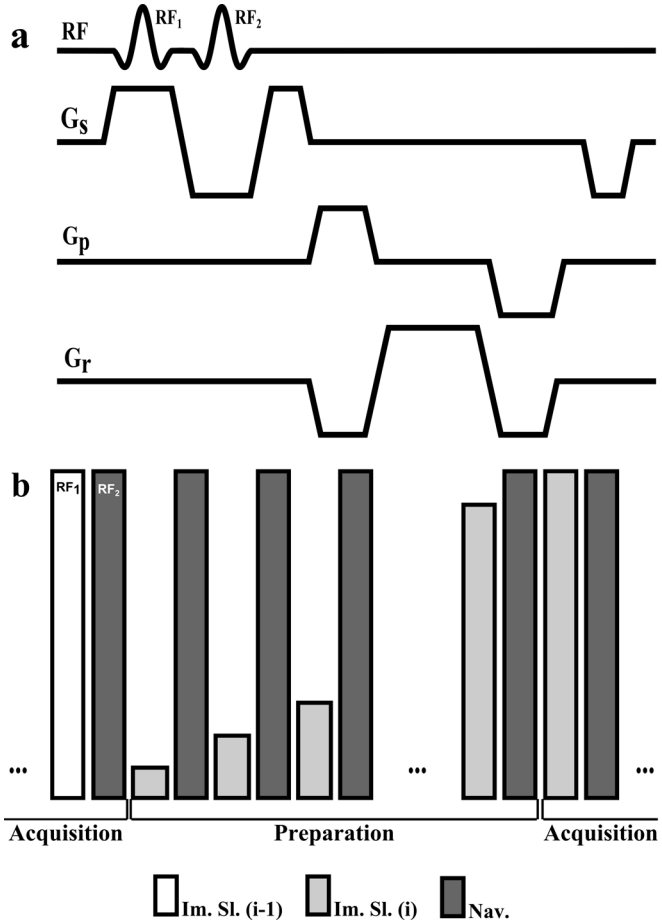

Figure 3.1 a) Exemplary diagram of the CAIPIRINHA 4D bSSFP sequence. The first RF pulse (RF_1) excites the image slice, while the second (RF_2) excites the navigator slice. The two signals are acquired simultaneously by means of a conventional bSSFP readout scheme. **b)** Descriptive representation of the RF pulse amplitude evolution during a change of image slices. A Kaiser-Bessel preparation is executed for the new image slice, while the navigator slice is kept in the steady state by constant amplitude RF pulses.

Coil sensitivity maps were acquired in free breathing with a proton-density-weighted spoiled gradient echo sequence (TE = 3.48 ms, TR = 7.2 ms, FA = 25º, BW = 260 Hz/pixel), having essentially the same resolution and FOV as the bSSFP images. Four averages were acquired to compensate for the respiratory motion.

The CAIPIRINHA images were reconstructed using the adapted sensitivity encoding (SENSE) [16] algorithm with the reduction factor of R = 2. All reconstructions were performed offline on a standalone personal computer (PC) in the Matlab programming environment (The Mathworks, Natick, MA).

The phantom experiments were performed on a spherical agar phantom using a 12-channel head coil. 20 repetitions of the proposed CAIPIRINHA sequence and 20 repetitions of the original 4D-MRI protocol, adapted to match spatial and temporal resolutions, were acquired. The protocol parameters of the original 4D-MRI were: TE = 1.38 ms, TR = 2.92 ms, FA = 50º, FOV = 27.3 × 34.9 cm2, matrix = 150 × 192, slice thickness = 6 mm, partial Fourier factor = 6/8, BW = 1184 Hz/pixel, SENSE with acceleration factor = 2. SNR maps were calculated by dividing the temporal average of the signal across the repetitions in each voxel by its standard deviation [17-19]. Average SNR was calculated over a large region of interest comprising most of the phantom.

In vivo experiments were performed in the abdomen of 4 healthy volunteers (3 male) with different amount of subcutaneous adipose tissue during free breathing to evaluate the robustness of the method with respect to the body shape. For these experiments, a standard 6-channel surface body coil and a 9-channel spine coil were used. Informed consent was obtained before the study from each volunteer.

In order to compare CAIPIRINHA-based 4D-MRI to the original method described in [7], we acquired a sequence of 90 consecutive repetitions of one of the healthy volunteers with the original 4D-MRI protocol [7], and with the here described sequence and protocol (total scan time of approximately 60 minutes). In both cases, the 4D-MRI reconstructions were computed retrospectively as described in [7]. However, in either case, no averaging among the best matches was performed when stacking the data slices. Instead, only the single best matching data slice for each navigator was used in order to avoid further obfuscation in the comparison. Another difference to [7] was the use of non-rigid image registration instead of simple template matching for determining the frame similarity of the navigators, which resulted in dense deformation fields instead of only a few tracked points. For that task, we used the NiftyReg library [20].

G-factor maps were calculated for each slice according to:

$$g_i = \sqrt{(\hat{C}^H \hat{C})_{ii} \left((\hat{C}^H \hat{C})^{-1}\right)_{ii}}, \tag{3.1}$$

where C is the coil sensitivity matrix. Also the g-factor maps for the original 4D-MRI approach with the in-plane SENSE with the acceleration factor of 2 (SENSE x2) was calculated for each slice. Region of interest (ROI) were drawn around the whole liver, as it was the organ of interest in this case, and the mean and maximum g-factors were calculated for each slice. Finally the relative SNR compared to the unaccelerated counterpart (SNRunac) was calculated according to:

$$\frac{SNR_{CAIP}}{SNR^{unac}} = \frac{1}{g_{CAIP}}, \tag{3.2}$$

$$\frac{SNR_{SENSEx2}}{SNR^{unac}} = \frac{1}{g_{SENSEx2}\sqrt{2}} . \quad (3.3)$$

Further theoretical details about the equations could be found in [11].

3.3 Results

In the phantom experiments, the method was able to acquire and unfold two slices simultaneously. In the originally acquired slices, the image and navigator slices appear superimposed on top of each other, shifted by half of the FOV. Generally, CAIPIRINHA-SENSE reconstruction separated the navigator from the image without any visible reconstruction artifacts (see Fig. 3.2, first three columns). The resulting signal is homogeneous, compatible with the composition of the phantom and a sum-of-squares reconstruction deriving from the 12-channel head coil. The SNR maps (Fig. 3.2, fourth and fifth columns) are more homogeneous in the case of CAIPIRINHA reconstruction due to its most efficient usage of coil sensitivities with respect to conventional parallel imaging used in the original 4D-MRI sequence [11]. The overall average SNR was also higher for the proposed CAIPIRINHA case with respect to the original sequence [7].

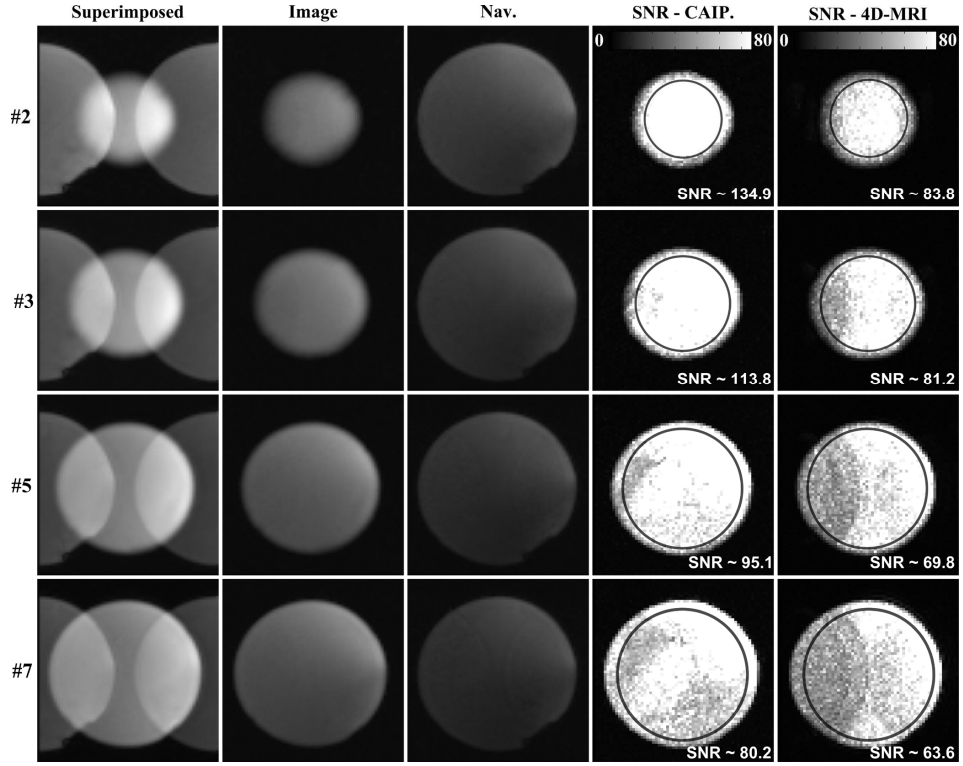

Figure 2 Phantom exemplary images. Superimposed images with their respective reconstructed image and navigator slices are shown for different slice positions (here 2, 3, 5, 7 represent slice numbers; total number of slices was 20; navigator slice was number 10). SNR maps calculated for each slice, are shown for both the

CAIPIRINHA approach and the reference 4D-MRI. Average SNRs calculated over the region of interest, are also provided.

The g-factor maps of an in vivo volunteer were calculated for the image and navigator for each slice position, and they are shown on Fig. 3.3a. The original 4D-MRI approach of performing the SENSE with the acceleration factor of 2 (here referred as SENSE x2) was evaluated as well, and the corresponding g-factor maps are shown on Fig. 3.3a for the same slice positions as for the image and navigator. On Fig. 3.3b, the calculated mean and minimum relative SNR for the CAIPIRINA and SENSE x2 approach are shown, as a function of the slice position. The navigator was the slice number 11, and is marked on the figure with the vertical line.

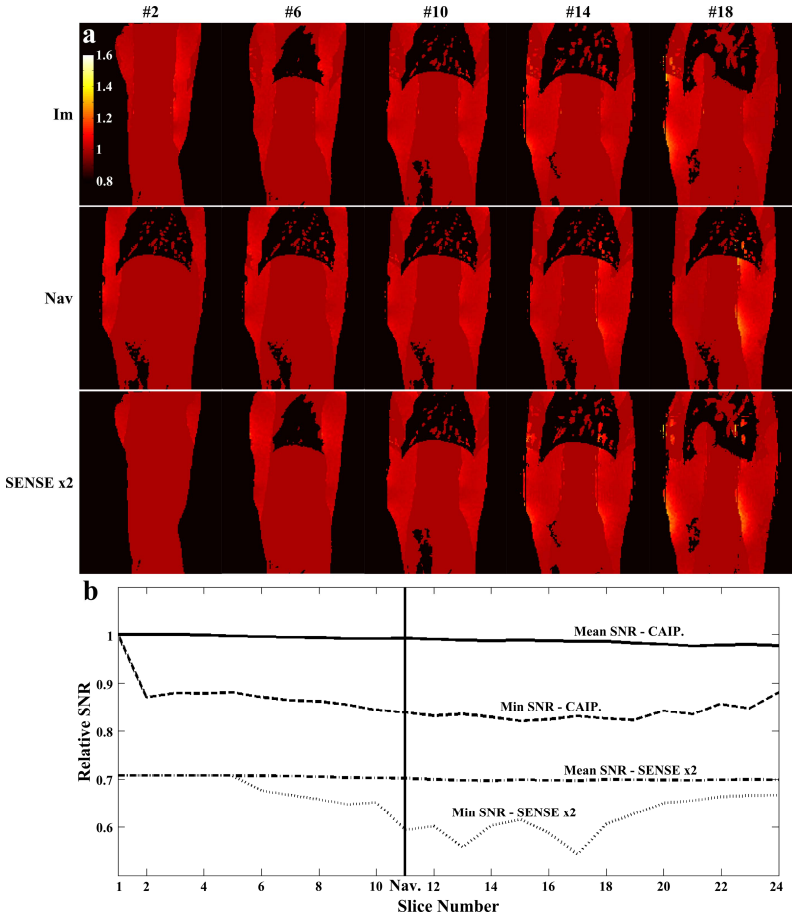

Figure 3.3 a) G-factor maps of the image and navigator slices for the different slice positions. G-factor maps of SENSE x2 for the same slice positions are shown for comparison. **b)** Plot of the calculated mean and minimum relative SNR for CAIPIRINHA and SENSE x2.

The four volunteers exhibited different amounts of adipose tissue, which appeared hyperintense in the bSSFP images. Despite these differences, the reconstruction was successful in all volunteer cases (see Fig. 3.4). There were no artifacts arising from the simultaneous acquisition. In some slices the liver parenchyma appeared darker because of the off-resonance profile of the bSSFP acquisition. In general, the navigator slices have a more pronounced inflow effect due to a higher saturation, since they are continuously excited. This is however beneficial for the retrospective stacking [7].

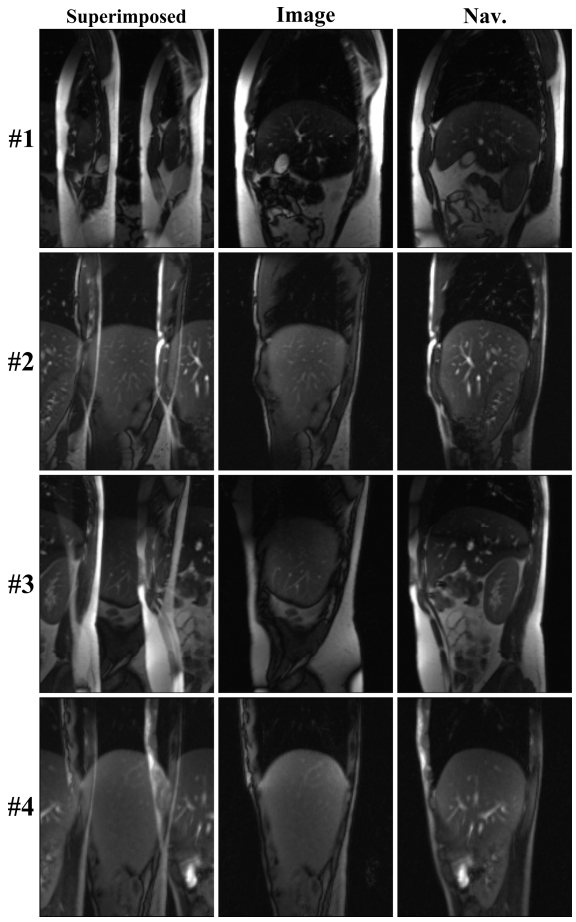

Figure 3.4 In vivo exemplary images of four healthy volunteers demonstrating the feasibility of unfolding. Superimposed images, and reconstructed image and navigator slices are presented in columns from left to right, respectively.

The stacking of a time-resolved three-dimensional dataset from the 90-repetition acquisition was successful both in the CAIPIRINHA and in the original 4D-MRI case. However, the original 4D-MRI presented some mismatching in the stacking due to the time difference between image and navigator slices. The image quality of the CAIPIRINHA stacks is noticeably improved, due to an increased SNR. On Fig. 3.5a-d and 3.5e-h the triplanar view and a respective 3D stack of the standard 4D-MRI and of our approach are presented, respectively.

The time-resolved 3D stacks are shown on Fig. 3.5i and 3.5j again for the 4D-MRI and for our approach, demonstrating the reduced mismatching (marked with white arrows) in our approach.

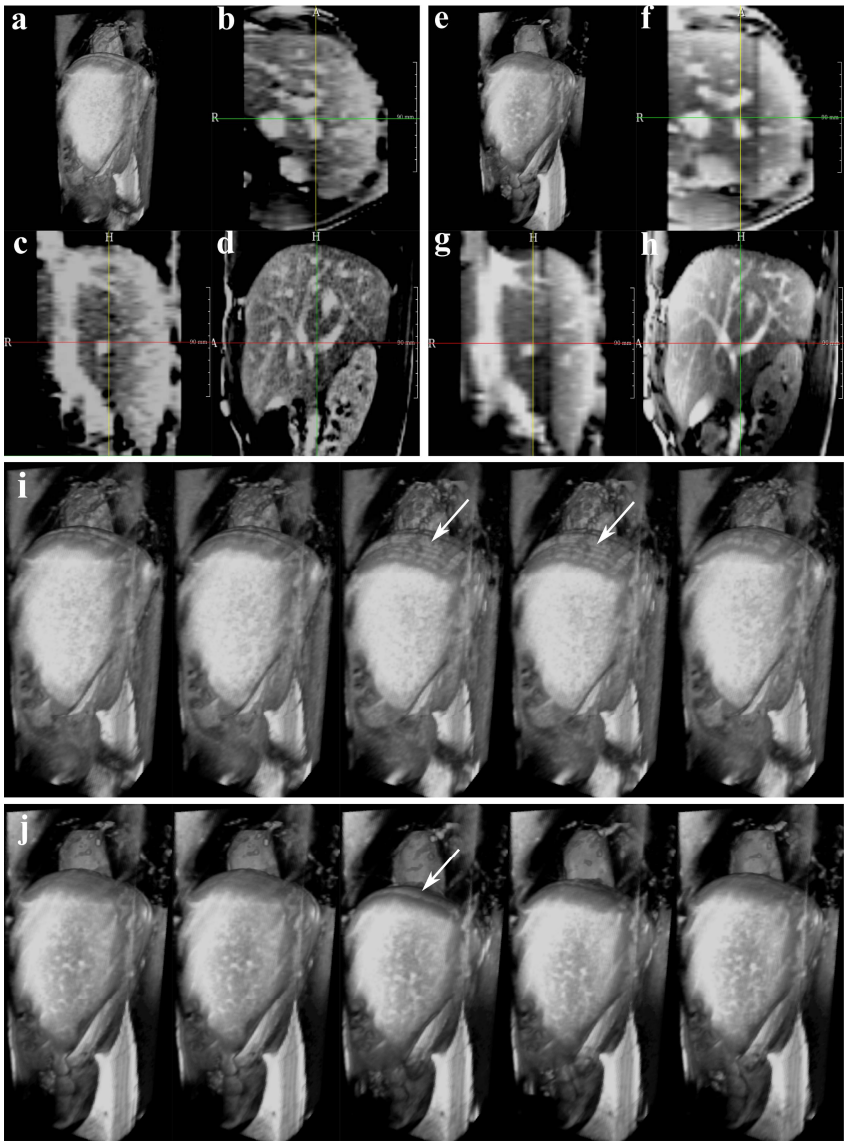

Figure 3.5 Triplanar views of 3D stacks of the original 4D-MRI **(a-d)** and CAIPIRINHA **(e-h)** acquisition. Time-resolved three-dimensional stacks produced from: **i)** a dataset acquired with the proposed CAIPIRINHA 4D-MRI method, and **j)** the original 4D-MRI acquisition. Note the mismatching artifacts (white arrows) in the original 4D-MRI method, which are less severe for the CAIPIRINHA-based acquisition. Note that vertical dark bands, discernible on f) and g), are caused by saturation of the navigator slice, which was kept in the steady state.

3.4 Discussion

A novel imaging method for simultaneous acquisition of image and navigator slices, using a flexible CAIPIRINHA acquisition strategy for 4D-MRI organ motion imaging, was presented. As a result and in contrast to the previous work [7], the image and navigator slices have no temporal mismatch. The major focus here is to produce time-resolved series of 3D image datasets to build motion models of internal organs. The final aim of these models is to guide "beam therapies" (i.e. high-intensity focused ultrasound (HIFU), proton beam therapy, etc.), where free breathing and motion tracking are preferred to breath-hold or triggered approaches. In particular, motion tracking is important in HIFU treatments, because it allows an effective targeting of the delivered thermal dose, which leads to a reduction of the collateral thermal damage to tissues surrounding the lesion [21, 22].

For this application, the superiority of using a full 2D navigator with respect to a more conventional diaphragm position tracking by a single pencil-beam navigator was proven in [8]. In addition to providing information concerning the respiratory phase, navigator images can also track non-periodic and long term motion, such as organ drifts over time.

In this work, scanning was performed on a standard 1.5 T clinical system, while processing of images was done offline, with no special requirements to the clinical setting. When used with a high flip angle to enhance the signal from blood vessels (by saturating the tissue and exploiting the inflow effect), the multi-slice CAIPIRINHA acquisition is limited by a specific absorption rate (SAR) and RF power amplifier limits.

However, in order to be suited for this application, the original CAIPIRINHA method needed some adaptation. Since the navigator and the image slice were acquired simultaneously with different phase cycles, the conventional π-phase cycling scheme of contemporary bSSFP protocols could not be used. Such a phase cycling scheme would result in an image acquired in the middle of the passband while the other one would be centered in the stopband of the bSSFP signal. Instead, a $+\pi/2$ and a $-\pi/2$ phase cycling scheme (as proposed in [12]) was preferably used for the image and the navigator slices, respectively. This allowed acquisition of both slices in the passband, but increased sensitivity to off-resonance effects and therefore banding artifacts, which limited imaging on MR systems with good field homogeneity and accurate shimming. Manually changing the phase cycling scheme of one of the slices helped optimize image quality in our set-up. Alternatively, the sequence could be modified by the introduction of a spoiling gradient at the end of TR to become a SSFP-FID or spoiled gradient echo sequence, eliminating the banding issue at the cost of a reduced signal level and different contrast.

Typically, simultaneous excitation of two slices is performed with alternating multiband RF pulses similar to Hadamard pulses [9]. Here, a novel and more flexible approach was used based on two separate RF pulses. This, in general, provides an easy setup for arbitrary flip angles (e.g., necessary for magnetization preparation of the image slice), or for a variable distance between slices, and, overall the implementation of that sequence is considerably simpler. Overall, this

only introduces a small penalty in TR and a shift in one of the two signals with respect to the center of the TR by an amount corresponding to the time difference between the two RF pulse peaks, which is in fact equal to the RF pulse duration plus the gradient ramp times. This shift introduces a T2*-weighting in the bSSFP signal [23]. However, in our case, this weighting is considered negligible as the timings involved here are much smaller than the typical T2* of the imaged tissues (850 μs versus more than 10 or 20 ms [24]). However, the frequency and phase encoding of the signals are performed at the same time, thus leading to truly simultaneous encoding of the spatial position, except for the minimal through plane motion happening between the two RF pulses, which is negligible for this setup (sagittal acquisition of respiratory motion).

As demonstrated on Fig. 3.3, the relative SNR in our approach is higher than the one obtain by the conventional 4D-MRI. Although the relative SNR is higher for the CAIPIRINHA case, the dependence of the SNR on the slice distance, between the image and navigator slice, was not observed. This is probably due to the lack of a significant coil sensitivity variance in the slice direction. Here, a body coil with 6-channels was used, while the slices were of a sagittal orientation, and this was significantly different than the simulated relative SNR on Fig. 8 in [11], that used 16-channel head-coil with significant sensitivity variations in the slice direction.

Since the temporal footprint of the acquisition of each image is increased with respect to conventional 4D-MRI, intra-view motion might become noticeable in case of very fast breathing motions. In our experimental results we did not observe any noticeable motion artifacts or blurring of the CAIPIRINHA images. However, even in case that such blurring occurs, it would not necessarily affect the registration in a negative way. In most registration approaches, both reference and floating image are blurred prior to matching since this removes the highest frequencies which often encode noise and affect the registration result.

In the 4D model building stage, due to the interleaved acquisition scheme of the original 4D-MRI, an accurate similarity measure between two data frames Di, Dj acquired at time i and j can only be estimated, as the exact breathing stage is not given. This is done by comparing the displacement field of both the preceding and succeeding pairs of navigators Ni-1, Nj-1 and Ni+1, Nj+1. Another problem is that the resulting two difference vectors must be combined and mapped to a cost c(i,j), which induces a dependency on breathing speed. With CAIPIRINHA, on the other hand, the respiratory state of Di is exactly represented by Ni, thus only a single pair of deformation fields needs to be compared. This is not only computationally more efficient, but also solves the above problems and leads to better results, as can be seen in Fig. 3.5.

The proposed method was specifically designed for the acquisition of 4D-MRI datasets of the abdominal region. However, it is evident that the concepts presented here can be generalized for other applications where the acquisition of an image together with a positional navigator is advisable (e.g. for respiratory motion compensation in cardiac imaging).

3.5 Conclusion

A novel imaging strategy for improved 4D-MRI of organ motion was proposed. The method enables the simultaneous acquisition of an image and a navigator slice with high temporal resolution and improved SNR compared to the reference 4D-MRI approach, at the potential cost of minor blurring of the images in case of very fast respiratory movements. Phantom and volunteer studies indicate that the presented method provides three-dimensional stacks with reduced mismatching compared to the reference method, potentially leading to more accurate images as a basis for learning motion models.

References

[1] M. Pernot, M. Tanter, and M. Fink, "3-D real-time motion correction in high-intensity focused ultrasound therapy," *Ultrasound Med Biol*, vol. 30, pp. 1239-1249, 2004.

[2] P. J. Keall, G. S. Mageras, J. M. Balter, R. S. Emery, K. M. Forster, S. B. Jiang, J. M. Kapatoes, D. A. Low, M. J. Murphy, C. R. Ramsey, M. B. Van Herk, S. S. Vedam, J. W. Wong, and E. Yorke, "The management of respiratory motion in radiation oncology report of AAPM Task Group 76," *Med Phys*, vol. 33, pp. 3874-3900, 2006.

[3] E. Rietzel, and C. Bert, "Respiratory motion management in particle therapy," *Med Phys*, vol. 37, pp. 449-460, 2010.

[4] T. Rohlfing, C. R. Maurer Jr, W. G. O'Dell, and J. Zhong, "Modeling liver motion and deformation during the respiratory cycle using intensity-based nonrigid registration of gated MR images," *Med Phys*, vol. 31, pp. 427:432, 2004.

[5] J. M. Blackall, S. Ahmad, M. E. Miguel, J. R. McClelland, D. B. Landau, and D. J. Hawkes, "MRI-based measurements of respiratory motion variability and assessment of imaging strategies for radiotherapy planning," *Phys Med Biol*, vol. 51, pp. 4147-4169, 2006.

[6] J. Tokuda, S. Morikawa, H. A. Haque, T. Tsukamoto, K. Matsumiya, H. Liao, K. Masamune, and T. Dohi, "Adaptive 4D MR imaging using navigator-based respiratory signal for MRI-guided therapy," *Magn Reson Med*, vol. 59, pp. 1051-1061, 2008.

[7] M von Siebenthal, G. Székely, U. Gamper, P. Boesiger, A. Lomax, and P. Cattin, "4D MR imaging of respiratory organ motion and its variability," *Phys Med Biol*, vol. 52, pp. 1547-1564, 2007.

[8] P. Arnold, F. Preiswerk, B. Fasel, R. Salomir, K. Scheffler, and P. C. Cattin, "3D organ motion prediction for MR-guided high intensity focused ultrasound," *Med Image Comput Comput Assist Interv*, vol. 14, pp. 623-630, 2011.

[9] S. P. Souza, J. Szumowski, C. L. Dumoulin, D. P. Plewes, and G. Glover, "SIMA: simultaneous multislice acquisition of MR images by Hadamard-encoded excitation," *J Comput Assist Tomogr*, vol. 12, pp. 1026-1030, 1988.

[10] S. Müller, "Simultaneous multislice imaging (SIMUSIM) for improved cardiac imaging," *Magn Reson Med*, vol. 10, pp. 145-155, 1989.

[11] F. A. Breuer, M. Blaimer, R. M. Heidemann, M. F. Mueller, M. A. Griswold, and P. M. Jakob, "Controlled aliasing in parallel imaging results in higher acceleration (CAIPIRINHA) for multi-slice imaging," *Magn Reson Med*, vol. 53, pp. 684-691, 2005.

[12] D. Stäb, C. O. Ritter, F. A. Breuer, A. M. Weng, D. Hahn, and H. Köstler, "CAIPIRINHA accelerated SSFP imaging," *Magn Reson Med*, vol. 65, pp. 157-164, 2011.

[13] Z. Celicanin, F. Preiswerk, P. Arnold, P. Cattin, K. Scheffler, and F. Santini, "Simultaneous acquisition of image and navigator slices using CAIPIRINHA," In Proceedings of the 19th Annual Meeting of ISMRM, Montréal, Québec, Canada, 2011. p. 4399.

[14] D. Giese, M. Buehrer, C. von Deuster, T. Schaeffter, and S. Kozerke, "Multi-slice free breathing liver imaging using a 2D CAIPIRINHA navigator," In Proceedings of the 21st Annual Meeting of ISMRM, Salt Lake City, Utah, USA, 2013. p. 307.

[15] P. Le Roux, "Simplified model and stabilization of SSFP sequences," *J Magn Reson*, vol. 163, pp. 23-37, 2003.

[16] K. P. Pruessmann, M. Weiger, M. B. Scheidegger, and P. Boesiger, "SENSE: sensitivity encoding for fast MRI," *Magn Reson Med*, vol. 42, pp. 952-962, 1999.

[17] C. D. Constantinides, E. Atalar, and E. R. McVeigh, "Signal-to-noise measurements in magnitude images from NMR phased arrays," *Magn Reson Med*, vol. 38, pp. 852-857, 1997.

[18] D. K. Sodickson, and W. J. Manning, "Simultaneous acquisition of spatial harmonics (SMASH): fast imaging with radiofrequency coil arrays," *Magn Reson Med*, vol. 38, pp. 591-603, 1997.

[19] O. Dietrich, J. G. Raya, S. B. Reeder, M. F. Reiser, and S. O. Schoenberg, "Measurement of signal-to-noise ratios in MR images: influence of multichannel coils, parallel imaging, and reconstruction filters," *J Magn Reson Imaging*, vol. 26, pp. 375-385, 2007.

[20] M. Modat, G. R. Ridgway, Z. A. Taylor, M. Lehmann, J. Barnes, D. J. Hawkes, N. C. Fox, and S. Ourselin, "Fast free-form deformation using graphics processing units," *Comput Methods Programs Biomed*, vol. 98, pp. 278-284, 2010.

[21] B. D. de Senneville, C. Mougenot, and C. T. Moonen, “Real-time adaptive methods for treatment of mobile organs by MRI-controlled high-intensity focused ultrasound,” *Magn Reson Med*, vol. 57, pp. 319-330, 2007.

[22] Z. Celicanin, V. Auboiroux, O. Bieri, L. Petrusca, F. Santini, M. Viallon, K. Scheffler, and R. Salomir, “Real-time method for motion-compensated MR thermometry and MRgHIFU treatment in abdominal organs,” *Magn Reson Med*, 2013. doi: 10.1002/mrm.25017.

[23] K. Scheffler, and S. Lehnhardt, “Principles and applications of balanced SSFP techniques,” *Eur Radiol*, vol. 13, pp. 2409-2418, 2003.

[24] H. Chandarana, R. P. Lim, J. H. Jensen, C. H. Hajdu, M. Losada, J. S. Babb, S. Huffman, and B. Taouli, “Hepatic iron deposition in patients with liver disease: preliminary experience with breath-hold multiecho T2*-weighted sequence,” *AJR Am J Roentgenol*, vol. 193, pp. 1261-1267, 2009.

Chapter 4

Spectrally Selective Crossed-Pair Navigator

An adapted version of this chapter has been presented as:
Z. Celicanin, O. Bieri, K. Scheffler, and F. Santini, "Spectrally Selective Crossed-Pair Navigator," In Proceedings of the 20th Annual Meeting of ISMRM, Melbourne, Australia, 2012. p. 3408.

4.1 Introduction

Organ motion monitoring by means of navigator echoes is required in many applications of magnetic resonance imaging (MRI), in which physiological motion causes image artifacts. Instead of tracking the diaphragm motion and correlating it to the motion of the imaging organ, tracking could be directly provided from the surrounding fatty tissue, without compromising image quality.

The position of the abdominal and thoracic organs is generally tracked by a diaphragmatic crossed-pair or one-dimensional (1D) pencil-beam navigator, which provides the indirect measure of the respiratory motion. However, direct measurement of cardiac motion was reported in [1] by a navigator approach, where the epicardial fat was used to provide a direct tracking signal. This approach was further investigated and corresponding results were reported in [2-6]. Respiratory motion correction based on the TR-perturbed balanced steady state free precession [7] was recently reported [8] and the feasibility of it was demonstrated for free-breathing three-dimensional (3D) cardiac imaging.

Besides the negative impact of respiratory motion on cardiac imaging, a significant issue in various interventional procedures, guided by magnetic resonance imaging (MRI), is respiratory motion of other organs. In magnetic resonance guided high-intensity focused ultrasound (MRgHIFU), organ motion is tracked by MRI, which is also used to provide a measure of treatment efficiency in a form of thermal dose maps [9]. This leads to interferences between the two imaging procedures, as both of them are performed on the same organ. A spectrally selective pencil-beam navigator based on a 1-$\overline{2}$-1 binomial pulse (subpulses consisted of spiral two-dimensional (2D) RF pulses) was used to track the surrounding adipose tissue of the liver and the kidney, and provided the information about the organ motion to the HIFU system [10].

T1-weighted 3D spoiled gradient-echo (SPGR) sequences acquired in a breathhold are used in general to assess liver tissue abnormalities [11, 12]. However, the quality of the volumetric images is compromised when acquired in a single breathhold, due to challenging compliance of some patients, including pediatric, geriatric, and uncommunicative patients. The navigator-gated approach [13] can be used during free-breathing to acquire multiple signals for averaging to improve signal-to-noise ratio (SNR) or to improve spatial resolution.

Here, a novel spectrally selective navigator is presented based on a spin echo sequence with two orthogonal planes for the excitation and refocusing. Both pulses, for excitation and refocusing, were made spectrally selective by converting them to theirs 1-$\overline{1}$ binomial counterparts.

4.2 Methods

A spectrally selective crossed-pair navigator was designed and implemented for organ motion tracking on a 1.5 T and a 3 T clinical whole-body scanner (MAGNETOM Avanto and Verio, respectively; Siemens Medical Solutions, Erlangen, Germany). The pulse sequence of the here presented navigator is shown

on Fig. 4.1. The two orthogonal planes for excitation and refocusing had a completely separate planning and protocol setup. The two planes could be tilted with respect to each other in order to control the navigator volume and profile. The time period between the subpulses in both an excitation and a refocusing RF pulse, on Fig. 4.1 designated by τ, could be controlled from the graphical user interface of the pulse sequence. For the subpulses, sinc-shaped excitation pulses of 1 ms duration with time-bandwidth product of 2.7 were used.

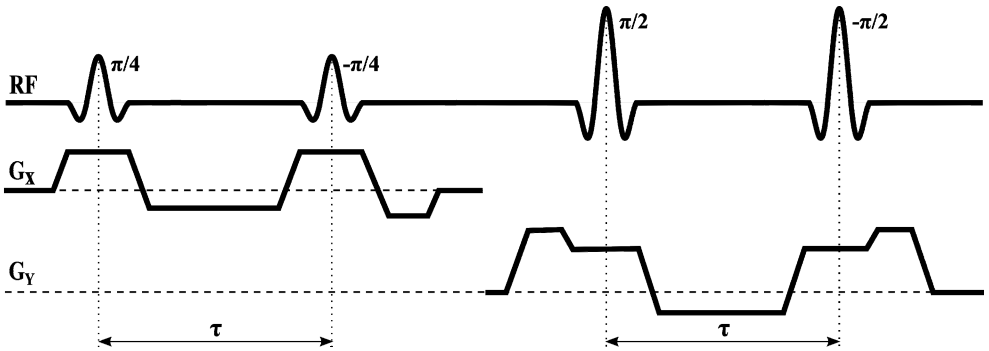

Figure 4.1 Pulse sequence diagram. Spectrally selective 1-$\bar{1}$ binomial crossed-pair excitation and refocusing pulses are shown with corresponding slice selection gradients. The binomial subpulse separation time is indicated by a parameter τ.

The navigator was evaluated on a phantom and in vivo on a 1.5 T and a 3 T clinical MRI system. The following pulse sequence parameters were used: TE = 5 ms, voxel size = 10 × 10 × 0.67 mm, readout FOV= 128 mm. The overall duration of the acquisition of the spectrally selective navigator was 8 ms. Tracking of the adipose tissue around the liver, the kidney and the heart was attempted. Three healthy volunteers were scanned in total. The impact of the saturation artifacts of the purposed navigator on a desired imaging sequence was evaluated on a phantom. Body coil with 6 channels was used for in vivo and phantom acquisitions. The phase accrual between water and fat of π and 3π was used at 1.5 T and 3 T, respectively. The imaging sequence for the phantom acquisition was balanced steady-state free precession (bSSFP) with the following parameters: TE = 1.9 ms, TR = 3.2 ms, FA = 70º, FOV = 300 × 300 mm, matrix = 128 × 128, slice thickness = 5 mm.

The practical application of the purposed navigator was investigated for a three-dimensional triggered acquisition of the liver. The standard crossed-pair navigator was used for the initial acquisition, following the acquisition in which the liver motion was tracked by the here developed spectrally selective navigator. In that case the navigator was positioned in the lower part of the liver, where a significant amount of adipose tissue was present, in contrast to the standard acquisitions, performed initially, where the navigator tracked the diaphragm motion. Informed consent was obtained from each volunteer before the study. The imaging pulse sequence of the liver was 3D gradient-recalled echo (GRE) with the following parameters: TE = 2.99 ms, TR = 457.45 ms, FA = 15º, FOV = 250 × 320 mm, matrix = 138 × 176, slice thickness = 2 mm, 72 slices.

The spectral selectivity of a 1-$\bar{1}$ binomial pulse at 1.5 and 3 T was evaluated offline starting from Bloch equations in Matlab programming environment (The Mathworks, Natick, MA), assuming a chemical shift between water and fat nuclei of 3.5 ppm (223 Hz at 1.5 T and 446 Hz at 3 T). The relaxation times were omitted from the simulation as the typical values are much longer compared to the interval period between the subpulses.

4.3 Results

The spectral selectivity of a 1-$\bar{1}$ binomial pulse, calculated starting from the Bloch equations, at 1.5 and 3 T is shown on Fig. 4.2, assuming a chemical shift between water and fat nuclei of 3.5 ppm (223 Hz at 1.5 T and 446 Hz at 3 T).

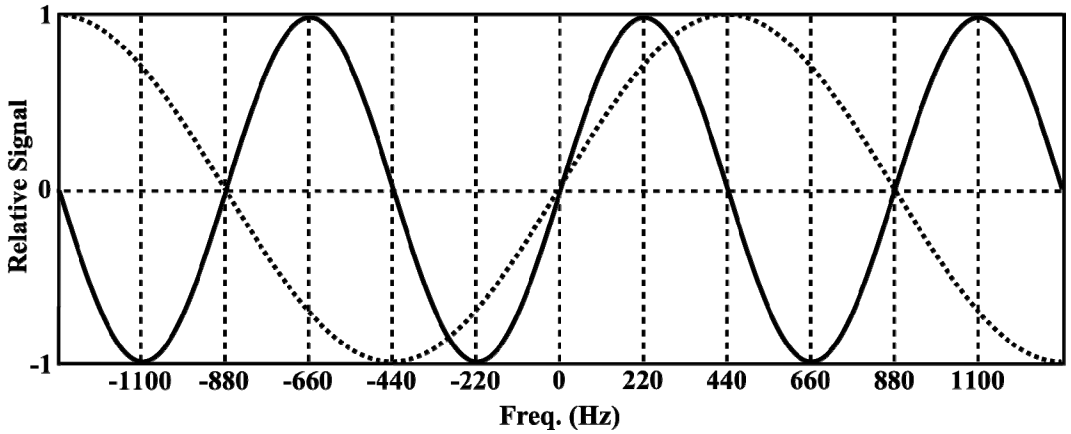

Figure 4.2 The spectral profile of the 1-$\bar{1}$ binomial pulse at 1.5 (full line) and 3 T (dotted line).

The images of the phantom acquired with the bSSFP sequence interleaved with the navigator are shown on Fig. 4.3. It can be observed that due to the spectral selectivity of the fat navigator, the saturation artifacts are significantly mitigated compared to the standard nonselective cross-paired navigator. Only in the areas of higher magnetic field inhomogeneities (lower part of the phantom), that the artifact becomes more pronounced.

The navigator tracking capability was evaluated in vivo on the liver, and the tracking signal is shown on Fig. 4.4a at 1.5 T and on Fig. 4.4b 3 T. The navigator was positioned in the lower part of the liver in order to track visceral fat. The SNR was comparable to the nonselective cross-paired navigator if enough adipose tissue was present, while not producing the saturation artifact. The tracking signal, reconstructed from the navigator profiles by least squares fitting [14], was stable and accurate.

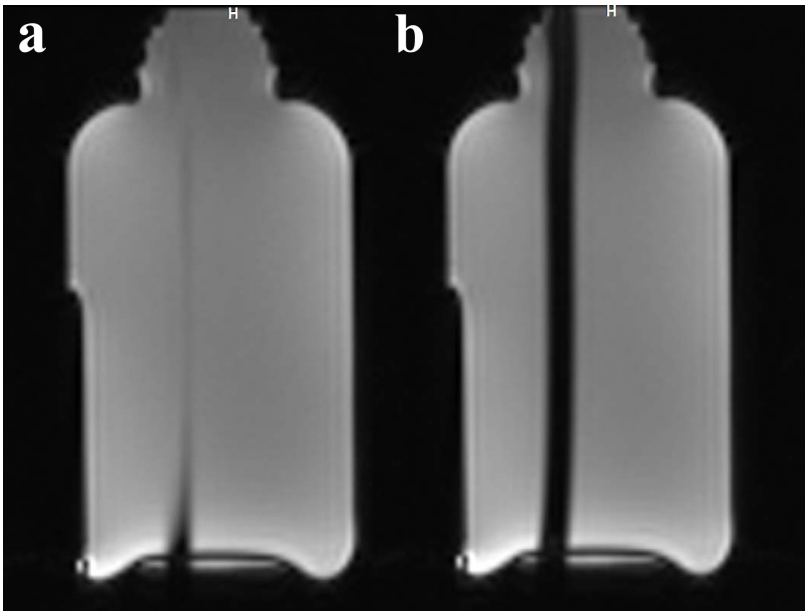

Figure 4.3 The saturation artifact due to the fat navigator **(a)** and due to the standard cross-paired navigator **(b)**. Note the significant reduction in the artifact appearance.

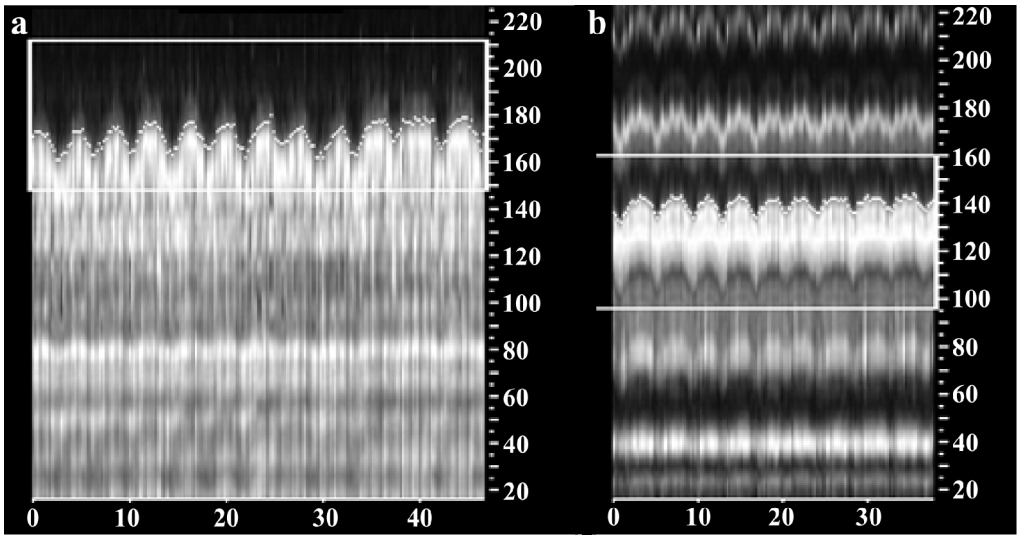

Figure 4.4 The tracking signal and navigator profiles of the spectrally selective crossed-pair navigator at 1.5 T **(a)** and 3 T **(b)**.

Two images of the liver acquired with the navigator-gated 3D spoiled gradient-recalled echo (GRE) pulse sequence are presented on Fig. 4.5. While both of them had the same imaging parameters, the image in a) was acquired while the liver motion was tracked with a standard crossed-pair navigator, in contrast to the acquisition of the image in b) where the tracking was performed with the here described spectrally selective crossed-pair navigator. It could be observed that the left image has pronounced saturation bands from the corresponding imaging

planes of the navigator, while the right image has no such artifacts due to the spectral selectivity of the navigator.

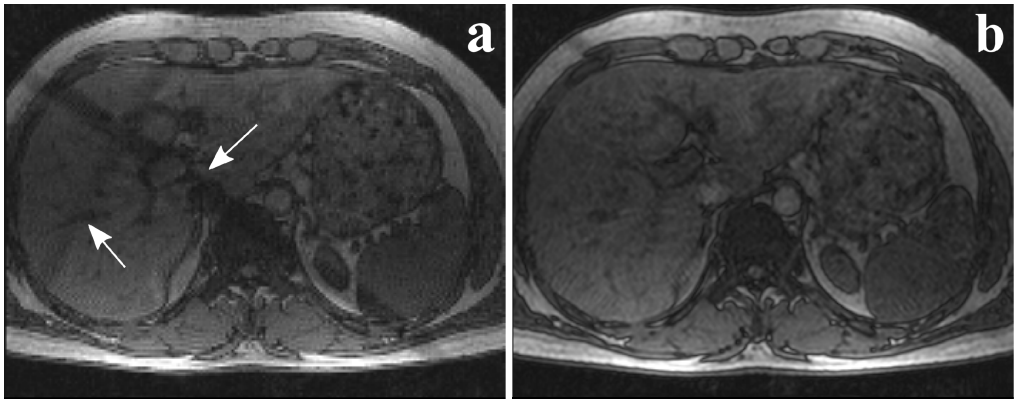

Figure 4.5 Three-dimensional gated liver images acquired using the standard crossed-pair navigator **(a)**, and with the purposed spectrally selective navigator **(b)**. Note the saturation bands from the two planes marked by white arrows in a).

4.4 Discussion

The spectrally selective crossed-pair navigator was designed to enable tracking of organ motion based on the signal from the surrounding adipose tissue of organs such as the liver, the kidney and the heart. Here, we demonstrated the tracking of the adipose tissue in the lower part of the liver, which was subsequently used to gate acquisitions of GRE sequence. Applications in cardiac imaging, as described in [6], could be also used in future, as well for the guidance of the HIFU system [10].

The spectral selectivity of the pulses was achieved by implementing the excitation and refocusing as 1-$\overline{1}$ binomial pulses. This is in contrast to the implementation in [10], that consisted of 1-$\overline{2}$-1 binomial pulse with 2D RF subpulses. Although the spectral selectivity of the tri-component binomial pulse is better, we used the simplest form of binomial pulses due to the efficiency and higher temporal resolution. 2D RF pulses are also in general more prone to B0 field inhomogeneities compared to crossed-pair excitation. Due to the relative long duration of the 2D RF pulses needed for a sufficiently dense coverage of the excitation k-space, it was not possible to achieve minimal interpulse interval τ, which is on the contrary achievable with the here presented navigator. This made the proposed 1-$\overline{2}$ -1 binomial pulse train more sensitive to B0 field inhomogeneities. However, our navigator was designed with $1/(2\pi)$ fat-water phase condition, which suggests that our navigator would be more suitable for applications on high-field MR systems.

This navigator in the presented application tracks the interface between liver parenchyma and the intraperitoneal fat, in contrast to the conventional approach that tracks the interface between lung air and liver tissue. Since the two portions

of the liver move differently, it is necessary to adapt the tracking factor when using the proposed navigator.

The saturation bands originating from the excitation and refocusing planes were not discernable on the 3D GRE liver image acquired with gating using our navigator. This is in particular valuable for tracking the organ motion and/or triggering/gating the image acquisition. Our results suggest that the purposed spectrally selective crossed-pair navigator could be used to track the adipose tissue around the imaging organs, like the liver or the heart, and can be used for triggering acquisitions to provide better image quality. The time required to acquire one navigator profile was around 8 ms, which is significantly less than the ones reported in [1, 10].

An extension of liver imaging is the obtainment of positional information of the target during the sonication with high-intensity focused ultrasound (HIFU) without interfering with MR thermometry or vice versa.

As shown in [1], another potential application for this navigator is cardiac and coronary imaging with reduced motion artifacts. The motion-correction methods used in coronary MRA [15], like slice-following algorithms could benefit from direct tracking of imaged-organ motion, as suggested in [1].

4.5 Conclusion

The spectrally selective crossed-pair navigator can be used to track the imaged organ based on the surrounding adipose tissue. As the organ is directly tracked, the accuracy of motion-correction methods is improved. This kind of navigator could be used in MRgHIFU treatments to directly measure organ motion without the adverse effects on MR thermometry and for tracking the cardiac motion in coronary MRA.

References

[1] T. D. Nguyen, A. Nuval, S. Mulukutla, and Y. Wang, “Direct monitoring of coronary artery motion with cardiac fat navigator echoes,” *Magn Reson Med*, vol. 50, pp. 235-241, 2003.

[2] T. D. Nguyen, P. Spincemaille, M. R. Prince, and Y. Wang, “Cardiac fat navigator-gated steady-state free precession 3D magnetic resonance angiography of coronary arteries,” *Magn Reson Med*, vol. 56, pp. 210-215, 2006.

[3] J. Keegan, P. D. Gatehouse, G. Z. Yang, and D. N. Firmin, “Non-model-based correction of respiratory motion using beat-to-beat 3D spiral fat-selective imaging,” *J Magn Reson Imaging*, vol. 26, pp. 624-629, 2007.

[4] T. D. Nguyen, P. Spincemaille, M. D. Cham, J. W. Weinsaft, M. R. Prince, and Y. Wang, "Free-breathing 3D steady-state free precession coronary magnetic resonance angiography: comparison of diaphragm and cardiac fat navigators," *J Magn Reson Imaging*, vol. 28, pp. 509-514, 2008.

[5] A. D. Scott, J. Keegan, and D. N. Firmin, "High-resolution 3D coronary vessel wall imaging with near 100% respiratory efficiency using epicardial fat tracking: reproducibility and comparison with standard methods," *J Magn Reson Imaging*, vol. 33, pp. 77-86, 2011.

[6] K. Kawaji, P. Spincemaille,T. D. Nguyen, N. Thimmappa, M. A. Cooper, M. R. Prince, and Y. Wang, "Direct coronary motion extraction from a 2D fat image navigator for prospectively gated coronary MR angiography," *Magn Reson Med*, 2013. doi: 10.1002/mrm.24698.

[7] R. R. Ingle, T. Cukur, and D. G. Nishimura, "The central signal singularity phenomenon in balanced SSFP and its application to positive-contrast imaging," *Magn Reson Med*, vol. 67, pp. 1673-1683, 2012.

[8] R. R. Ingle, T. Shin, and D. G. Nishimura, "Respiratory motion correction using TR-perturbed bSSFP for fat navigator acquisition and imaging," In Proceedings of the 20th Annual Meeting of ISMRM, Melbourne, Australia, 2012. p. 603.

[9] Z. Celicanin, V. Auboiroux, O. Bieri, L. Petrusca, F. Santini, M. Viallon, K. Scheffler, and R. Salomir, "Real-time method for motion-compensated MR thermometry and MRgHIFU treatment in abdominal organs," *Magn Reson Med*, 2013, doi: 10.1002/mrm.25017.

[10] M. O. Köhler, D. B. Senneville, B. Quesson, C. T. Moonen, and M. Ries, "Spectrally selective pencil-beam navigator for motion compensation of MR-guided high-intensity focused ultrasound therapy of abdominal organs," *Magn Reson Med*, vol. 66, pp. 102-111, 2011.

[11] V. S. Lee, M. T. Lavelle, N. M. Rofsky, G. Laub, D. M. Thomasson, G. A. Krinsky, and J. C. Weinreb, "Hepatic MR imaging with a dynamic contrast-enhanced isotropic volumetric interpolated breath-hold examination: feasibility, reproducibility, and technical quality," *Radiology*, vol. 215, pp. 365-372, 2000.

[12] J. A. Goncalves Neto, E. Altun, M. Elazzazi, G. D. Vaidean, M. Chaney, and R. C. Semelka, "Enhancement of abdominal organs on hepatic arterial phase: quantitative comparison between 1.5- and 3.0-T magnetic resonance imaging," *Magn Reson Imaging*, vol. 28, pp. 47-55, 2010.

[13] Y. Iwadate, A. C. Brau, S. S. Vasanawala, and H. Kabasawa, "Enhancement of respiratory navigator-gated three-dimensional spoiled gradient-recalled echo sequence with variable flip angle scheme," *Magn Reson Med*, 2013. doi: 10.1002/mrm.24902.

[14] Y. Wang, R. C. Grimm, J. P. Felmlee, S. J. Riederer, and R. L. Ehman, "Algorithms for extracting motion information from navigator echoes," *Magn Reson Med*, vol. 36, pp. 117-123, 1996.

[15] P. G. Danias, M. V. McConnell, V. C. Khasgiwala, M. L. Chuang, R. R. Edelman, and W. J. Manning, "Prospective navigator correction of image position for coronary MR angiography," *Radiology*, vol. 203, pp. 733-736, 1997.

Chapter 5

Hybrid US-MR guided HIFU Treatment Method with 3D Motion Compensation

---

An adapted version of this chapter has been submitted as:
Z. Celicanin, L. Petrusca, K. Scheffler, V. Auboiroux, Y. Natsuaki, F. Santini, S. Terraz, O. Bieri, R. Salomir, “Hybrid US-MR guided HIFU Treatment Method with 3D Motion Compensation,” submitted to *BioMed Research Journal*, 2014.

5.1 Introduction

High-intensity focused ultrasound (HIFU) is the concept of using acoustic energy to induce thermal coagulation inside the human body [1]. Although initially developed in the 1940s, the technique was significantly advanced in the 1990s with the introduction of accurate thermal ablation monitoring by magnetic resonance imaging (MRI). Combining MRI and HIFU into magnetic resonance guided high-intensity focused ultrasound (MRgHIFU) gave rise to clinically approved therapies [2-5]. During the developmental process, various imaging modalities to guide HIFU were investigated, from X-rays to computed tomography (CT). MRI and ultrasound (US) imaging were established as the preferred guiding modalities; they are innocuous in a clinical setting, while having complementary guiding characteristics in terms of spatial-temporal resolution and image contrast.

MR imaging offers excellent soft tissue delineation, necessary for treatment planning and evaluation of the treatment outcome. Contrarily, US imaging generally offers poor contrast between soft tissues, limiting its guiding capabilities. Furthermore, MRI is the only clinically proven imaging modality capable of monitoring thermotherapies by providing thermal quantitative maps. However, considering that an US system is by far the most affordable imaging modality and taking into account its high temporal and spatial resolution (current state-of-the-art is sub-millimeter) as well as its immunity to geometrical distortions, US imaging is also a suitable candidate for guiding HIFU.

Considering the strengths and weaknesses of the imaging capabilities of both MRI and US, the two techniques could be combined to form a hybrid US-MRI guiding method. MRI-compatible US imaging transducers have already been developed, tested and reported [6-8].

Abdominal organ motion, caused by respiration and other physiological processes, renders the already developed clinical methods for local therapy in immobile organs, e.g. the prostate [9] or uterine fibroids [10], inapplicable to the abdominal region. Previous attempts to handle respiratory organ motion guided solely by MRI include: organ motion compensation using principle component analysis, used in a pretreatment step to record the organ motion pattern [11]; estimation of the motion pattern during an initial learning phase, with monitoring of the target motion by image registration (in-plane motion) and a pencil-beam navigator (out-of-plane motion) during treatment [12]; an external respiratory bellow used in a treatment phase to provide target motion estimation from a pre-mapped signal acquired in an initial preparative training [13]; HIFU beam steering and simultaneous prospective motion compensation of MR thermometry using a 1D MR pencil-beam navigator [14]. In [15], an ex vivo feasibility study demonstrated the ability of ultrasound to guide HIFU therapy simultaneously to MR thermometry, enabling the focal point to follow the organ motion in two dimensions. This study contained no out-of-plane motion compensation due to the unavailability of a three-dimensional MR compatible US transducer. Furthermore no explicit intra-scan motion correction was applied to the MR data, simply a rapid acquisition (300 ms/slice) was performed in order to alleviate intra-scan ghosting artifacts. Respiratory-gated MRgHIFU in the upper abdomen using an

MR-compatible in-bore digital camera was recently reported [16]. Contrarily to US-image-based monitoring of abdominal motion, the use of an optical camera does not require an additional acoustic window, however only the surface of the body can be analyzed with no direct visualization of the target tissue motion.

Temperature imaging based on the proton resonance frequency (PRF) shift is the favored method to measure the temperature distribution as it is tissue independent, linear and provides a high signal-to-noise ratio (SNR) [17]. The application of PRF shift-based temperature mapping in the abdominal region requires organ motion compensation. Various approaches had been suggested to deal with the motion, of which the baseline and multi-baseline approaches were the most common. However, the reference-less temperature calculation method has been demonstrated to greatly improve the stability of the temperature maps since no baseline is required [18-19]. An extension to reference-less thermometry enabling an estimation of the background phase in the presence of phase discontinuities between aqueous and fatty tissues was described in [20].

Here, a truly hybrid US-MR-guided HIFU (US-MRgHIFU) method using an ex vivo study is demonstrated with electronic steering of the acoustic beam in three dimensions and prospective motion compensation (PMC) of multi-slice MR thermometry. An optical flow detection algorithm was applied to US images, acquired in the coronal orientation, in order to extract information about target in-plane motion, while an MR-based pencil-beam navigator [21-22], oriented perpendicular to the US imaging plane (Oy or, equivalent, AP direction), provided the tracking information in the remaining third dimension in order to achieve full 3D organ motion compensation. The 3D target motion vectors were sent in real-time to the HIFU system, enabling its focal point to be repositioned. The same information was simultaneously used for PMC of MR thermometry, which was acquired using a segmented gradient-recalled echo (GRE) echo-planar imaging (EPI) pulse sequence.

5.2 Materials and Methods

All measurements were performed using a 3 Tesla (T) whole-body MR system (MAGNETOM Trio, Siemens AG, Erlangen, Germany). The HIFU transducer (Imasonic, Besançon, France) consisted of 256 phased-array elements (frequency range f = 974-1049 kHz, focal length R = 130 mm, aperture D = 140 mm). The HIFU platform used a 256-channel generator, while piezo-electric motors were used for the adjustment of the transducer position in the coronal (horizontal) plane (Image Guided Therapy, Pessac, France).

The acquisition of ultrasound images was performed using a clinical US system (ACUSON Antares, Siemens Healthcare, Mountain View, USA). The abdominal CH4.1 imaging probe (256-element phased-array transducer) was modified to ensure MR compatibility by replacing various magnetic materials with MR-compatible ones. A 7 m long multi-channel cable was used to transfer the signals between the US probe and the stand-up control unit, which was placed outside the MR room. The cable was shielded against electromagnetic interference by an aluminum coating, which was set to common ground with the Faraday cage.

Additional adjustment of the impedance matching was performed to compensate for the increased capacity of the long cable. The US probe (shown on Fig. 5.1) was placed inside a dedicated holder, which was shielded with a copper coating. Standard acoustic gel, contained in a bag, was placed in front of the transducer to ensure good acoustic coupling of the transducer with the object to be imaged. Further technical details of the MR-compatible ultrasound imaging probe can be found in [23].

A pencil-beam MR navigator was used to track the motion along the AP direction, perpendicular to the US imaging plane, which was oriented approximately coronal (see Fig. 5.1). The MR navigator consisted of a 2D spatially-selective echo-planar RF pulse, used to excite a strip-shaped column, followed by a gradient echo. The acquisition duration of the pencil-beam navigator was approximately 20 ms, while the navigator volume was a rectangular column of dimension (5 to 10) x (5 to 10) x 180 mm. Further details are provided in [14]. The in-plane projection of the motion vector of the tissue (see blue vector on Fig. 5.1) was imaged and tracked by US. In order to have the complete 3D motion vector, the MR navigator was used to track the remaining direction. Thus, complete 3D tracking was obtained by the hybrid US-MR system.

The US field depth was approximately 10-18 cm with single-focus scanning. The frame rate varied between 15-30 images per second depending on the field depth and angular aperture. The slice thickness of the US imaging plane was approximately 4 mm (carrier frequency 2.2 MHz, second harmonic imaging mode).

The US images were sent in real-time to an external PC, which controlled the HIFU system. In order to control the exact position and orientation of the US probe in the MR coordinate system (and therefore the US imaging plane), volume imaging with T1-weigthed 3D GRE pulse sequence was performed (TE = 2.99 ms, TR = 6.88 ms, FA = 10°, voxel size = 1.2 × 1.2 × 2 mm3). The registration of the US probe on the multi-planar reconstructed MR data was based on 1) the known shape of the transducer's holder and 2) the spatially smooth MR signal of the acoustic coupling gel used to fill the gap between transducer, holder and sample.

Ex vivo bovine liver was used for the experiments. It was placed in a water-filled container, acoustically coupled with the water tank hosting the HIFU transducer. A mechanical ventilator was used to produce a breathing-like motion pattern by pumping air in and out of the balloon, which acted as a lung. A wooden ring was used to provide the support of a rotation axis, such that the suspended sample underwent periodic oscillations driven by the inflating balloon. The US probe was positioned to acquire images of the moving sample in the coronal (horizontal) plane, approximately. Periodic motion was obtained by the gravitational force pushing the sample towards its equilibrium position. The main direction of motion was along the Oz direction of the MR scanner. The total amplitude of the simulated breathing-like motion was approximately 6-15 mm, controlled by the volume of air pumped by the ventilator. The period of the motion was approximately 6-10 s, similar to the typical breathing pattern of a human subject. A single element receive-only 11 cm diameter loop coil (Siemens AG, Erlangen, Germany) was positioned above the sample to acquire the MR

signal. Several HIFU sonications were performed with and without motion compensation of duration and acoustic power 36 s / 150 W.

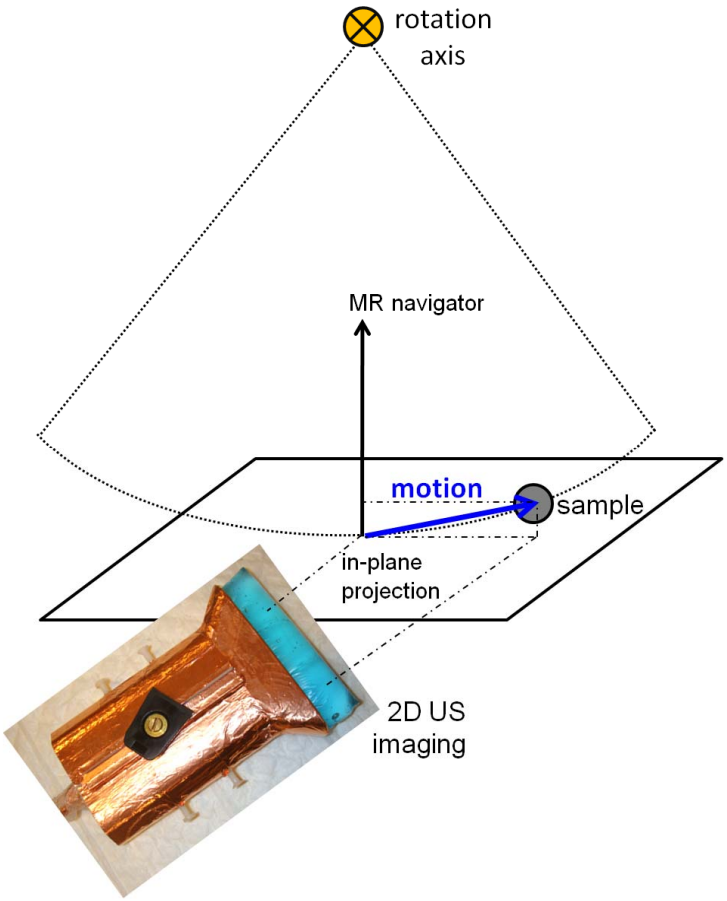

Figure 5.1 Set-up of the US and MR imaging. The MR navigator is orientated perpendicular to the US imaging plane. The sample undergoes circular motion, with the principal component in the US imaging plane and the vertical displacement detected by the MR navigator.

The interrelation scheme between the different parts of the complete system with the estimated delay times is shown on Fig. 5.2. Note that single line arrows correspond to 1D information, double line to 2D and triple line to 3D. Once the US image was imported into the external PC, an optical flow algorithm was used to calculate the average displacement vector within a user-defined region-of-interest (ROI), achieved using an in-house developed program based on OpenCV libraries (Open Source Computer Vision Library, http://www.opencv.org/) running on a standard personal computer (Intel Core Duo P8700 CPU 2.53GHz 2GB RAM). Registration points were automatically assigned to sharp edge-features inside the user-defined ROI using a feature-detecting algorithm, see Fig. 5.3. This was achieved using the OpenCV 'GoodFeaturesToTrack' method, which was implemented based on the algorithm described in [24]. Once initialized, the

displacement could be tracked by computing the optical flow using the iterative Lucas-Kanade method [25] and pyramidal implementation [26]. The two-dimensional vector extracted from US data (motion along Ox and Oz axes of the MR magnet) was then sent to the MR system via an Ethernet connection. The image reconstruction unit combined the out-of-plane motion measured by the MR pencil-beam navigator with the US tracking to form a complete 3D motion vector, which was then sent back via Ethernet to the HIFU beam-former driving application. The update frequency of the HIFU focal spot steering (including motion detection, HIFU signals phase calculation and transfer of the information to the beam-former) was equal to 1/TR of the MR thermometry pulse sequence, i.e. approximately 15 Hz.

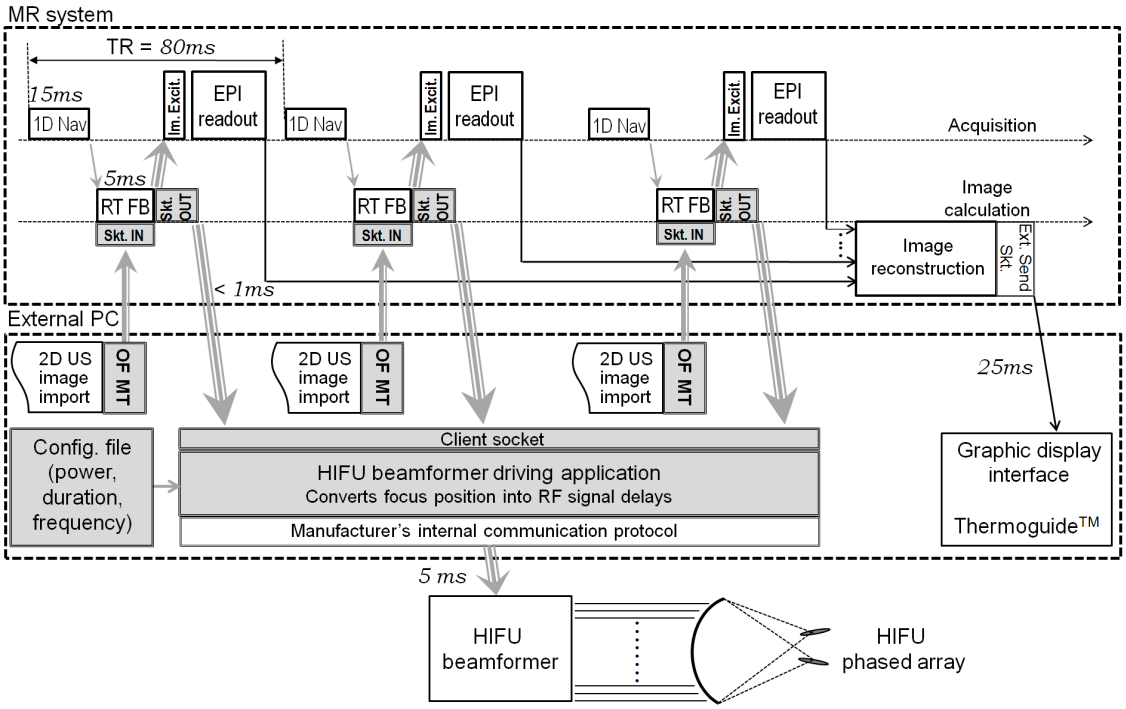

Figure 5.2 Diagram of the system showing the relationship and information exchange between the MR system, external PC and HIFU system. The latencies of the essential processes are provided. The dimensionality of the motion information is indicated by the line style of the arrows (single, double or triple for respectively 1D projection, 2D projection or full 3D vector).

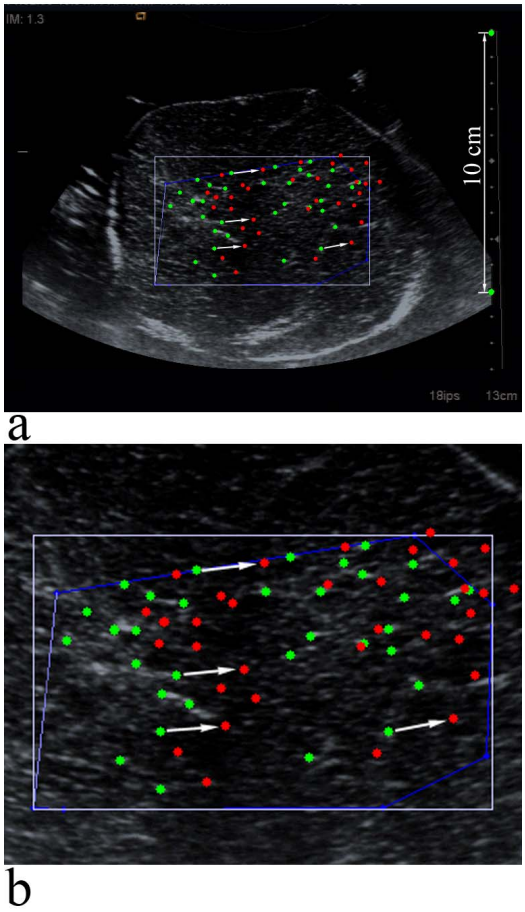

Figure 5.3 Ultrasound imaging-based motion tracking in the coronal plane. **a)** Second harmonic data from the ex vivo tissue is shown as background (Fo=2.2 MHz, mechanical index = 1.3, frame rate = 18 fps). The registration points for feature tracking are overlaid. Two extreme situations are shown, corresponding to the high volume (red dots) and the low volume of air (green dots) in the inflating balloon, i.e. similar to exhalation and inspiration. A few 2D motion vectors are indicated with white arrows. US data was acquired simultaneously with MR thermometry, free of electromagnetic interferences. Note the distance scale on the right side. **b)** Zoom-in by a factor of 2 of the region of interest of the above image.

MR thermometry was performed using a segmented GRE-EPI based on the proton resonance frequency (PRF) shift. The imaging parameters were as follows: TE = 10.5 ms, TR = 68 ms, FOV = 205 × 186 mm2, FA = 15º, acquisition matrix 128 x 116, reconstructed matrix = 256 × 232, slice thickness = 6 mm, BW = 797 Hz/pix, EPI factor = 13. Note that the TR parameter of GRE-EPI thermometry sequence, provided above, also includes the duration of the MR navigator. The fat suppression was implemented using a water selective 1-2-1 binomial RF pulse for slice excitation. In order to motion compensate the imaging, and thus allow easier calculation of thermal build-up with a reference-less method [19], while also increasing the SNR, the imaging plane was repositioned for each new segment of k-space. This was achieved by adapting the parameters of the excitation RF

pulses, the respective slice selection gradients, and by adjusting the readout accordingly. In order to have multiple-axis control of the sonication, the MR thermometry was performed in two perpendicular planes – the first in coronal orientation (i.e. parallel to the HIFU transducer) and the second in sagittal orientation. The slices were acquired sequentially; the complete k-space of each plane was acquired before beginning the acquisition of the second plane. The duration to acquire one slice was 0.9 s resulting in a temporal resolution of 1.8 s. It is important to note that the temporal resolution of the motion compensation was the repetition time (TR) of RF slice excitation (here 68 ms) and not the temporal resolution of the MR thermometry imaging. The acquired images were reconstructed and exported in real-time via an Ethernet connection to the external PC. A software package, Thermoguide (Image Guided Therapy, Pessac, France), was used for the calculation of thermal maps based on a 2D near-harmonic reference-less PRF shift method [19], which was implemented using the closed border variant in the coronal plane (perpendicular to the HIFU beam) and using the open border variant in the sagittal plane (parallel to the beam). An open border variant was required along the beam in order to avoid contamination of the border phase from ultrasound heating and subsequent temperature underestimation. Typically, 30% of the circular perimeter was open symmetrically, both proximal and distal to the HIFU transducer.

Aiming to examine the effectiveness of the motion-compensated treatment, two series of experiments were performed: without motion-compensation of the HIFU ablation, and with 3D motion-compensation of the HIFU ablation. MR thermometry was motion compensated for both series of experiments to enable accurate monitoring of the resulting thermal build-up. The anisotropy and shape of the thermal build-up and gross pathology, as performed immediately after the experiment, were used to assess the quality of the motion-compensated ablation. Similar to [14], calibration experiments using the same set-up but in static tissue (ventilator off) were performed to guarantee that there was no intrinsic acoustical aberration of the HIFU beam (data not shown here).

5.3 Results

Simultaneous imaging with US and MRI did not cause mutual interference. The US images were of standard quality, enabling the tracking algorithm to be both stable and accurate. HIFU sonication produced detectable acoustic interference in the far field of the US images. Interferences increased as the applied HIFU power was increased and could be attenuated by appropriate adjustment of the transmitted power and the US imaging receiver gain. Overall, the region of interest for US motion tracking was free from any significant interference under the present experimental conditions.

The sagittal and coronal MR thermometry images are shown on Fig. 5.4, demonstrating the geometry of the HIFU beam and the position of the MR pencil-beam navigator, see the dark saturation-induced region (indicated by a white arrow).

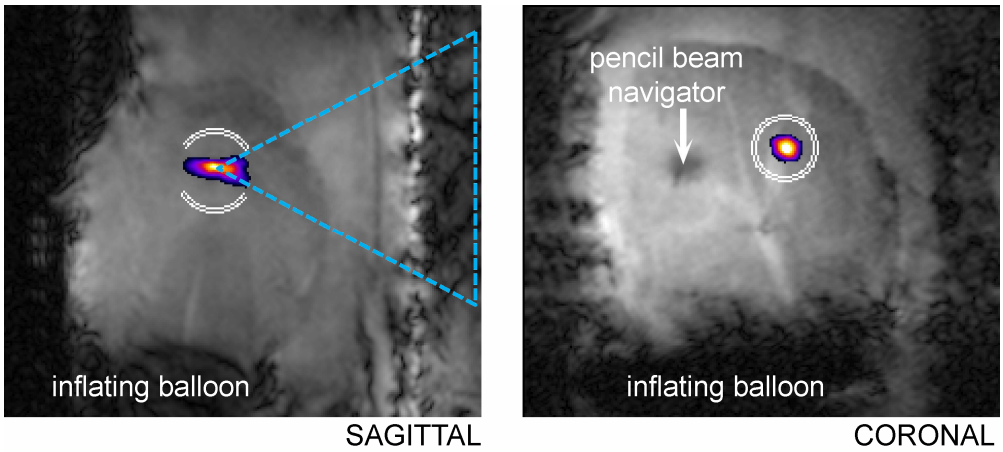

Figure 5.4 The set-up of the HIFU sonication cone and MR pencil-beam navigator. Magnitude data and reference-less thermometry are shown in two orthogonal planes.

Fig. 5.5 shows the results of HIFU sonication achieved without motion compensation. The elevated temperature at the sonication end-point (36 s) is shown in two orientations, sagittal and coronal, and the corresponding thermal dose in coronal orientation is calculated according to [27] and shown in the last column. It can be seen that due to the motion of the ex vivo liver, the acoustic energy is dispersed around the desired focal point, resulting in lower temperature elevation, elongated thermal build-up and reduced precision of the ablation. Note that the temperature distribution in the coronal plane represents the histogram of tissue mass-point positions, after convolution with the in-plane profile of HIFU acoustic intensity and with Gaussian point-spread-function due to heat diffusion.

In contrast to Fig. 5.5, Fig. 5.6 shows the ablation achieved by the hybrid US-MR guided HIFU with full motion compensation. Sagittal and coronal views of the elevated temperature at the sonication end-point (36 s) and the corresponding thermal dose maps are presented. From the gross pathology, performed after the experiment, it can be seen that the ablated tissue (decolored area) is mainly isotropic. The elevated temperatures, greater than 30ºC, were high enough to cause the coagulation of the liver tissue. It should be noted however that fresh tissue cutting cannot guarantee a perfect alignment with the MR coronal plane used in the treatment set-up. In some cases, the MR thermometry sagittal slice was slightly misaligned from the focal point trajectory; in these cases the temperatures measured are therefore not representative of the highest thermal build-up actually produced in the tissue. The coronal plane always captured the focal spot due to its elongated shape. In a series of repeated independent experiments on samples prepared from the same organ (ex vivo bovine liver), the in-plane maximum spatial temperature achieved at the end of a 36 s sonication was 29.5 ± 8.8 °C with motion compensation on 4 experiments, and, respectively, 15.8 ± 1.4 °C without motion compensation on 3 experiments ($p = 0.026$ one tailed t-test). This corresponds to a statistically significant improvement of the highest temperature elevation in the treated tissue by a factor of approximately 2.

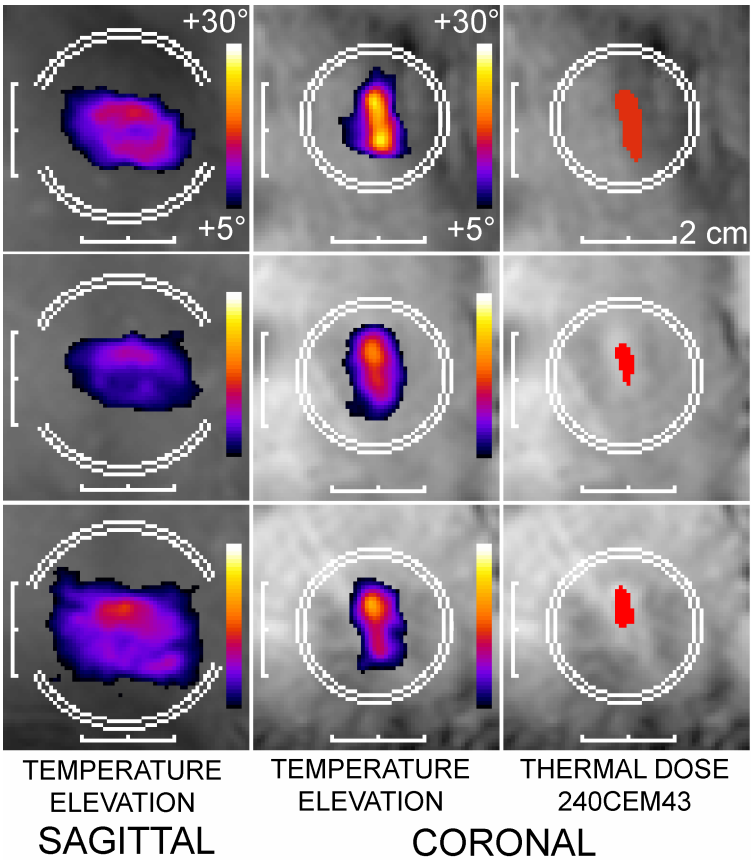

Figure 5.5 Hybrid US-MR-guided HIFU ablation without motion compensation in three individual experiments (each row corresponds to a different experiment). The circular border (open in the sagittal plane, closed in the coronal plane) for near-harmonic reference-less thermometry is shown in white. Note the embedded scales of distances and temperature elevation color bar.

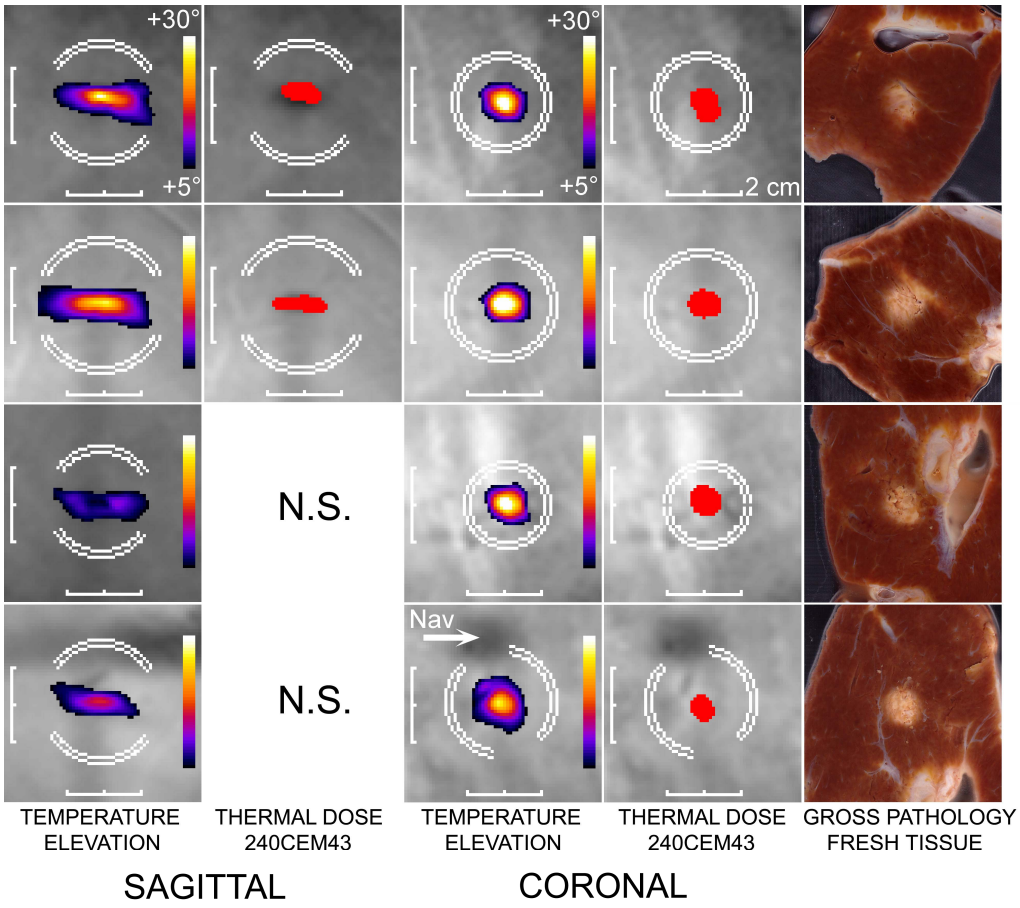

Figure 5.6 Full motion-compensated sonication with US-MRgHIFU from four individual experiments (each row corresponds to a different experiment). The circular border (open in the sagittal plane, closed it the coronal plane) for near-harmonic reference-less thermometry is shown in white. Note the embedded scale of distances and temperature elevation color bar.

The temperature of the pixel with the highest temperature during the experiment with and without motion compensation is shown on Fig. 5.7, on tissue samples taken from the same ex vivo liver. Motion compensation clearly enables a higher temperature elevation to be achieved than sonication without motion compensation. The periodical waveform of the pixel-wise temperature of the non-compensated approach was caused by the periodic exposure of the chosen pixel to the HIFU beam, as the focal point was static in the laboratory frame while the slice position was locked-on the moving tissue and therefore moving together with the tissue in the laboratory frame.

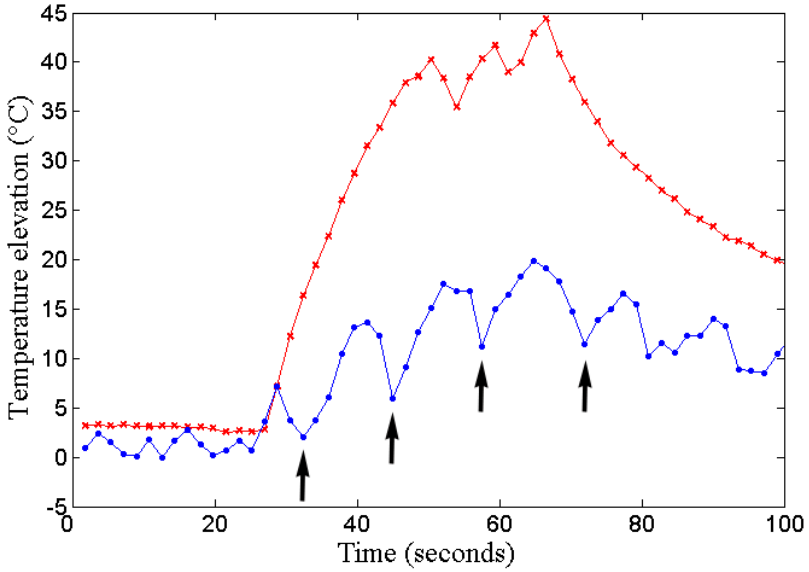

Figure 5.7 Temperature evolution of the pixel with the highest temperature elevation in the coronal plane with motion compensation (red plot) and without motion compensation (blue plot). Except for dynamic beam steering, the same acoustic parameters (36 s / 150 W) were applied for each experiment. Vertical arrows indicate the breathing cycles.

5.4 Discussion

The application of HIFU to the abdominal and thoracic region requires tracking of the motion of the targeted organs, and acoustic beam steering. This could be achieved using a hybrid guiding technique involving US and MRI, complementary and non-invasive imaging modalities, offering high temporal resolution and precision of the tracking signal. The active motion tracking enabled a sonication of nearly 100% duty cycle to be achieved. Without motion compensation, the acoustic energy is dispersed, creating a risk of thermal damage to critical structures in the treated organ, as well as ineffective heating of the focal spot, therefore requiring increased energy to elevate the temperature, assuming the other parameters remain constant. Increasing the delivered energy increases the risk of side effects.

A hybrid US-MRgHIFU method using an ex vivo study is demonstrated, achieving full 3D motion compensation. The improvement is evident when the sonications performed with and without motion compensation are compared. As this is a real-time method without any background model, non-periodic motion can also be handled, requiring no preparation stage prior to treatment. In addition to respiratory motion, upper abdomen targets may also be affected by motion due to coughing, cardiac motion or peristaltic motion. Our objective is to provide a clinically applicable method for conscious free-breathing patients.

The prospective motion compensation of the MR thermometry is advantageous as it is not necessary to register the temperature maps in moving tissue for the

reference-less calculation. The thermal dose calculation and the gross pathologies after the experiment both indicated that the acoustic energy was precisely focused on the moving target in all three directions within SD ± 1 mm, even though the ex vivo tissue was moving and deforming during the sonication. Before beginning the experiments, it was necessary to adjust the scaling factors between the measured motion vectors and the applied compensation, as the motion information was not obtained directly from the treated region. These scaling factors typically ranged between 0.4 and 1.25. The US imaging plane was set in general 10 to 15 mm above the HIFU focal point, while the MR navigator captured the information of tissue-to-air interface. In principle, the adjustment of the scaling factors can be achieved automatically by minimizing the residual motion of the ROI in the MR thermometry magnitude data.

The set-up used 2D US imaging that is fast, motion-robust, readily available and inexpensive, combined with a 1D MR pencil-beam navigator that required limited additional delays in the MR pulse sequence. The simultaneous use of three orthogonal pencil-beam navigators may be time consuming in MR pulse sequence chronogram and furthermore would produce inconvenient signal-void saturation regions on thermometry images. The principal component of the motion (SI) was monitored and tracked using US, minimizing the out-of-plane motion in the US images. Some adjustment of the US imaging probe position was required to acquire as much as possible the principal component of motion in the US imaging plane. In fact, the US imaging plane was set slightly oblique, parallel to the time-averaged motion vector of the sample. Motion through the US imaging plane may reduce the stability of the optical flow tracking algorithm.

A limitation of this study was the absence of a true histological reference detectable both in pre-operative MRI and in post-mortem macroscopic slices [28], as absolute proof of the ballistic accuracy of the motion-compensated US-MRgHIFU.

Sharply delineated and static-tissue-like lesions were produced with motion-compensated single-focus sonications in moving bulk tissue, however, the accurate positioning of the focal point on a true target at a pre-defined location was not addressed in this report. Another limitation was the lack of active temperature control at the focus. Therefore the temperature elevation was not accurately reproducible from one experiment to another under identical set-up and identical acoustic parameters (36 s / 150 W / 5.4 kJ), mainly due to slightly different geometries of samples (i.e. incidence angle of the HIFU beam on the tissue surface, focal point depth etc). Nonetheless, the difference of the focal point temperature elevation with and without motion compensation was clearly demonstrated as the improvement largely exceeded the inter-experiment data fluctuation. A more accurate method would be to force the same evolution of the temperature at the focus using a closed-loop feedback controller and to compare the energy delivered with and without motion compensation.

Further validation of the method is required in vivo, involving additional experimental challenges such as non-periodic motion, blood perfusion in liver parenchyma and avoiding near and far field side effects.

5.5 Conclusion

The hybrid US-MRgHIFU 3D method for the treatment of abdominal organs with HIFU guided simultaneously by US and MRI, was demonstrated as proof-of-concept in an ex vivo feasibility study. It enabled motion-compensated ablations, that appear similar to the static-like conditions. The MR thermometry was prospectively motion-compensated, which provided high quality temperature maps.

References

[1] F. A. Jolesz, "MRI-guided focused ultrasound surgery," Annu Rev Med, vol. 60, pp. 417-430, 2009.

[2] J. Hindley, W. M. Gedroyc, L. Regan, E. Stewart, C. Tempany, K. Hynyen, N. Mcdannold, Y. Inbar, Y. Itzchak, J. Rabinovici, H. S. Kim, J. F. Geschwind, G. Hesley, B. Gostout, T. Ehrenstein, S. Hengst, M. Sklair-Levy, A. Shushan, and F. Jolesz, "MRI guidance of focused ultrasound therapy of uterine fibroids: early results," AJR Am J Roentgenol, vol. 183, pp. 1713-1719, 2004.

[3] P. E. Huber, J. W. Jenne, R. Rastert, I. Simiantonakis, H. P. Sinn, H. J. Strittmatter, D. von Fournier, M. F. Wannenmacher, and J. Debus, "A new noninvasive approach in breast cancer therapy using magnetic resonance imaging-guided focused ultrasound surgery," Cancer Res, vol. 61, pp. 8441-8447, 2001.

[4] E. Martin, D. Jeanmonod, A. Morel, E. Zadicario, and B. Werner, "High-intensity focused ultrasound for noninvasive functional neurosurgery," Ann Neurol, vol. 66, pp. 858-861, 2009.

[5] R. Catane, A. Beck, Y. Inbar, T. Rabin, N. Shabshin, S. Hengst, R. M. Pfeffer, A. Hanannel, O. Dogadkin, B. Liberman, and D. Kopelman, "MR-guided focused ultrasound surgery (MRgFUS) for the palliation of pain in patients with bone metastases--preliminary clinical experience," Ann Oncol, vol. 18, pp. 163-167, 2007.

[6] P. L. de Oliveira, B. D. de Senneville, I. Dragonu, and C. T. Moonen, "Rapid motion correction in MR-guided high-intensity focused ultrasound heating using real-time ultrasound echo information," NMR Biomed, vol. 23, pp. 1103-1108, 2010.

[7] D. A. Feinberg, D. Giese, D. A. Bongers, S. Ramanna, M. Zaitsev, M. Markl, and M. Günther, "Hybrid ultrasound MRI for improved cardiac imaging and real-time respiration control," Magn Reson Med, vol. 63, pp. 290-296, 2010.

[8] C. D. Arvanitis, M. S. Livingstone, and N. McDannold, "Combined ultrasound and MR imaging to guide focused ultrasound therapies in the brain," Phys Med Biol, vol. 58, pp. 4749-4761, 2013.

[9] A. Marien, I. Gill, O. Ukimura, B. Nacim, and A. Villers, "Target ablation-Image-guided therapy in prostate cancer," Urol Oncol, 2014; doi: 10.1016/j.urolonc.2013.10.014.

[10] L. E. Rueff, and S. S. Raman, "Clinical and Technical Aspects of MR-Guided High Intensity Focused Ultrasound for Treatment of Symptomatic Uterine Fibroids," Semin Intervent Radiol, vol. 30, pp. 347-353, 2013.

[11] B. D. de Senneville, M. Ries, G. Maclair, and C. Moonen, "MR-guided thermotherapy of abdominal organs using a robust PCA-based motion descriptor," IEEE Trans Med Imaging, vol. 30, pp. 1987-1995, 2011.

[12] M. Ries, B. D. de Senneville, S. Roujol, Y. Berber, B. Quesson, and C. Moonen, "Real-time 3D target tracking in MRI guided focused ultrasound ablations in moving tissues," Magn Reson Med, vol. 64, pp. 1704-1712, 2010.

[13] A. B. Holbrook, P. Ghanouni, J. M. Santos, C. Dumoulin, Y. Medan, and K. B. Pauly, "Respiration based steering for high intensity focused ultrasound liver ablation," Magn Reson Med, 2013; doi: 10.1002/mrm.24695.

[14] Z. Celicanin, V. Auboiroux, O. Bieri, L. Petrusca, F. Santini, M. Viallon, K. Scheffler, and R. Salomir, "Real-time method for motion-compensated MR thermometry and MRgHIFU treatment in abdominal organs," Magn Reson Med, 2013. doi: 10.1002/mrm.25017.

[15] V. Auboiroux, L. Petrusca, M. Viallon, T. Goget, C. D. Becker, and R. Salomir, "Ultrasonography-based 2D motion-compensated HIFU sonication integrated with reference-free MR temperature monitoring: a feasibility study ex vivo," Phys Med Biol, vol. 57, pp. N159-N171, 2012.

[16] V. Auboiroux, L. Petrusca, M. Viallon, A. Muller, S. Terraz, R. Breguet, X. Montet, C. D. Becker and R. Salomir, "Respiratory-gated MRgHIFU in upper abdomen using an MR-compatible in-bore digital camera," BioMed Research International, 2014, in press

[17] V. Rieke, and K. B. Pauly, "MR thermometry," J Magn Reson Imaging, vol. 27, pp. 376-390, 2008.

[18] V. Rieke, K. K. Vigen, G. Sommer, B. L. Daniel, J. M. Pauly, and K. Butts, "Referenceless PRF shift thermometry," Magn Reson Med, vol. 51, pp. 1223-1231, 2004.

[19] R. Salomir, M. Viallon, A. Kickhefel, J. Roland, D. R. Morel, L. Petrusca, V. Auboiroux, T. Goget, S. Terraz, C. D. Becker, and P. Gross, "Reference-free PRFS MR-thermometry using near-harmonic 2-D reconstruction of the background phase," IEEE Trans Med Imaging, vol. 31, pp. 287-301, 2012.

[20] V. Rieke, A.M. Kinsey, A.B. Ross, W.H. Nau, C.J. Diederich, G. Sommer, and K.B. Pauly, "Referenceless MR thermometry for monitoring thermal ablation in the prostate," IEEE Trans Med Imaging, vol. 26, pp. 813-821, 2007.

[21] C. J. Hardy, J. D. Pearlman, J. R. Moore, P. B. Roemer, and H. E. Cline, "Rapid NMR cardiography with a half-echo M-mode method," J Comput Assist Tomogr, vol. 15, pp. 868-874, 1991.

[22] K. Nehrke, P. Börnert, J. Groen, J. Smink, and J. C. Böck, "On the performance and accuracy of 2D navigator pulses," Magn Reson Imaging, vol. 17, pp. 1173-1181, 1999.

[23] L. Petrusca, P. Cattin, V. de Luca, F. Preiswerk, Z. Celicanin, V. Auboiroux, M. Viallon, P. Arnold, F. Santini, S. Terraz, K. Scheffler, C. D. Becker, and R. Salomir, “Hybrid ultrasound/magnetic resonance simultaneous acquisition and image fusion for motion monitoring in the upper abdomen,” Invest Radiol, vol. 48, pp. 333–340, 2013.

[24] J. Shi, and C. Tomasi, “Good features to track,” in Proceedings of the IEEE Computer Society Conference on Computer Vision and Pattern Recognition, pp. 593–600, 1994.

[25] B. Lucas, and T. Kanade, “An iterative image registration technique with an application in stereo vision,” in Proceedings of the International Joint Conference on Artificial Intelligence, pp. 674–679, 1981.

[26] J. Y. von Bouguet, “Pyramidal implementation of the Lucas-Kanade feature tracker,” OpenCV Documentation, Intel Corp., Microprocessor Research Labs, 1999.

[27] S. A. Sapareto, and W. C. Dewey, “Thermal dose determination in cancer therapy,” Int J Radiat Oncol Biol Phys, vol. 10, pp. 787–800, 1984.

[28] L. Petrusca, M. Viallon, R. Breguet, S. Terraz, G. Manasseh, V. Auboiroux, T. Goget, L. Baboi, P. Gross, K. M. Sekins, C. D. Becker, and R. Salomir, "An experimental model to investigate the targeting accuracy of MR-guided focused ultrasound ablation in liver," J Transl Med, 2014; doi: 10.1186/1479-5876-12-12.

Chapter 6

Summary and Outlook

6.1 Summary

Interventional MRI has seen a significant progress over the past decades, especially an increase in noninvasive surgical procedures such as high-intensity focused ultrasound with a potential to treat many types of tissue abnormalities. However, the application of this technology for treatments in the abdominal and thoracic region is hindered by respiratory organ motion.

The main objective of this thesis was to deal with challenges of tracking and imaging respiratory organ motion, and proving methods for high-intensity focused ultrasound motion-compensated treatment in the liver.

Acquisition of volumetric time-resolved three dimensional images of organs in the abdominal region for subsequent organ motion modeling and prediction of organ motion is an important step in the interventional treatment planning. MRI is the preferred choice over the other imaging modalities for this aim due to its excellent soft-tissue contrast, the ability to perform image acquisition in arbitrary orientation and the noninvasive nature of the MR imaging. However, currently it is not possible to acquire the time-resolved volumes with high spatial and temporal resolution, high signal-to-noise ratio, which would be required to plan treatments and guide procedures. A novel acquisition scheme was developed for 4D-MRI based on the CAIPIRINHA method, which acquires the image and navigator slices simultaneously in order to reduce the lag between the two and have more accurate imaging and subsequently improved motion models.

MR navigator echoes are commonly used to track organ position and provide information about the respiratory phase. The acquisition of the navigator and imaging sequence are interleaved in order to have the information about the breathing phase in which the acquisition took place. Tracking of organ motion for either guiding an interventional MRI therapy or gating/triggering the MR image acquisition is in general performed by an MR pencil-beam navigator, a crossed-pair navigator, or external tracking methods, e.g. breathing belt. In case of MR-based navigators, saturation artifact appears in case the navigator is place on the same organ, which is imaged. Indirect tracking by a spectrally-selective crossed-pair navigator was proven here to provide an accurate information about the position of the organ and that concept is immune to saturation artifacts.

Magnetic resonance guided high-intensity focused ultrasound has been recognized as a promising technique for noninvasive ablation of abnormal tissue by an acoustic energy. Different attempts have been made in the past to motion-compensate the treatment by steering the focal point. Two methods have been described in this thesis. An MR pencil-beam navigator has been used to track the motion of a treated organ, here the liver, and the tracking signal was simultaneously sent to reposition the focal point and to adjust the imaging volume of the MR acquisition to have motion-compensated MR thermometry. In the other approach, a hybrid imaging modality comprising an MR-compatible ultrasound imaging system and an MRI was developed to guide efficiently the treatment and achieve the full three-dimensional compensation. The ablated lesions were isotropic in the plane perpendicular to the HIFU beam which indicate that the guiding of the HIFU focus was accurate.

6.2 Outlook

The application of high intensity focused ultrasound to a clinical routine for the treatment of patients demands high safety standards and the treatment outcome should be more favorable compared to other competing treatment options. Upper abdominal organs, such as the liver and the kidney, are particularly sensitive and critical organs, in which the HIFU ablation could produce serious side effects, such as internal bleeding and thrombosis. Therefore, the safety must be first evaluated before the full exploitation of the benefits of the acoustic therapy with the methods presented in this thesis.

MR-based pencil-beam navigator was proven to accurately track respiratory organ motion and its tracking information was fed to a HIFU system for focal point repositioning, while an MR system also used the same tracking information for prospective motion compensation. This method could be applied for the treatment of the liver abnormalities (e.g. liver cancer). However, ballistic accuracy of the acoustic beam must be first evaluated. The pretreatment anatomical images must be analyzed and the exact spatial location in the MR coordinate system must be obtained for the HIFU focus to be accurately targeted on a tumor.

The amount of thermal energy delivered to the region of interest should be controlled during ablation. Automatic temperature control is one approach to achieve this by controlling the acoustic power delivery according to the measured focal point temperature [1-3]. A proportional-integral-derivative controller (PID controller) can be used for this purpose to establish a feedback control mechanism [4].

Acquisition of pretreatment data to model the organ shape transformation driven by respiration could be performed by [5]. Modeling organ motion and predicting the future positions of the target to avoid system time lag was purposed in [6, 7], and could be readily integrated with a MRgHIFU and hybrid US-MRgHIFU method presented in this thesis.

The hybrid US-MRgHIFU method was so far evaluated on an ex vivo liver tissue in a feasibility study. The in vivo potential of this method should be investigated for the treatment of the liver in sheep and human subjects. The optimal positioning of the US plane and the MR-based pencil-beam navigator should be inferred to maximize the tracking capabilities of the hybrid system, which would result in a more accurate and therefore safer treatment. The collateral damping of the acoustic energy on the solid body parts such as ribs, should be prevented by reflective strips to mitigate potential side effects [8].

Tracking organ motion based on the adipose tissue around the organ of interest is gaining more interest especially in the imaging of coronary magnetic resonance angiography [9, 10]. The spectrally selective crossed-pair navigator can be applied for this purpose, and the reproducibility and accuracy of tracking should be evaluated. The image quality of coronary angiographies, acquired using a motion compensated approach based on the spectrally selective crossed-pair navigator, should be compared against the standard methods.

The spectrally selective crossed-pair navigator could be also applied for tracking of the liver motion during ablations with high intensity focused ultrasound, similar to [11].

To conclude, the aim of this thesis was to developed novel treatment methods to be used in interventional MRI with a particular focus on respiratory organ motion issues occurring in high intensity focused ultrasound ablations of the liver. Indirect organ motion tracking was developed to benefit future interventional MRI therapies that require organ motion position in real-time. And finally, the novel approach for 4D MRI data acquisition for organ motion modeling was developed. The hope is that these methods will provide an incentive for future developments in the field of interventional MRI.

References

[1] F. C. Vimeux, J. A. de Zwart, J. Palussiere, R. Fawaz, C. Delalande, P. Canioni, N. Grenier, and C. T. Moonen, "Real-time control of focused ultrasound heating based on rapid MR thermometry," *Invest Radiol*, vol. 34, pp. 190-193, 1999.

[2] R. Salomir, F. Vimeux, J. A. de Zwart, N. Grenier, and C. T. Moonen, "Hyperthermia by MR-guided focused ultrasound: accurate temperature control based on fast MRI and a physical model of local energy deposition and heat conduction," *Magn Reson Med*, vol. 43, pp. 342-347, 2000.

[3] B. Quesson, F. Vimeux, R. Salomir, J. A. de Zwart, and C. T. Moonen, "Automatic control of hyperthermic therapy based on real-time Fourier analysis of MR temperature maps," *Magn Reson Med*, vol. 47, pp. 1065-1072.

[4] S. H. Zak, "Systems and Control," *Oxford University Press*, USA, 2002.

[5] Z. Celicanin, O. Bieri, F. Preiswerk, P. Cattin, K. Scheffler, and F. Santini, "Simultaneous acquisition of image and navigator slices using CAIPIRINHA for 4D MRI," *Magn Reson Med*, doi: 10.1002/mrm.25134, 2014.

[6] P. Arnold, F. Preiswerk, B. Fasel, R. Salomir, K. Scheffler, and P. C. Cattin, "3D organ motion prediction for MR-guided high intensity focused ultrasound," *Med Image Comput Assist Interv*, vol. 14, pp. 623-630, 2011.

[7] D. Kokuryo, E. Kumamoto, Y. Takao, S. Fujii, T. Kaihara, and K. Kuroda, "Evaluation of a vessel-tracking-based technique for dynamic targeting in human liver," *Magn Reson Med*, vol. 67, pp. 156-163, 2012.

[8] R. Salomir, L. Petrusca, V. Auboiroux, A. Muller, M. I. Vargas, D. R. Morel, T. Goget, R. Breguet, S. Terraz, J. Hopple, X. Montet, C. D. Becker, and M. Viallon, "Magnetic resonance-guided shielding of prefocal acoustic obstacles in focused ultrasound therapy: application to intercostal ablation in liver," *Invest Radiol*, vol. 48, pp. 366-380, 2013.

[9] K. Kawaji, O. Spincemaille, T. D. Nguyen, N. Thimmappa, M. A. Cooper, M. R. Prince, and Y. Wang, "Direct coronary motion extraction from a 2D

fat image navigator for prospective gated coronary MR angiography," *Magn Reson Med*, doi: 10.1002/mrm.24698, 2013.

[10] A. D. Scott, J. Keegan, and D. N. Firmin, "High-resolution 3D coronary vessel wall imaging with near 100% respiratory efficiency using epicardial fat tracking: reproducibility and comparison with standard methods," *J Magn Reson Imaging*, vol. 33, pp. 77-86, 2011.

[11] M. O. Köhler, D. B. de Senneville, B. Quesson, C. T. Moonen, and M. Ries, "Spectrally selective pencil-beam navigator for motion compensation of MR-guided high-intensity focused ultrasound therapy of abdominal organs," *Magn Reson Med*, vol. 66, pp. 102-111, 2011.

Acknowledgement

I would like to thank to Prof. Klaus Scheffler, Prof. Michael Bock, Prof. Oliver Bieri, Prof. Philippe Cattin, Dr. Rares Salomir, Dr. Francesco Santini, Dr. Lorena Petrusca, and Dr. Frank Preiswerk for their help, which I received during the work on this thesis.

I would like to acknowledge the collaborations with the Radiology Department, University of Geneva, team of Dr. Rares Salomir and the Medical Image Analysis Center, University of Basel, team of Prof. Philippe Cattin for the collaborative work and joined publications.

And I would like to thank to the Swiss National Science Foundation for the financial support. Grant Numbers: CRS1I2_127549, CR32I3_125499, and CR33I3_143980.